QUALITY ENGINEERING APPLICATIONS ON SINGLE AND MULTIPLE NONLINEAR PROFILES

by

SHIH-HSIUNG CHOU

B.A., Tung-Hai University, 2001
M.S., National Taipei University of Technology, 2003

AN ABSTRACT OF A DISSERTATION

submitted in partial fulfillment of the requirements for the degree

DOCTOR OF PHILOSOPHY

Department of Industrial and Manufacturing Systems Engineering
College of Engineering

KANSAS STATE UNIVERSITY
Manhattan, Kansas

2014

Abstract

Profile analysis has drawn attention in quality engineering applications due to the growing use of sensors and information technologies. Unlike the conventional quality characteristics of interest, a profile is formed functionally dependent on one or more explanatory variables. A single profile may contain hundred or thousand data points. The conventional charting tools cannot handle such high dimensional datasets. In this dissertation, six unsolved issues are investigated. First, Chang and Yadama's method (2010) shows competitive results in nonlinear profile monitoring. However, the effectiveness of removing noise from given nonlinear profile by using B-splines fitting with and without wavelet transformation is unclear. Second, many researches dealt with profile analysis problem considering whether profile shape change only or variance change only. Those methods cannot identify whether the process is out-of-control due to mean or variance shift. Third, methods dealing with detecting profile shape change always assume that a gold standard profile exists. The existing profile shape change detecting methods are hard to be implemented directly. Fourth, multiple nonlinear profiles situation may exist in real world applications, so that conventional single profile analysis methods may result in high false alarm rate when dealing multiple profile scenario. Fifth, Multiple nonlinear profiles situation may be also happened in designs of experiment. In a conventional experimental design, the response variable is usually considered a single value or a vector. The conventional approach cannot deal with when the format of the response factor as multiple nonlinear profiles. Finally, profile fault diagnosis is an important step after detecting out-of-control signal. However, current approaches will lead to large number of combinations if the number of sections is too large.

The organization of this dissertation is as following. Chapter 1 introduces the profile analysis, current solutions, and challenges; Chapter 2 to Chapter 4 explore the unsolved challenges in single profile analysis; Chapter 5 and Chapter 6 investigate multiple profiles issues in profile monitoring analysis and experimental design method. Chapter 7 proposed a novel high-dimensional diagnosis control chart to diagnose the cause of out-of-control signal via visualization aid. Finally, Chapter 8 summarizes the achievements and contributions of this research.

QUALITY ENGINEERING APPLICATIONS ON SINGLE AND MULTIPLE NONLINEAR PROFILES

by

SHIH-HSIUNG CHOU

B.A., Tung-Hai University, 2001
M.S., National Taipei University of Technology, 2003

A DISSERTATION

submitted in partial fulfillment of the requirements for the degree

DOCTOR OF PHILOSOPHY

Department of Industrial and Manufacturing Systems Engineering
College of Engineering

KANSAS STATE UNIVERSITY
Manhattan, Kansas

2014

Approved by:

Major Professor
Dr. Shing I Chang

Abstract

Profile analysis has drawn attention in quality engineering applications due to the growing use of sensors and information technologies. Unlike the conventional quality characteristics of interest, a profile is formed functionally dependent on one or more explanatory variables. A single profile may contain hundred or thousand data points. The conventional charting tools cannot handle such high dimensional datasets. In this dissertation, six unsolved issues are investigated. First, Chang and Yadama's method (2010) shows competitive results in nonlinear profile monitoring. However, the effectiveness of removing noise from given nonlinear profile by using B-splines fitting with and without wavelet transformation is unclear. Second, many researches dealt with profile analysis problem considering whether profile shape change only or variance change only. Those methods cannot identify whether the process is out-of-control due to mean or variance shift. Third, methods dealing with detecting profile shape change always assume that a gold standard profile exists. The existing profile shape change detecting methods are hard to be implemented directly. Fourth, multiple nonlinear profiles situation may exist in real world applications, so that conventional single profile analysis methods may result in high false alarm rate when dealing multiple profile scenario. Fifth, Multiple nonlinear profiles situation may be also happened in designs of experiment. In a conventional experimental design, the response variable is usually considered a single value or a vector. The conventional approach cannot deal with when the format of the response factor as multiple nonlinear profiles. Finally, profile fault diagnosis is an important step after detecting out-of-control signal. However, current approaches will lead to large number of combinations if the number of sections is too large.

The organization of this dissertation is as following. Chapter 1 introduce the profile analysis, current solutions, and challenges; Chapter 2 to Chapter 4 explore the unsolved challenges in single profile analysis; Chapter 5 and Chapter 6 investigate multiple profiles issues in profile monitoring analysis and experimental design method. Chapter 7 proposed a novel high-dimensional diagnosis control chart to diagnose the cause of out-of-control signal via visualization aid. Finally, Chapter 8 summarizes the achievements and contributions of this research.

Table of Contents

List of Figures xi

List of Tables xv

Acknowledgements xvi

Chapter 1 Introduction 1

1.1 Introduction of Quality Engineering Applications on Profile Analysis 1

1.2 Current Process Monitoring Methods in Profile Analysis 5

1.3 Challenges in Profile Analysis 7

1.3 Objectives and Scope of this Research 9

1.4 The Contribution of this Research 11

References 12

Chapter 2 A Study of Using Wavelet Transformation and B-Spline Approximation for Nonlinear Profiles Monitoring 14

Abstract 14

2.1 Introduction 15

2.2 Background of Wavelet Transformation and B-Spline Approximations 16

2.2.1 Wavelet Transformation 16

2.2.2 B-Spline Approximation 17

2.2.3 Chang and Yadama's Work 18

2.3 Methodology 18

2.4 Experimental Result and Analysis 19

2.4.1 Simple Profile Case 19

2.4.2 Complex Profile Case 20

2.5 Conclusions and Future Study 20

References 22

Chapter 3 Detecting and Diagnosing Shape and Variation Changes in Nonlinear Profiles 24

Abstract 24

3.1 Introduction 25

3.2 Background of Wavelet Transformation and B-Spline Approximations 27

3.2.1 Wavelet Transformation 27
3.2.2 B-Spline Approximation 28
3.2.3 Chang and Yadama's Work 28
3.2.4 Levene Transformation 29
3.3 The Proposed Methodology 29
3.3.1 Phase II Process 29
3.4 Experimental Design 30
3.4.1 Profile Function 31
3.4.2 Types of Shape Change 32
3.4.3 Variance Change 32
3.4.4 Mixture 33
3.5 Simulation Results and Discussion 33
3.5.1 Case of Shape Change Only 34
3.5.2 Case of Variation Change Only 34
3.5.3 Case of Mixture Situations 34
3.6 Conclusions and Future Study 35
References 35
Chapter 4 Monitoring Waveform Profiles with No Gold Standard Reference 37
Abstract 37
4.1 Process Description 38
4.2 Data Collection 42
4.2.1 The Proposed Framework 43
4.2.2 Fast Fourier Transformation Component 44
4.2.3 Clustering Component 46
Partition Around Medoids (PAM) 48
4.2.4 Classifier Component 49
4.2.5 Dimension Reduction Component 50
4.2.6 Control Chart Component 51
4.3 Experimental Design 52
Data 53
Domain 53

Clustering 53
SVM Classifier Kernel Function (if clustering method is applied) 53
Dimension Reduction 53
Control Chart 53
Performance Comparison 53
4.4 Performance Comparison 54
4.5 Analyses and Interpretations 55
4.5.1 Phase I Process 55
4.5.2 Phase II Process 59
4.6 Conclusions and Recommendations 60
Reference 62
Chapter 5 On Monitoring of Multiple Non-linear Profiles 65
Abstract 65
5.1 Introduction 66
5.2 The Proposed Methods 70
5.2.1 Modified Chang and Yadama's Method 70
5.2.2 Multivariate EWMA Control Chart 72
Method I: One Chart for All Profiles and One Segment per Profile 72
Method II: One Chart for All Profiles and Multiple Segments per Profile 73
5.3 A Simulation Study 73
5.4 Experimental Design 75
5.4.1 Only the shape of either profile A or B is shifted 76
Scenario 1: The shape of profile A shifts entirely and the shape of profile B unchanged 76
Scenario 2: The shape of profile B shifts partially and the shape of profile A unchanged 77
5.4.2 Shapes of both profiles are shifted 77
Scenario 3: Shapes of both profiles A and B are shifted entirely 77
Scenario 4: Shapes of both profiles A and B are partially changed 77
Scenario 5: Shape of profile A is shifted entirely and the shape of profile B is shifted partially 78
5.5 Simulation Results and Discussion 79

5.6 A Case Study: a Curing Process of High-Pressure Hose Products 81
5.7 Conclusion and Future Study 84
Reference 86
Appendix 89
Chapter 6 Optimizing Cellulosic Biomass Pellets Quality via Multiple Temperature Profiles using PCA and Desirability Functions 92
Abstract 92
6.1 Introduction 93
6.2 Experiment Details 94
6.2.1 Experiment Setup 95
6.2.2 Design of Experiments 96
6.2.3 Input Variables of the Experiment 97
Pelleting Pressure (PSI) 97
Ultrasonic Power (%UVA) 97
Biomass Pellet Weight 98
6.2.4 Measurements of Response Variables 98
Measurement of Pellet Density 99
Measurement of Pellet Durability 99
Measurement of Temperature Profiles 100
6.3 Methodology 100
6.3.1 Principal Component Analysis (PCA) 101
6.3.2 Desirability Functions 102
6.4 Experimental Results and Discussion 103
6.5 Conclusion and Future Study 107
Reference 108
Appendix 110
Chapter 7 A Visualization Decision Support Tool for Multivariate SPC Diagnosis using Marginal CUSUM Glyphs 113
Abstract 113
7.1 Introduction 114
7.2 Background 118

7.2.1 Trellis Displays 118
7.2.2 Star Glyphs 119
7.2.3 Standardized Two-Side Univariate CUSUM (SD2CUSUM) 120
7.2.4 The Multivariate CUSUM Chart 122
7.3 The Proposed Marginal CUSUM Glyphs 123
7.3.1 An Example to Demonstrate the Use of the Proposed Method 125
To Determine Which Variables Contribute to the Out-of-control Signal 126
7.4 A Simulation Study 130
Magnitude of h 130
Number of Dimensions 131
Number of Dimensions Shifted 131
Types of Correlation-Coefficient Structure 131
7.4.1 Simulation Results and Discussions 131
7.5 Conclusions and Future Study 139
References 141
Chapter 8 Conclusions 143
8.1 Summaries and Conclusions of this Research 143
8.2 Future Study 145
References 145

List of Figures

Figure 1.1 Vertical density profile (adapted from Walker and Write, 2002) 2
Figure 1.2 Schematic diagram of monitoring vertical density profiles of wood board manufacturing process. 3
Figure 1.3 One example of Noorossana et al.'s study (adapted from Noorossana *et al.,* 2010)..... 4
Figure 1.4 One air temperature and pressure profile of the curing process of high-pressure hose product. 5
Figure 1.5 Research map of this dissertation 10
Figure 2.1 Two Functions of True Profile. 19
Figure 2.2 (a) Boxplot of Simple Profile with Low, Medium, and High Signal-to-Noise Ratio; (b) Boxplot of Complex Profile with Low, Medium, and High Signal-to-Noise Ratio. 21
Figure 3.1 (a) Simple profile without noise; (b) Simple profile with noise which follows normal distribution with mean 0 and stand deviation 0.1; (c) Three different types of magnitude change; (c) Three types of phase shift. 31
Figure 3.2 (a) Variance changed in the entire profile, (b) Variance changed in half of profile, and (c) An example of mixture change—magnitude shape change with variance changed on the half of a profile.. 33
Figure 4.1 Steps of curing process for high-pressure hose products. 40
Figure 4.2 A schematic diagram of vulcanizer. 40
Figure 4.3 An example of condensation water temperature profile.. 41
Figure 4.4 Example of three in-control condensation water profiles.. 41
Figure 4.5 The proposed framework for condensation water temperature monitoring. 44
Figure 4.6 Condensation water temperature profile 15 in (a) time domain and (b) frequency domain.. 46
Figure 4.7 Profile 5 and 15 in frequency domain. 47
Figure 4.8 PAM algorithm.. 49
Figure 4.9 The experimental design of the proposed SPC implementation framework for the condensation water temperature profiles. 53
Figure 4.10 Six abnormal condensation water temperature profiles in phase II process (thick solid line: abnormal profiles; thin dot lines: overall 146 in-control profiles)...................... 54

Figure 4.11 A confusion matrix for positive and negative tuples (adapted from Han et al., 2006). 55
Figure 4.12 Bar chart of the four dimension reduction methods and their average false alarm rates. 57
Figure 4.13 The IX chart of 146 in-control waveform profiles in phase I process using FFT+BS method. 57
Figure 4.14 The IX charts of 146 in-control waveform profiles in phase I process for each cluster using FFT+PAM+BS method. 58
Figure 4.15 The IX charts of 146 in-control waveform profiles in phase I process for each cluster using FFT+PAM+ED. 58
Figure 4.16 The IX charts of Cluster 1 using FFT+PAM+BS and FFT+PAM+ED with out-of-control points removed in constructing phase I process. 58
Figure 5.1 Overall air temperature and pressure profiles from the curing process of high-pressure hose products. 69
Figure 5.2 Procedure of Chang and Yadama's Method. 71
Figure 5.3 Procedure of Modified Chang and Yadama's Method 71
Figure 5.4 An example of 25-pair in-control profiles. 75
Figure 5.5 Design of experiment of simulation study 76
Figure 5.6 Scenarios of simulation study, (a) entire Profile A shifted only; (b) partial Profile B shifted only; (c) both Profile A and Profile B shifted entirely; (d) both Profile A and Profile B changed partially; (e) entire Profile A changed and partial Profile B changed. 78
Figure 5.7 Abnormal (a) temperature profiles and (b) pressure profiles superimposed on in-control profiles. 82
Figure 5.8 The phase I process MEWMA control charts of curing process of high-pressure hose products using (a) method I and (b) method II. 83
Figure 5.9 Phase I control charts of the curing process using the hybrid method. 84
Figure 6.1 The schematic UV-A machine setup. 96
Figure 6.2 Six locations of placing thermocouples in the (a) side view and (b) top view of the mold. 96
Figure 6.3 Temperature profiles recorded from six-location of the mold during the pelleting process with various input setting. 100

Figure 6.4 Contour plot of density, durability, BC, BS, MC, MS, TC, and TS.......................... 104
Figure 6.5 The desirability functions result for density and durability of biomass pellets......... 105
Figure 6.6 The desirability functions result for the temperature profiles 105
Figure 6.7 Regression analysis of density versus six-location temperature profiles. 106
Figure 6.8 Regression analysis of durability versus six-location temperature profiles. 107
Figure 7.1 (a) The Example of the Mosaicplot for 2009 Automobile Dataset; (b) The Example of the Scatter Plot Matrix for the Three-Dimensional Dataset... 115
Figure 7.2 (a) An Simple Example of 5 observations, 3-dimensional dataset; (b) Example of 100 observations, 20-dimensional dataset with one step mean shift. 116
Figure 7.3 A Trellis displays of the Oats data. 119
Figure 7.4. Examples of Star glyphs where (f) Represents the Legend..................................... 120
Figure 7.5. An Example of the CUSUM Chart. The first 25 dataset was generated from $N(10,1^2)$, while the rest 5 dataset was from $N(12,1^2)$. 121
Figure 7.6 Pseudocode of Procedure of Tabular CUSUM 122
Figure 7.7. The scatter plot of the given example... 127
Figure 7.8. MCUSUM control chart of the given example. 127
Figure 7.9. The CMCUSUM glyphs of the given example with c=0. 129
Figure 7.10. The CMCUSUM glyphs of the given example with c=3. 129
Figure 7.11. Experimental design of the proposed method at different types of h. 130
Figure 7.12.Performance statistics for small level of number of dimensions shifted with (a) ρ=0, (b) ρ=0.5, and (c) ρ=0.9 under different h. The y axes of plots (1) to (4) are correct classification percentage, average absolute value of deviation, type I error rate in percentage, and type II error rate in percentage, respectively. The x axis represents the numbers dimension for last-in-control location. 134
Figure 7.13. Performance statistics for medium level of number of dimensions shifted with (a) ρ=0, (b) ρ=0.5, and (c) ρ=0.9 under different h. The y axes of plots (1) to (4) are correct classification percentage, average absolute value of deviation, type I error rate in percentage, and type II error rate in percentage, respectively. The x axis represents the numbers dimension for last-in-control location. 135
Figure 7.14. Performance statistics for large level of number of dimensions shifted with (a) ρ=0, (b) ρ=0.5, and (c) ρ=0.9 under different h. The y axes of plots (1) to (3) are correct

classification percentage, average absolute value of deviation, and type II error rate in percentage, respectively. The x axis represents the numbers dimension for last-in-control location. 136
Figure 7.15. Simulation results of small number of dimensions shifted. 137
Figure 7.16. Simulation results of medium number of dimensions shifted. 137
Figure 7.17. Simulation results of large number of dimensions shifted. 137

List of Tables

Table 2.1 Average MSE of B-Spline and B-Spline with Wavelet for Simple Profile.................. 20
Table 2.2 Average MSE of B-Spline and B-Spline with Wavelet for Complex Profile 20
Table 3.1 Simulation results for the case of shape change only. 34
Table 4.1 Clustering methods examined in this study. 48
Table 4.2 Performance results of the experiment for phase I data... 56
Table 4.3 Performance results of the experiment for phase II data 60
Table 5.1 The smallest ARL_1 method I method II under different correlation structures in all scenarios. 79
Table 6.1 Scheme of the input variables studied in the experiment. 97
Table 6.2 Summary of first five PC scores 102
Table 7.1 Chosen value of *k* and *h* with different kinds of dimension *p* under two in-control ARLs. 123
Table 7.2. 5-dimensional, 20 observations dataset. 127
Table 7.3. The result of two-side standardized CUSUM for the given example. 128
Table 7.4. Simulation results of small number of dimensions shifted. 137
Table 7.5. Simulation results of medium number of dimensions shifted. 137
Table 7.6. Simulation results of large number of dimensions shifted. 137

Acknowledgements

I would like to thank my committees, Dr. Lee, Dr. Hsu, and Dr. Wang. During my Ph.D study, they helped me develop knowledge that I could apply to my dissertation. Also, they gave me a lot of valuable suggestions so that my dissertation can be better. I would like to thank Dr. Wu, who is also my committee and my supervisor when I was the System Administrator of IMSE Department at Kanas State University. Dr. Wu taught me a lot of skills in Linux system, networking, and researches principles. Many thanks to my advisor and my brother in Christ, Dr. Shing I Chang. He not only gave many advises in my researches, but also taught me God's words of the Bible.

There are too many people that I would like to give my thanks as well. First, my family, they raise me and support me and love me. And I love them very much. In addition, many thanks to my brothers and sisters in Christ—Helen, Yufan, Xiaochuan, Hongzhou, Fuhua, Jingpen, Pastor Shih, Pastor Mao, Pastor Ko, Cindy, Xuming, Kanglin, Huang Ning, Honwang, Xiyang, Eric, Zoe, Jingya, Chih-Ching, Xiaojing, Qingling, Ross, Marci, and Hsun. Special thanks to Tiffany Wang, she led me to Jesus Christ and gave me my first Bible. May God bless them all. I would like to give thanks to people in IMSE Department and other departments—Dr. Kramer, Dr. Pei, Dr. Lei, Dr. Rys, Dr. Ben-Arieh, Dr. Easton, Dr. Heier Stamm, Dr. Cong, Dr. Zheng, Dr. Tsai, Dr. Yusiang Lin, Dr. Dennis Lin, Vicky, Doris, and Luke.

Thanks to my wife and daughter, Chih-Chieh and Anya, they gave me love and support. I really love them. Finally, I would like to thank God. He love me and give me salvation. The following is the verse that God gave to me when I first believed.

Isaiah 41:10

Fear thou not, for I am with thee;
be not dismayed, for I am thy God:
I will strengthen thee; yea, I will help thee;
yea, I will uphold thee with the right hand of my righteousness.

Chapter 1 Introduction

1.1 Introduction of Quality Engineering Applications on Profile Analysis

Quality engineering applications can be found in many fields, such as, organization strategy, manufacturing process, distribution, transportation, financial services, healthcare, government process (Montgomery 2009), bioinformatics (Zhang et al. 2004), or software developing ("ISO/IEC 9126-1:2001", 2013). In each field, the quality characteristics of interest may vary. For example, quality characteristics may include: the percentage of reducing customer resolution cycle time in organization strategy; temperature data recording over time for each product in high pressure hose products manufacturing process; percentage of a product remaining in a store before next shipping in distribution field; statistics of shipment in transportation field; statistics of on-time payment of credit card in financial services field; or a particular disease incidence rate in healthcare field.

Most quality characteristics of interest may consider only one measurement in a variable (univariate) or in several related variables (multivariate) during a process monitoring. However, with the growing use of sensors during a manufacturing process, a single measurement on a product may contain a set of hundred or thousand data points. Such a set of values is called a profile. Montgomery (2009) defines the profile monitoring as "*Profiles occur when a critical-to-quality characteristic is functionally dependent on one or more explanatory, or independent, variables. Thus, instead of observing a single measurement on each unit or product we observe a set of values over a range, when plotted, takes the shape of a curve. That is, there is a response variable y and one or more explanatory variables* $x_1, x_2, \ldots, x_k$ *and the situation is like regression analysis*". Such profile monitoring analysis is called single profile monitoring analysis.

Examples of single profile monitoring analysis can be found in the following applications: the stamping tonnage data over time within a cycle examined by Jin and Shi (1999); a calibration issue during the etch step of the semiconductor manufacturing process introduced by Kang and Albin (2000); the vertical density of wood board data over depth across the thickness of a section of the wood board studied by Walker and Wright (2002); the monitoring stability of a calibration process in order to assure its accuracy studied by Chang and Gan (2006); the pressing force profile signals in a valve seat assembly operation presented by

Paynabar and Jin (2011); the temperature data over time recording from a curing process for high-pressure hose products investigated by Chang et al. (2012).

Considering Walker and Write's (2002) study for example, they considered vertical density data collected by a laser device from the wood board manufacturing process. Each wood board was combined a particleboard and a medium density fiberboard. The data of measurement was the vertical density and its associated depth across the thickness of a section of the wood board (2×2 inch). The shape of the profile is like a bathtub. One of the vertical density profiles is shown in Figure 1.1. The x-axis is the depth while the y-axis records the density. Moreover, Figure 1.2 shows the schematic diagram of monitoring vertical density profiles of wood board manufacturing process. The objective of monitoring was to maintain the stability of the process, so that each vertical density profile would be statistically identical. The first four profiles can be deemed in-control profiles while the last two profiles are out-of-control.

Figure 1.1 Vertical density profile (adapted from Walker and Write, 2002)

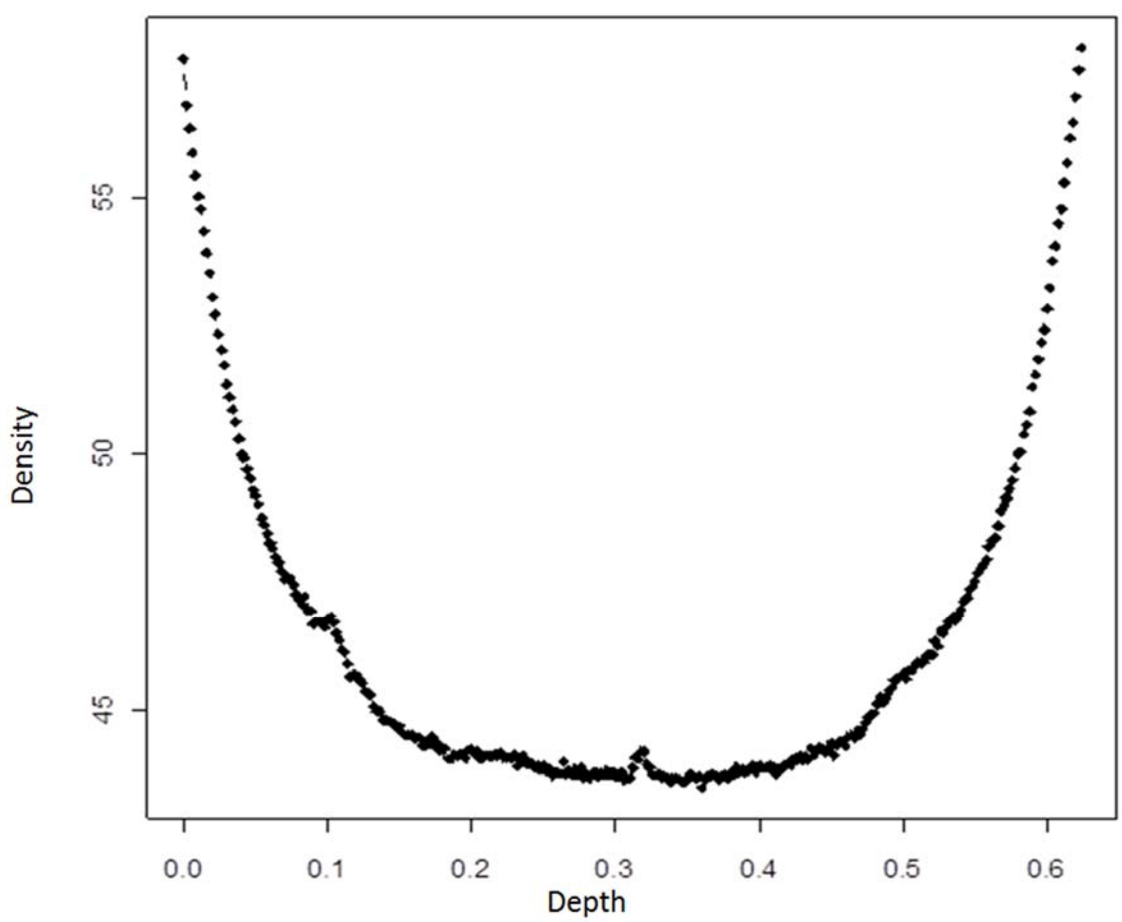

Figure 1.2 Schematic diagram of monitoring vertical density profiles of wood board manufacturing process.

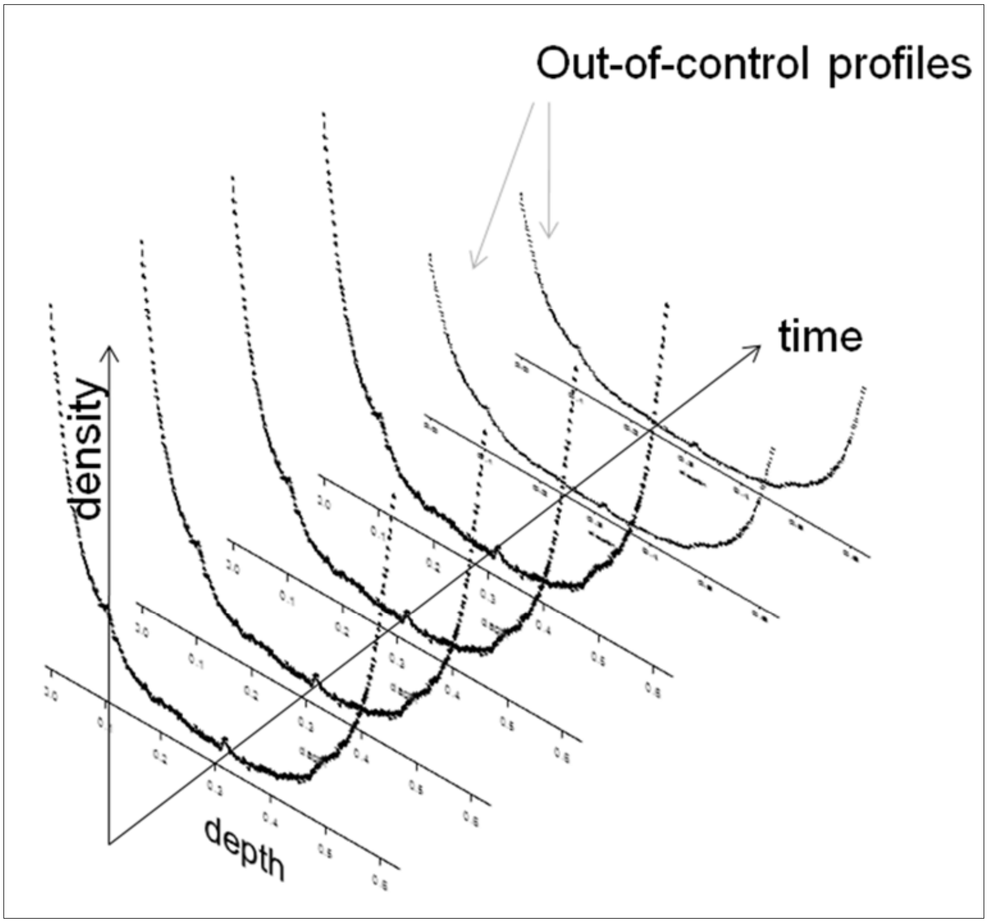

Other than the single profile monitoring analysis, multiple profiles monitoring analysis is also studied in this research. Unlike a single profile, monitoring a set of data points that collected from a process or system can be characterized by two or more profiles in a process monitoring is called multiple profiles monitoring analysis. In other words, each observation contains more than one type of profiles during the monitoring. Noorossana *et al.* (2010) showed an example of a multiple linear profiles: a calibration application between desired force and the real force produced by 1600-ton hydraulic press machine. The machine controlled by a programmable logic controller (PLC) consists of a set of cylinders, pistons and hydraulic pipe. The input variable of the machine known as the desired force or nominal force is given by a motor placed on the top of machine. The output variables (four real forces) collected from four cylinders of the press machine were measured by the PLC. One example of Noorossana *et al.'s* (2010) study is shown in Figure 1.3. Four response variables are considered as correlated linear profiles, and the shapes of four profiles are highly similar. Note that, the ideal output force is expected to be identical to the input force.

Figure 1.3 One example of Noorossana et al.'s study (adapted from Noorossana *et al.,* 2010)

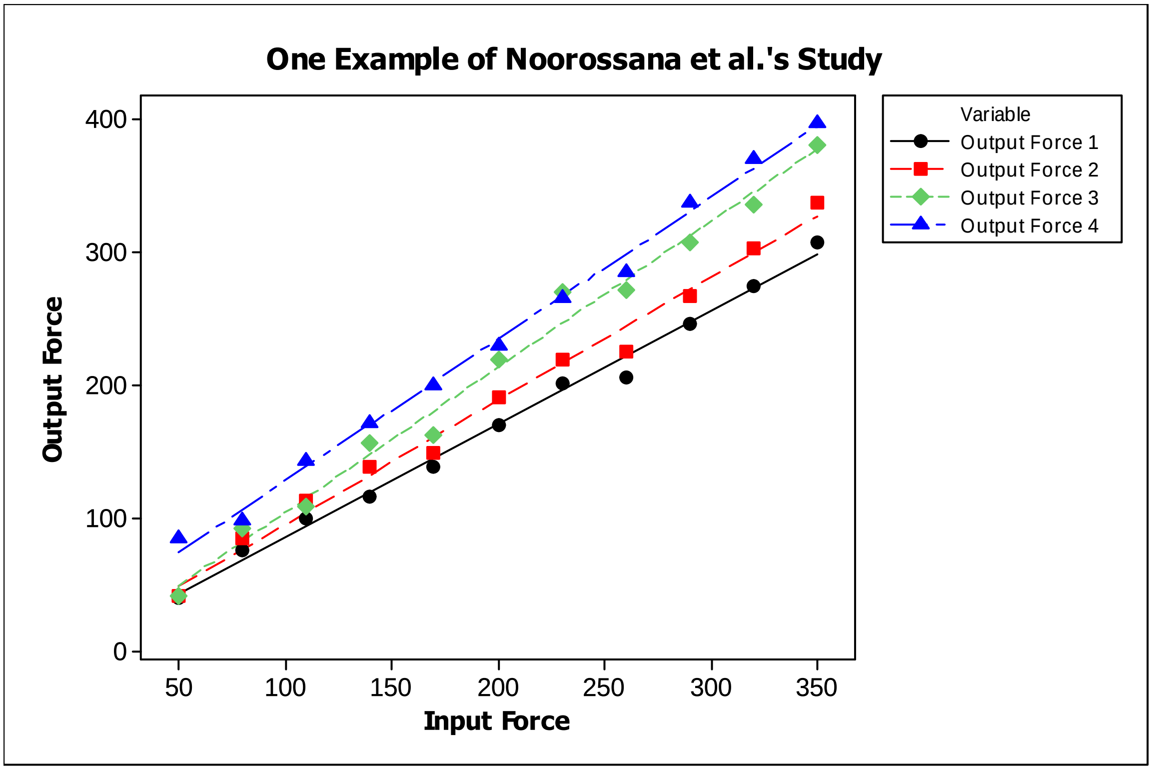

Another example of multiple profiles can be found in a curing process of high-pressure hose products manufacturing. This kind of hose product is wrapped by layers of rubbers and metal wires, which is required to be loaded and cured in an autoclave or vulcanizer as its final step to activate cross-linking reaction (Hoster et al., 2009). In the vulcanizer, there are several sensors in different locations of the chamber for monitoring air temperature, condensation water temperature, and chamber pressure. More details of products' manufacturing process refer to Chang et al. (2012). Figure 1.4 shows an example of air temperature and pressure profile of the curing process of high-pressure hose product. From the Figure 1.4, the temperature and pressure profile is highly correlated nonlinear multiple profiles. Unlike Noorossana *et al.'s* (2010) application, the temperature and pressure profile should be highly correlated instead of identical.

Figure 1.4 One air temperature and pressure profile of the curing process of high-pressure hose product.

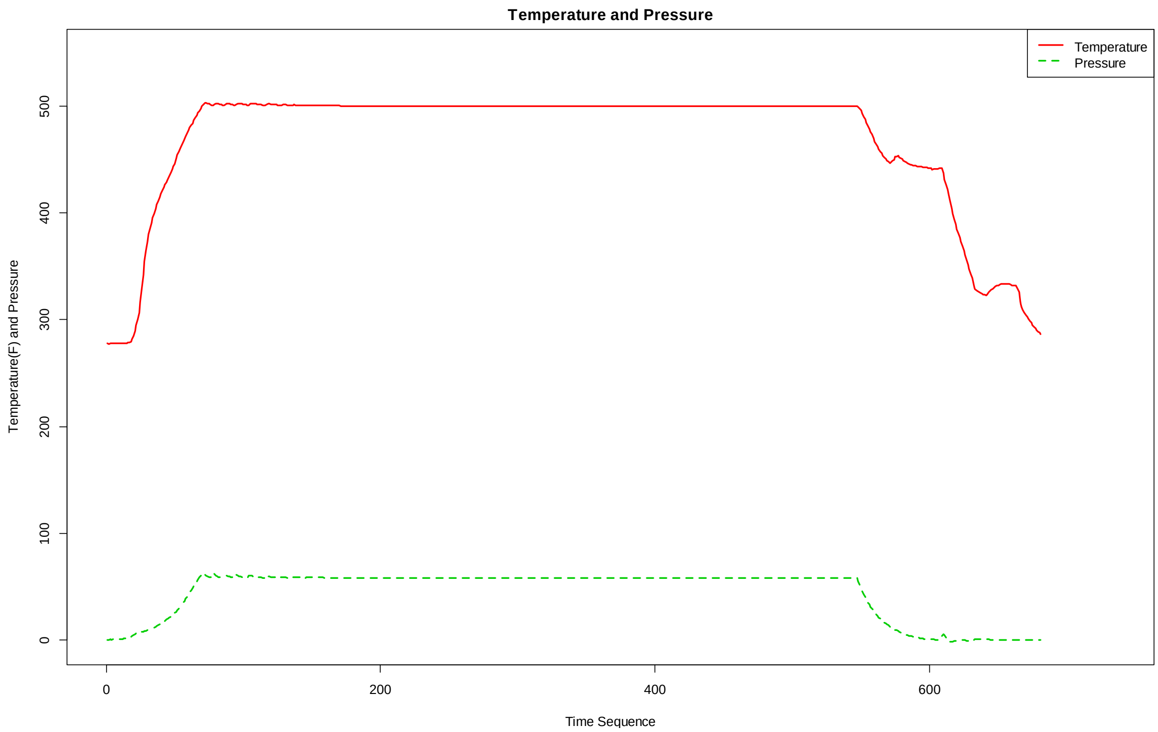

1.2 Current Process Monitoring Methods in Profile Analysis

Methodologies that deal with single profile monitoring problem can be categorized into two aspects according to Woodall (2007), linear and nonlinear profile with regard to profile shape. To deal with linear profile problem, many studies monitored parameters of the linear regression model, such as, intercept or slope parameter. For example, Kang and Albin (2000) used the Hotelling's T^2 control chart as first method to detect abnormal profiles by monitoring slope and intercept parameters. They also monitored average residuals between sample profiles and reference profile followed by EWMA and R chart as their second proposed method. Kim *et al.* (2003) monitored slope, intercept, and the variance of deviation between samples and regression line simultaneously by their proposed three univariate EWMA charts. Since this research is focus on nonlinear profile monitoring analysis, more details regarding linear profile analysis methods please refer to Noorossana et al. (2011).

To deal with nonlinear profile analysis problem, Woodall (2007) categorized this problem into four types. (1) applying multiple and polynomial regression (Zou et al., 2007; Kazemzadeh et al. 2008; Mahmoud 2008); (2) applying nonlinear regression models (Ding et al., 2006; Williams et al., 2007; Shiau et al., 2009; Chang and Yadama 2010; Chen and Nembhard 2011); (3) use of mixed models (Jensen et al., 2008; Jensen and Birch, 2009; Qiu et al., 2010; Paynabar and Jin, 2011); and (4) use of wavelets (Reis and Saraiva, 2006; Zhou et al., 2006; Chicken et al., 2009). This research will focus on Chang and Yadama's (2010) method in the latter chapter because of the following reasons. First, their method can detect an out-of-control profile under the desirable false alarm rate; second, unlike parametric models, the method allow user to isolate the caused section within the out-of-control profile. Detail of other approaches to monitor the process stability can be found in Woodall (2007) and Noorossana *et al.* (2011).

The methods introduced above focus on shape change only. In other words, those methods will deem a profile as an out-of-control profile when the profile shape is changed. However, it is possible that the variation of profiles is not stable. Paynabar and Jin (2011) investigated profiles' variation in the application of a valve seat pressing operation, an engine head assembly process. They proposed a framework to detect the process variation between profiles. Their method first used the discrete wavelet transformation to reduce the dimensions, followed by estimating random-effect coefficients for profile variations. Then a likelihood ratio test (LRT)-based change-point model is used for clustering profiles, so that the model estimation may become more accurate. Finally, the log likelihood ratio is generated as the statistic to determine if variation change occurs or not. Although their method successfully detect the profile variation change, it is difficult for their method to isolate whether the shape and variance are changed at the same time. This research will discuss this challenge in the Chapter 3.

With regard to dealing with multiple profiles, very few researches have worked on this problem. As mentioned in the 1.1 section of this chapter, Noorossana et al. (2010) investigated four multiple linear profiles simultaneously generated from a 1600-ton hydraulic press machine. They proposed a multivariate simple linear profile model to generate parameters, such as, intercept and slope. Then those parameters were used as plotting statistics in their three proposed approaches. The three approaches are: (1) the use of single multivariate exponentially weighted moving average (MEWMA) control chart to monitor all parameters ($\hat{\beta}$); (2) combining MEWMA and chi-square control chart to monitor the difference between observations and reference profiles as well as their variability, which very similar to X-bar and R chart in univariate case; (3) the use of three MEWMA control charts to monitor intercept, slope, and variability, simultaneously.

Although their proposed methods were promising of solving multiple linear profiles of the same type, their method cannot be applied to multiple correlated nonlinear profiles of different types.

1.3 Challenges in Profile Analysis

Methods dealing with profile analysis problems introduced above are promising in their problem domain. For example, assumption of mean or shape shifted only, variance shifted only, gold standard reference is existed, the application is formed a single profile, or formed linear profile. In real world, these assumptions may not be realistic. Furthermore, the models used may not be accurate. For example, the bathtub shape profile that generated from wood board manufacturing profile is a nonlinear profile. It is not suitable to apply a simple linear regression model to the profile. Therefore, those methods may not be adequate if the underlining assumptions no longer exist.

A list of unsolved challenges or possible issues for improvement in profile analysis discussed above is summarized here:

1. Chang and Yadama's (2010) method showed competitive results to detect an out-of-control profile under the desirable false alarm rate. Also, their method is adequate to detect the cause section of the out-of-control profile that contribute the out-of-control signal that deemed by the Hotelling's T^2 control chart. Their proposed method consists of three components, wavelet transformation, B-splines fitting, and the Hotelling's T^2 control chart. The role of the wavelet transformation is to decompose the original signal to mean and variance channel, so that the noise of the reconstructed signal along with all zero variance channel can be removed. However, the B-splines fitting may have the same capability of removing noise. In other words, the wavelet transformation maybe a redundant procedure for detecting profile shape change only situation.
2. Many researches dealt with profile analysis problem considering whether profile shape change only or variance change only. However, in the real world, it may happen at the same time. Methods detecting profile shape only cannot deal with variance change problem, and vice versa. Also, those methods cannot identify whether the process is out-of-control due to mean or variance shift.

3. Methods dealing with detecting profile shape change always assume that a gold standard profile exists. However, some applications may not have this underline assumption. For example, the condensation water temperature profile that collected from a high-pressure hose products manufacturing profess shows that no gold standard profile exists. Therefore, the existing profile shape change detecting methods are hard to be implemented directly.
4. Multiple nonlinear profiles situation may exist in real world applications, but very few researches dealt with this problem. Although Noorossana et al.'s (2010) method is a promising approach to handle the multiple linear profile problems, their method cannot be applied to the multiple nonlinear profiles situation. Other than Noorossana et al's approach, it is possible to monitor multiple nonlinear profiles using multiple univariate control charts simultaneously. However, this approach may result in high false alarm rate.
5. Multiple nonlinear profiles situation may be also happened in designs of experiment. In a conventional experimental design, the response variable is usually considered a single value or a vector. Very few studies considered the format of the response factor as multiple nonlinear profiles. In an application of cellulosic biomass pelleting process, the response factor is six temperature profiles recorded in six-location of each biomass pellet. Usually, the conventional approach is to use the highest temperature of each location as response factor results for experimental design analysis. However, the heat-up stage and steady-state of the temperature at each location is also important to the quality of biomass. The conventional approach can not quantify both heat-up stage and steady-state of temperature profiles.
6. One of the advantages of Chang and Yadama's (2010) method is that it can isolate the cause of section that contributed the out-of-control signal using Mason, Young and Tracy's (1995) MYT decomposition. However, MYT decomposition will lead to a very large number of combinations if the number of sections is too large. For example, three segments' profile will result 3!=6 combinations of decomposition of one T^2 value. Moreover, their method cannot be visualized. With this among of data set after running the MYT decomposition, it will be difficult for on-line operators to identify the contributor of out-of-control signal.

1.3 Objectives and Scope of this Research

A research map of this dissertation is shown in Figure 1.5. In order to provide solutions for the challenges and difficulties presented in the previous section, this dissertation presents potential solutions and improvements in each chapter. The following objectives and scope of this research provide an organization of this dissertation.

1. Chapter 2: To investigate the effectiveness of removing noise from given nonlinear profile by using B-splines fitting with and without wavelet transformation.
2. Chapter 3: To solve the situation when there is no underline assumption of profile shape change or variance change only situation. The proposed method should be able to isolate the cause of out-of-control signal due to shape or variance change or both.
3. Chapter 4: To deal with the situation when monitoring the process without the gold standard profile provided. And the proposed method should be able to monitor the real world case, condensation water temperature profiles generated from a curing process of high-pressure hose products manufacturing.
4. Chapter 5: To monitor process when the quality characteristics of interest are multiple nonlinear profiles. And the proposed method should be capable of detecting abnormal profiles in the real world case where air temperature and pressure profiles are two correlated nonlinear profiles collected from a curing process of high-pressure hose products manufacturing.
5. Chapter 6: To analyze the experimental design results when the response factor is no longer a single value or a vector, but a multiple nonlinear profiles.
6. Chapter 7: To provide a method not only can help profile analysis methods to identify which section of the profile contributes triggering out-of-control signal detected from a multivariate control chart, but also allow users to diagnose the causes of out-of-control signal through the visualization aid.
7. Chapter 8: To summarize the achievements and contributions of this research.

Figure 1.5 Research map of this dissertation

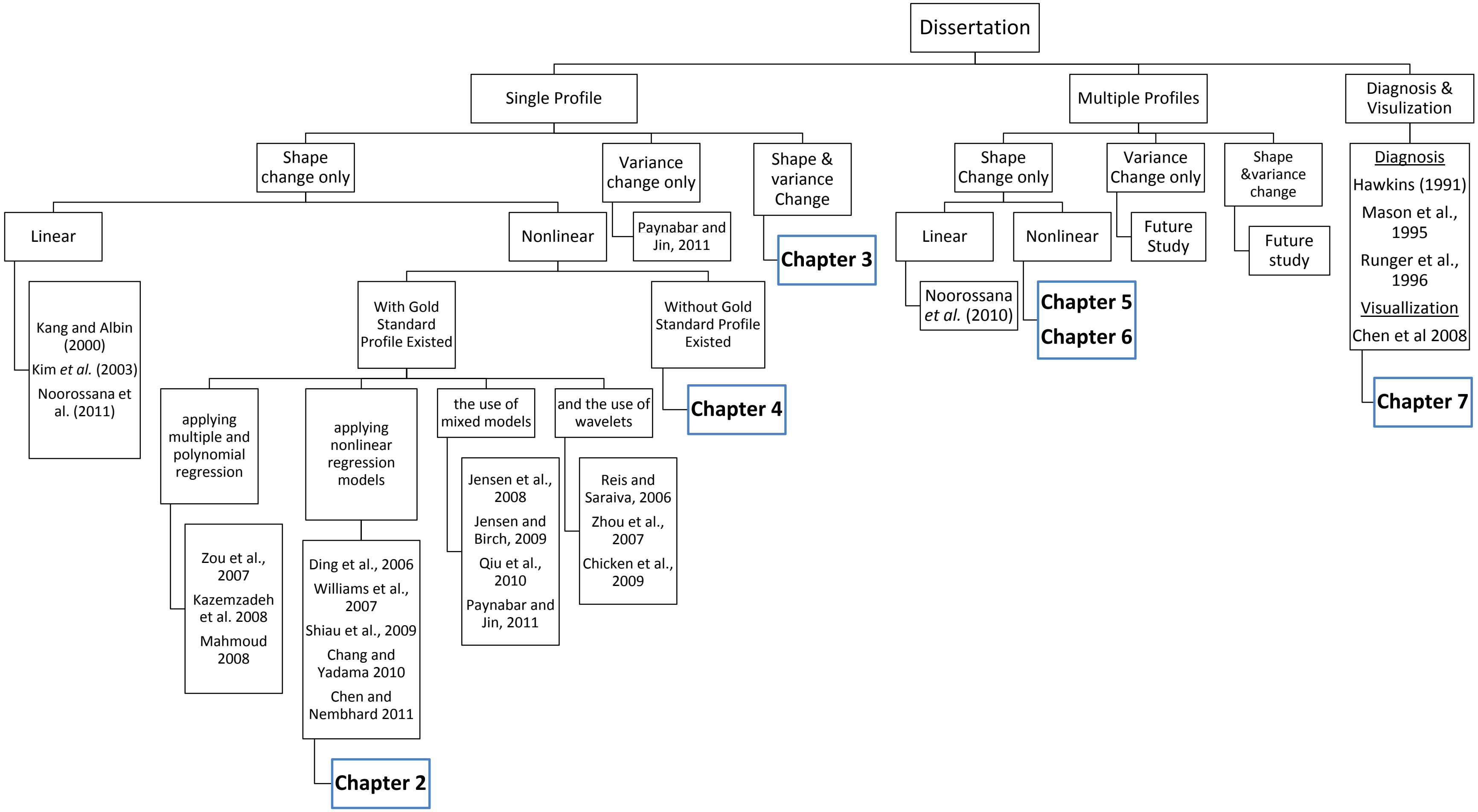

1.4 The Contribution of this Research

The contributions of this research can be listed as following:

1. This research shows the scientific evidence that the effectiveness of removing noise from the given nonlinear profile by using B-splines fitting with and without wavelet transformation has no significant difference. This evidence confirms that one can use B-splines fitting without applying wavelet transformation to the profile first if the profile shape monitoring is the only consideration; otherwise the wavelet transformation should be considered first for extracting profile variation information.
2. This research proposed a novel approach to isolate the cause of out-of-control signal due to shape or variance change or both. Specifically, the proposed method not only shows if the process is statistical stable but also indicates the contributor of out-of-control signal with regard to shape or variance or both.
3. This research succeeded in dealing with waveform profile with no gold standard profile exists. Moreover, the proposed method provides a competitive result of phase I process and the robust performance among other profile analysis methods.
4. This research proposed a novel approach to monitor a process when its quality characteristics of interest are multiple nonlinear profiles. Also, the proposed method is capable of monitoring the real world case in which two nonlinear correlated profiles are of interest, i.e., temperature and pressure profiles recorded from curing process of high pressure hose products manufacturing.
5. This research solved the problem of multiple nonlinear profiles as response factor in factorial design by using the proposed method. Also, this research showed the temperature profiles recorded from six-location of biomass pellet can be surrogate variables to the conventional ones, i.e., density and durability of the biomass pellets.
6. This research proposed a novel visualization aid for multiple profiles analysis diagnosis using marginal CUSUM glyphs. Not only the proposed method can show the given dataset, but also it can decompose out-of-control signals over time. In other words, it is capable of indicating when and which variables contributing to the cause.

References

Chang, S.I., Tsai, T.R., Lin, D.K.J., Chou, S.H., and Lin, Y.S. (2012). Statistical Process Control for Monitoring Nonlinear Profiles: A Six Sigma Project on Curing Process, *Quality Engineering*, 24:251-263.

Chang, T. C., Gan, F. F. (2006). Monitoring Linearity of Measurement Gauges. *Journal of Statistical Computation and Simulation*, 76(10): 889-911.

Chang, S.I. and Yadama, S. (2010). Statistical Process control for Monitoring Non-linear Profiles using Wavelet Filtering and B-Spline Approximation*, International Journal of Production Research*, 48(4), 1049-1068.

Chicken, E. Pignatiello, Jr., J., andSimpson, J.R. (2009) Statistical Process Monitoring of Nonlinear Profiles Using Wavelets, *Journal of Quality Technology*, 41(2), 198-212.

Chen, S. and Nembhard, H.B., (2011). A High-dimensional Control Chart for Profile Monitoring, *Quality and Reliability Engineering International*, 27(4), 451-464.

Ding, Y., Zeng, L., and Zhou, S. (2006). Phase I Analysis for Monitoring Nonlinear Profiles in Manufacturing Processes, *Journal of Quality Technology*, 38(3), 199-216.

Hoster, B., Jaunich, M., and Stark, W. (2009). Monitoring of the Vulcanisation Process by Ultrasound during Injection Moulding," *ndt.net*, 14(9), 1-9.

Jensen, W.A. and Birch, J.B. (2009). Profile Monitoring Via Nonlinear Mixed Models, *Journal of Quality Technology* 41(1), 18-34.

Jensen, W.A., Birch, J.B., and Woodall, W.H. (2008). Monitoring Correlation within Linear Profiles using Mixed Models, *Journal of Quality Technology*, 40(2), 167-183.

ISO/IEC 9126-1:2001. (2013). Retrieved September 9, 2013, from http://www.iso.org/iso/iso_catalogue/catalogue_tc/catalogue_detail.htm?csnumber=22749

Jin, J., and Shi, J. (1999). Feature-Preserving Data Compression of Stamping Tonnage Information Using Wavelets, *Technometrics* 41(4): 327–339.

Kang, L.; Albin, S. L. (2000). On-Line Monitoring when the Process Yields a Linear Profile, *Journal of Quality Technology*, 32(4): 418-426.

Kazemzadeh, R.B., Noorossana, R., Amiri, A. (2008). Phase I Monitoring of Polynomial Profiles, *Communications in Statistics—Theory and Methods*, 37(10), 1671-1686.

Mahmoud, M. A. (2008). Phase I Analysis of Multiple Regression Linear Profiles, *Communications in Statistics - Simulation and Computation*, 37(10), 2106-2130.

Mason, R. L., Tracy, N. D., and Young, J. C. (1995). Decomposition of T2 for multivariate control chart interpretation. *Journal of Quality Technology*, 27(2): 99-108.

Montgomery, D.C. (2009). *Introduction to statistical quality control*. New York, NY: John Wiley & Sons.

Noorossana, R, Eyvazian, M., Vaghefi, A. (2010). Phase II Monitoring of Multivariate Simple Linear Profiles, *Computers & Industrial Engineering*, 58, 563-570.

Noorossana, R., Saghaei, A., and Amiri, A. (2011). *Statistical Analysis of Profile Monitoring*, Hoboken, New Jersey: John Wiley & Sons, Inc.

Paynabar, K. and Jin, J. (2011). Characterization of Non-linear Profiles Variations using Mixed-effect Models and Wavelets, *IIE Transactions*, 43(4), 275-290.

Qiu, P., Zou, C. and Wang, Z. (2010). Nonparametric Profile Monitoring by Mixed Effects Modeling, *Technometrics*, Vol. 52(3):265-277.

Reis, M.S., SARAIVA, P.M. (2006). Multiscale Statistical Process Control of Paper Surface Profiles, *Quality Technology and Quantitative Management*, 3(3), 263-282.

Shiau, J.J.H., Huang, H.L., Lin, S.H., and Tsai, M.Y. (2009). Monitoring Nonlinear Profiles with Random Effects by Nonparametric Regression, *Communications in Statistics-Theory and Methods*, 38(10), 1664-1679.

Walker, E. and Wright, S. P. (2002). Comparing Curves Using Additive Models, *Journal of Quality Technology*, 34(1), 118-129.

Williams, J. D., Woodall, W. H., and Birch, J. B. (2007). Statistical Monitoring of Nonlinear Product and Process Quality Profiles, *Quality & Reliability Engineering International*, 23(7), 925-941.

Woodall, W.H. (2007). Current Research on Profile monitoring, *Produção* 17(3): 420-425.

Zhang, W., Shmulevich, I., and Astola, J. (2004). *Microarray Quality Control*, Hoboken, N.J.: Wiley-Liss.

Zhou, S.Y., Sun, B.C., and Shi, J.J. (2006). An SPC Monitoring System for Cycle-based Waveform Signals using Haar Transform. *IEEE Transactions on Automation Science and Engineering*, 3(1), 60- 72.

Zou, C.,Tsung, F., and Wang, Z. (2007). Monitoring General Linear Profiles Using Multivariate Exponentially Weighted Moving Average Schemes, *Technometrics*, 49(4), 395-408.

Chapter 2 A Study of Using Wavelet Transformation and B-Spline Approximation for Nonlinear Profiles Monitoring

Paper Title:
A Study of Using Wavelet Transformation and B-Spline Approximation for Nonlinear Profiles Monitoring

Published in:
Proceedings of the 2009 Industrial Engineering Research Conference (IERC). pp. 1567-1572, Miami, Florida, June, 2009.

Author's Name:
Dr. Shing I Chang and Shih-Hsiung Chou

Authors' Affiliations:
Department of Industrial and Manufacturing Systems Engineering
Kansas State University

Abstract

This research studies the effectiveness of wavelet transformation in nonlinear profiles monitoring. Wavelet filtering is applied to separate signals containing shape information from noise of a nonlinear profile. Then B-spline approximation is applied to the filtered profile to reduce dimensionality. In this study, we examine the performance of B-spline fitting with and without wavelet filtering. Two types of nonlinear profiles under three levels of noise were studied. Our preliminary simulation results show that there is no difference whether wavelet is used or not. In other words, B-spline approximation can be directly applied to a noisy profile without sacrificing detection power.

Keywords: Statistic Process Control, Wavelet Transformation, B-spline Approximation.

2.1 Introduction

Profile monitoring is a complicated topic in the Statistical Process Control. In many industrial applications, quality characteristics of process or product involve observations collected as a set of data points that forms a profile, waveform, or signature. For example, Jin and Shi (2001) monitor the torque produced by engine against engine speed in RPM. Gardner et al. (1997) measure pressure for a mass flow controller against the set points for flow. Walker and Wright (2002) study the vertical density against depth produced by a springboard.

Dealing with this high-dimensional data set (a profile data), researchers had been constructing control charts for either linear or nonlinear profiles. In linear profile cases, Kang and Albin (2000) combine the EWMA chart with R chart (EWMA-R chart) for Phase II linear profile monitoring. Kim et al. (2003) combine three EWMA charts for Phase II monitoring. They claim that their method could detect shifts faster than EWMA/R chart. Mahmoud and Woodall (2004) suggest an F-test approach using indicator (dummy) variables in a multiple regression model, and propose a likelihood ratio test for detecting changes in one or more regression parameters.

For nonlinear profile cases, Brill (2001) applies a T^2 monitoring approach by monitoring the estimated regression coefficients in the nonlinear regression model. Williams et al. (2007) fit a nonlinear regression to model the vertical density profiles (VDP) data. They compare three T^2 control charts using sample covariance matrix, successive differences, and intra-profile pooling as estimates of the covariance matrix to monitor the VDP data.

To monitor nonlinear profiles is difficult. One of the main challenges is to find a proper model with a reasonable number of unknown parameter to fit a complex profile. Jin and Shi (2001) propose a feature-preserving method that first compresses the stamping tonnage information. Then, they recommend the monitoring of changes in wavelet coefficients instead of extracting features to represent some specific faults. Bernadette and Jonathan (2005) review three approaches for analyzing the results of experimental design when the response is a curve. Three methods studied are parametric nonlinear pre-processing, pointwise functional regression, and B-spline transformation pre-processing. They conclude that the B-spline approach provides the best result amount of those three methods studied.

Chang and Yadama (2010) further combine wavelet transformation and B-spline for nonlinear profile monitoring. They apply discrete wavelet transformation to separate the original profile into feature and noise signal. Then B-spline plays the role to define the shape of a profile. They also suggest that users divide a profile into multiple segments and then calculate the distance difference statistic for each segment. This statistic can be monitored by any multivariate control chart, e.g. a Hotelling T^2 chart.

In this study we are interested in finding out whether wavelet filtering improves B-Spline fitting. The performance criterion is the mean square error between the fitted and the true models. Both simple and complex nonlinear profiles under three levels of noise are studied. In both cases 1000 simulated profiles with random noise are compared. The organization of this paper is listed as follows. Background of wavelet and B-spline will be introduced in next section followed by the methodology and performance criterion. Finally, the experimental results will be discussed and the conclusion will be made.

2.2 Background of Wavelet Transformation and B-Spline Approximations

2.2.1 Wavelet Transformation

Wavelet theory is a relatively new development in applied mathematics, although similar ideas and constructions took place as early as the nineteenth century. Much of early work on wavelets was closely tied to a particular application or traditional theoretical framework (Graps, 1995). The signal processing community started to pay attention to wavelet decomposition in 1989 when Daubechies and Mallat demonstrated the use of discrete signal processing instead of analog signal process via Fourier transformation (Daubechies, 1988; Mallat, 1989). Since then, a number of theoretical as well as practical contributions have been made on various aspects of wavelet decomposition. This subject is growing rapidly. The basic concept of the wavelet transformation is briefly summarized here base on Gilbert and Truong (1997).

From the viewpoint of the nonlinear profile, a function *f(t)* can often be described as a linear combination function:

$$f(t) = \sum_{j,k} a_{j,k} \psi_{j,k}(t) \tag{1}$$

where $a_{j,k}$ is called filter coefficient at decomposition level j and location k; t represents time; $\psi_{j,k}$ is the wavelet function which form an orthogonal basis, meaning ,

$$\langle \psi_k(t), \psi_l(t) \rangle = \int \psi_k(t) \psi_l(t) dt = 0\,, k \neq l \tag{2}$$

Typically, the wavelet function $\psi_{j,k}$ can be expressed by the following equation:

$$\psi_{\mathrm{j},k}(t) = \psi(2^j t - k) \tag{3}$$

Moreover, Mallat (1989) in his paper provided an algorithm to decompose a signal using discrete wavelet transform (DWT) by two channels, lowpass filter (moving average) and highpass filter (moving difference). This process is called downsampling or decimation. Then the nonlinear profile *f(t)* can be form as:

$$f(t) = \sum_{\mathrm{j},k} a_{\mathrm{j},k}\psi_{\mathrm{j},k}(t) = \sum_k a_{j-1,k}\psi_{j-1,k}(t) + \sum_k b_{j-1,k}\phi_{j-1,k}(t) \tag{4}$$

where $b_{j-1,k}$ is the scaling coefficient and $\phi_{j-1,k}(t)$ is scaling function at decomposition level j-1 and location *k.* In addition, the scaling function is also called approximation channel that catches the low frequency components, which also represent the shape of the given profile.

In this study, haar is the primary mother wavelet used in the wavelet transformation. Also, for implementation, wavelets package of R is using in this study. The function dwt() is the discrete wavelet transformation, and dw.filter("haar") states that haar as the mother wavelet for the dwt() function.

2.2.2 B-Spline Approximation

De Boor (2001) shows a *p*-degree B-Spline curve is defined by

$$\mathrm{C}(u) = \sum_{i=0}^{n} \mathrm{N}_{i,p}(u)P_i \quad 0 \le u \le 1 \tag{5}$$

where P_i are the control points, and $N_{i,p}(u)$ are the p^{th}-degree B-spline basis functions. The i^{th} basis function $N_{i,p}(u)$ is defined by

$$N_{i,p}(u) = \frac{u-u_i}{u_{i+p}-u_i} N_{i,p-1}(u) + \frac{u_{i+p+1}-u}{u_{i+p+1}-u_{i+1}} N_{i+1,p-1}(u) \tag{6}$$

where $N_{i,0}(u) = \begin{cases} 1 & if\ u_i \le u < u_{i+1} \\ 0 & otherwise \end{cases}$ and knot vectors is

$$U=\{\underbrace{0,\ldots,0}_{P+1}, u_{p+1}, \ldots, u_{M+p-1}, \underbrace{1,\ldots,1}_{P+1}\} \tag{7}$$

where $M=n+p+1$ and number of control point $=n$+1. Then cubic B-Spline used in Chang and Yadama (2010) can be specified as following form:

$$C_i(t) = \sum_{k=0}^{3} P_{i-3+k} u_{i-3+k}(t)\,;\, t \in [0,1] \tag{8}$$

where $C_i(t)$ is the i^{th} B-Spline segment and *P* is the set of knots. When the distance of each knots (or control points) is equal, the B-Spline is uniform. Then the uniform cubic B-Spline—the cubic B-spline with uniform knot-vector can be expressed the following matrix form, which is the most commonly used from B-spline.

$$C_i(t) = [t^3\ t^3\ t^3\ t]\frac{1}{6}\begin{bmatrix} -1 & 3 & -3 & 1 \\ 3 & -6 & 3 & 0 \\ -3 & 0 & 3 & 0 \\ 1 & 4 & 1 & 0 \end{bmatrix}\ t \in [0,1] \tag{9}$$

2.2.3 Chang and Yadama's Work

Chang and Yadama (2010) propose a process to monitor nonlinear profiles for identifying mean shifts or shape changes in a profile. The main idea is, first, to use discrete wavelet transform to decompose a profile by lowpass and highpass filtering as described in section 2.2. Then, reconstruction step reverses the process of decomposition by setting all wavelet coefficients in the detailed channels to zero. The output of this step is the shape signals without noise. Then the reconstructed signal is partitioned into various segments according to engineering knowledge. Within each segment, users choose a fix number of control points to generate a B-Spline to fit model, and each segment is applied fitted by a B-Spline. Users then calculate the distance vector d using the control point matrix that stores control points by each profile. After that, mean difference distance vector of each segment is computed. The Hotelling's T^2 statistics is then adopted on the vector statistics for process monitoring. Their simulation result shows the proposed method is capable of detecting and diagnosing shifts of profiles. In this study, we would like to explore the possibility of skipping the wavelet filtering stage. If the B-spline fitting is the same without using the wavelet transformation, then we can skip this step for monitoring profile shape changes.

2.3 Methodology

This section introduces a simulation to test B-Spline fitting with and without the wavelet filtering. Two functions—a simple profile and a complex profile are studied. The simple profile is $f(x)=\begin{cases} 5, \text{if } x \le 0.5 \\ 10, \text{if } x > 0.5 \end{cases}$ while the complex profile is : $y=sin^3(2\pi x^3)$. Each profile contains 512 data points. The error terms are assumed to be normally distributed. Three levels of signal-to-noise ratio to explored, SD(f)/ σ=2, 5, and 10, where SD(f) is $max(f)-min(f)$ and σ is the standard deviation of the error term, such that, $y=f(x)+\varepsilon$, where $\varepsilon \sim N(0,\sigma^2)$. Figure 2.1 demonstrates the true functions of (a) the simple and (b) the complex profile, as well as their simulated profiles at low signal-to-noise ratio ($SD(f)/\sigma$=10) ((c) and (d)), respectively. Moreover, the statistic Mean Square Error (MSE) is chosen as the performance measure. Specifically, a two-sample t test will be applied to test the hypothesis that the performance of the B-Spline with the wavelet filtering is the same as that without the filtering. The MSE is defined in equation (10)

$$\overline{MSE} = \frac{\sum_{j=1}^{m} MSE_j}{m}, \tag{10}$$

where $MSE_j = \frac{\sum_{i=1}^{n}(\hat{y}_i - y_i)^2}{n}$, m is the number of replications, (m=1000 in this study); y_i is the value of i^{th} data point from either simple or complex profile; $\hat{y}_i$ is the estimate of the i^{th} profile y_i; n is the number of data points in a profile. The simulation codes were written in R (2009) while the hypothesis tests were carried out in Minitab15 (2009).

Figure 2.1 Two Functions of True Profile.

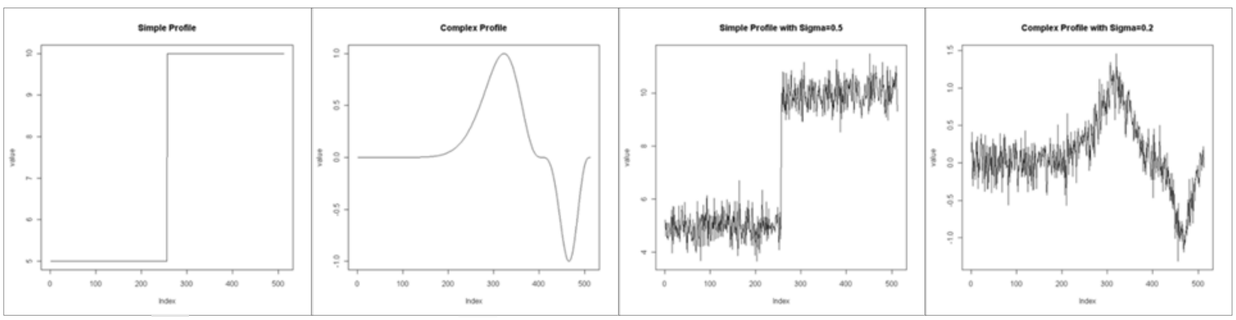

(a) (b) (c) (d)

2.4 Experimental Result and Analysis

We generate 1000 profiles for each function defined in the previous section. The average MSE values and their corresponding hypothesis testing results are provided in Table 2-1 and Table 2-2. A two sample t-test is conducted to test if there is a difference between the MSE of B-spline fitting on wavelet filtered profiles and that of B-spline fitting with the noisy profile.

2.4.1 Simple Profile Case

In this case, the results, in term of MSE, of both B-Spline and B-Spline with Wavelet filtering approximation model are showing in Table 2-1. Although the average MSE of B-Spline with Wavelet is slightly smaller than that of only B-Spline fitting, the t-test results showing large p-values suggests that we cannot reject the null hypothesis. In other words, there is no statistical difference between these two fitting approaches. The same conclusion can be made regardless of the noise level. Figure 2.2 (a) provides further evidences that the spread of the MSE distributions from these two B-spline fitting approaches are very similar.

Table 2-1 Average MSE of B-Spline and B-Spline with Wavelet for Simple Profile

	B-Spline only	B-Spline with Wavelet	P-Value
Low Noise Signal	0.2607128	0.2606352	0.235
Medium Noise Signal	0.2795273	0.2792172	0.235
High Noise Signal	0.4112292	0.4092905	0.235

2.4.2 Complex Profile Case

The simulated complex profile was generated by function $f(x)=sin^3(2\pi x^3)$ with error term that follows the Normal Distribution under three noise magnitudes. The computational results of average MSE of using B-Spline only and B-Spline with Wavelet are showing in Table 2-2 as well as two-sample *t*-test that examines the performance of these two approaches. Figure 2.2 (b) depicts three boxplots that show the dispersion of the MSE statistics. The conclusions that we made for the simple profile case can be extended to the complex profile case as well.

Table 2-2 Average MSE of B-Spline and B-Spline with Wavelet for Complex Profile

	B-Spline only	B-Spline with Wavelet	P-Value
Low Noise Signal	0.003142120	0.003140324	0.541
Medium Noise Signal	0.006152447	0.006113389	0.715
High Noise Signal	0.02722474	0.02692501	0.757

2.5 Conclusions and Future Study

In this study, we examine the effectiveness of wavelet filtering when the B-Spline fitting is used to approximate nonlinear profiles. B-Spline is capable of providing an effective estimating smooth function while the wavelet transformation can be used to reduce noise from a profile. Chang and Yadama (2010) have proposed to combine these two methods to improve profile monitoring. However, according to the experimental results in this study, B-spline fitting is effective without the help of wavelet filtering when the monitoring of profile changes is the only consideration. Therefore, we suggest that one can just use B-Spline approximation without applying wavelet filtering first. If variance changes also need to be considered, the wavelet decomposition will still useful to extract the variation change information. For the future studies, other situations such as variance shifts or mixture of both mean and variance shifts should be explored.

Figure 2.2 (a) Boxplot of Simple Profile with Low, Medium, and High Signal-to-Noise Ratio; (b) Boxplot of Complex Profile with Low, Medium, and High Signal-to-Noise Ratio.

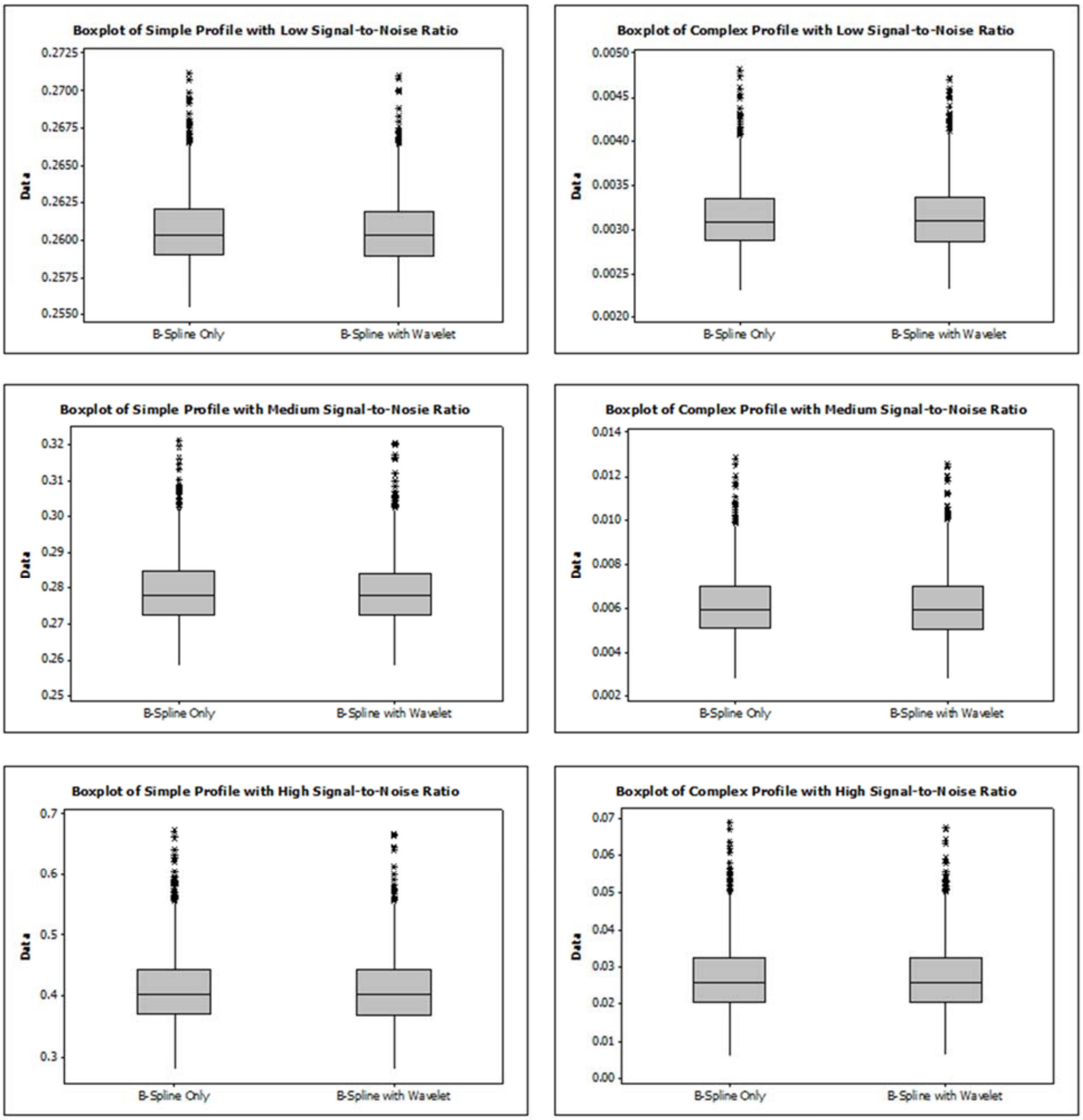

(a) (b)

References

Bernadette, G. and Jonathan, N., (2005), "Analysing the Results of a Designed Experiment when the Response is a Curve: Methodology and Application in Metal Injection Moulding." *Quality and Reliability Engineering International*. 21, pp. 509-520.

Brill, R. V., (2001), "A Case Study for Control Charting a Product Quality Measure That is a Continuous Function Over Time". Presentation at the 45thAnnual Fall Technical Conference, Toronto, Ontario.

Chang, S.I., Yadama, S., (2008), "Statistical Process Control for Monitoring Nonlinear Profiles Using Wavelet Filtering and B-Spline Approximation." *International Journal of Production Research*. (iFirst, Nov 26, 2008)

Chang, S. I., and S. Yadama (2010), "Statistical Process Control for Monitoring Nonlinear Profiles Using Wavelet Filtering and B-Spline Approximation," *International Journal of Production Research*, 48, 4, 1049-1068.

Daubechies, I., (1988), "Orthonormal bases of compactly supported wavelets." *Comm. in Pure and Applied Math.*, 41(7), pp. 909-996.

de Boor, C.,(2001), *A Practical Guide to Splines*. New York, NY: Springer-Verlag.

Gardner, M.M.; Lu, J. –C; Gyurcsik, R. S.; Wortman, J. J.; Hornung, G. E.; Heinisch, H.H.; Rying, E. A.; Rao, S.; Davis, J.C.; and Mozumder, P. K., (1997), "Equipment Fault Detection Using Spatial Signatures". *IEEE Transactions on Components, Packaging, and Manufacturing Technology—Part C* 20, 295-304.

Gilbert, S. and Truong, N., (1997), *Wavelets and Filter Banks*. Wellesley, MA: Wellesley-Cambridge Press.

Graps, A., (1995), "An introduction to wavelets." *IEEE Computational Science and Engineering*, pp. 50-61.

Jin, J. and Shi, J., (2001), "Automatic Feature Extraction of Waveform Signals for In-Process diagnostic Performance Improvement." *Journal of Intelligent Manufacturing* 12, pp.257-268.

Kang, L. and Albin, S. L., (2000), "On-Line Monitoring When the Process Yields a Linear Profile." *Journal of quality Technology*, 32, 418-426.

Kim, K., Mahmoud, M. A., and Woodall, W. H., (2003), "On the Monitoring of Linear Profiles." *Journal of Quality Technology,* 35(3), 317-328.

Mahmoud M. A. and Woodall, W. H., (2004), "Phase I Analysis of Linear Profiles With Calibration Applications." *Technometrics,* 46, 380-391.

Mallat, S., (1989), "A theory for multiresolution signal decomposition: the wavelet representation." *IEEE Trans. on Pattern Analysis and Machine Intell*, 11(7), 674-693.

"The R project for statistical computing." Retrieved 1/29/2009, 2009, from http://www.r-project.org/

"Statistical analysis: Data analysis and statistics software and training | minitab." Retrieved 1/29/2009, 2009, from http://www.minitab.com/

Walker, E. and Wright, S.P., (2002), "Comparing curves using additive models." *Journal of Quality Technology, 34*(1), 118.

Williams, J.D., Woodall, W.H., Birch, J.B., (2007), "Statistical monitoring of nonlinear product and process quality profiles." *Quality and Reliability Engineering International*, 23, 925-941.

Chapter 3 Detecting and Diagnosing Shape and Variation Changes in Nonlinear Profiles

Paper Title:
Detecting and Diagnosing Shape and Variation Changes in Nonlinear Profiles

Published in:
Proceedings of the 2011 Industrial Engineering Research Conference, T.Doolen and E. Van Aken, eds., Reno, Nevada, May 21-25, 2011.

Author's Name:
Dr. Shing I Chang and Shih-Hsiung Chou

Authors' Affiliations:
Department of Industrial and Manufacturing Systems Engineering
Kansas State University

Abstract

In profile analysis, a profile may contain a few hundred or thousand observations. Conventional multivariate statistical process control (SPC) tools cannot be applied directly without modifications due to high dimensions. Most existing methods for monitoring nonlinear profiles focus on detecting shape changes only. This study provides a framework for detecting shape as well as variation changes of a nonlinear profile. The proposed method first separates a given nonlinear profile into two channels using a discrete wavelet transformation (DWT). The first channel contains the information of overall contour of the profile while the second channel captures the noise around this contour. A Levene transformation is applied to signals in the variation (or noise) channel so that the problem of detecting variance changes is converted into the problem of detecting mean shifts. A B-spline approximation is then used on both the shape channel and the Levene transformed channel to generate knots or control points for dimension reduction. The proposed plotting statistic is defined as the average deviation between the actual

profiles and B-spline fitted profiles at the locations of the B-spline knots. Then a pair of univariate control charts, such as, EWMA charts, is used to monitor the process that produces the profile. Similar to X-bar and R charts, the proposed charting method aims to detect assignable causes of variation due to either mean or/and variance changes in profiles. A simulation study is conducted to evaluate the performance of the proposed method.

Keywords: Statistic Process Control, Wavelet Transformation, B-spline Approximation, Profile Analysis.

3.1 Introduction

In many industrial applications, it is necessary to describe quality characteristics of process as a profile instead of a number. For example, Jin and Shi (2001) monitor the tonnage signal for a stamping process. Gardner et al. (1997) measure pressure for a mass flow controller against the set points for flow. Walker and Wright (2002) study the vertical density against depth of a springboard.

A profile may contain a few hundred or thousand observations. As a consequence conventional multivariate statistical process control (SPC) tools cannot be applied directly without modifications due to high dimensions. Many studies of SPC techniques for profile analysis can be categorized according to the shape of a profile either linear or nonlinear. In linear profile cases, Kang and Albin (2000) combine the EWMA chart with R chart (EWMA-R chart) for Phase II linear profile monitoring. Kim et al. (2003) combine three EWMA charts for Phase II monitoring. They claim that their method could detect shifts faster than EWMA/R chart. Mahmoud and Woodall (2004) suggest an F-test approach using indicator (dummy) variables in a multiple regression model, and propose a likelihood ratio test for detecting changes in one or more regression parameters. Chang and Gan (2006) considered several Shewhart control charts to monitor the slopes of relationships between two or more measurement processes.

When the shape of profiles cannot be easily represented by a linear model, for example, the use of linear regression is inappropriate to apply to those profiles, nonlinear models should be considered. Brill (2001) applies a T^2 monitoring approach by monitoring the estimated regression coefficients in a nonlinear regression model. Williams et al. (2007) fit a nonlinear regression to model the vertical density profiles (VDP) data. They compare three T^2 control charts using sample covariance matrix, successive differences, and intra-profile pooling as estimates of the covariance matrix to monitor the VDP data.

To monitor nonlinear profiles is difficult. One of the main challenges is to find a proper model with a reasonable number of unknown parameter to fit a complex profile. Jin and Shi (2001) propose the use of wavelet decomposition, a feature-preserving method that first compresses the stamping tonnage information. Then, they recommend the monitoring of changes in wavelet coefficients instead of extracting features to represent some specific faults. Bernadette and Jonathan (2005) review three approaches for analyzing the results of experimental design when the response is a curve. Three methods studied are parametric nonlinear pre-processing, point-wise functional regression, and B-spline transformation pre-processing. They conclude that the B-spline approach provides the best result among three methods studied.

Chang and Yadama (2010) further combine wavelet transformation and B-spline for linear and nonlinear profile monitoring. They apply discrete wavelet transformation to separate the original profile into shape and noise signals. Then a B-spline model plays the role of defining the shape of a profile. Further, the mean square error (MSE) of the associated control point locations between observations and the target profile based on the B-spline model is then calculated. They also suggest that users divide a profile into multiple segments and then calculate the MSE statistic for each segment. This statistic can be monitored by any multivariate control chart, e.g. a Hotelling T^2 chart. In this study, a profile is considered as a whole i.e. segmentation is not implemented.

All of the above mentioned methods focus on detecting shape change only. In this study, we propose a framework of detecting and diagnosing shape as well as variance changes of a nonlinear profile. A profile during phase II monitoring is first applied to the DWT to be separated into two channels, i.e., shape and variance channels. Once the original profile is decomposed to certain level, both shape and variance channels will be reconstructed to the original domain. Note that the variance channel should be entered as all zeros when reconstructing the shape channel, while the shape channel is consisted of all zeros when reconstructing the variance channel. Then the Levene transformation is applied to the reconstructed variance channel, so that problem of detecting variance change becomes the one to detect shape changes. A B-spline fitting is then obtained to both the shape and Levene transformed variance channel, such that, the associated knots locations can be represented to shape and variance channel. Finally, the MSE between an observed and the target profile is calculated as a plotting statistic for each profile. Those statistics are then plotting into a couple of EWMA charts to monitor both profile shape changes and variation simultaneously. The organization of this study is the following. The next section introduces the background of wavelet transformation B-spline approximation, and Chang and Yadama's method, followed by the framework of the proposed method. Further, the experimental design is described, and then the simulation results are discussed. Finally, the conclusion and future work will be made in the study.

3.2 Background of Wavelet Transformation and B-Spline Approximations

3.2.1 Wavelet Transformation

Much of early work on wavelets was closely tied to a particular application or traditional theoretical framework (Graps, 1995). The signal processing community started to pay attention to wavelet decomposition in 1989 when Daubechies and Mallat demonstrated the use of discrete signal processing instead of analog signal process via Fourier transformation (Daubechies, 1988; Mallat, 1989). Since then, a number of theoretical as well as practical contributions have been made on various aspects of wavelet decomposition. This subject has been growing rapidly. The basic concept of the wavelet transformation is briefly summarized here base on Gilbert and Truong (1997).

From the viewpoint of the nonlinear profile, a function *f(t)* can often be described as a linear combination function:

$$f(t) = \sum_{j,k} a_{j,k} \psi_{j,k}(t) \tag{1}$$

where $a_{j,k}$ is called filter coefficient at decomposition level j and location k; t represents time; $\psi_{j,k}$ is the wavelet function which forms an orthogonal basis, meaning ,

$$\langle \psi_k(t), \psi_l(t) \rangle = \int \psi_k(t)\psi_l(t)dt = 0\,, k \neq l \tag{2}$$

Typically, the wavelet function $\psi_{j,k}$ can be expressed by the following equation:

$$\psi_{\mathrm{j},k}(t) = \psi(2^j t - k) \tag{3}$$

Moreover, Mallat 1989 in his paper provided an algorithm to decompose a signal using discrete wavelet transform (DWT) by two channels, lowpass filter (moving average) and highpass filter (moving difference). This process is called downsampling or decimation. Then a nonlinear profile $f(t)$ can be form as:

$$f(t) = \sum_{j,k} a_{j,k}\psi_{j,k}(t) = \sum_k a_{j-1,k}\psi_{j-1,k}(t) + \sum_k b_{j-1,k}\phi_{j-1,k}(t) \tag{4}$$

where $b_{j-1,k}$ is the scaling coefficient and $\phi_{j-1,k}(t)$ is scaling function at decomposition level j-1 and location k. In addition, the scaling function is also called approximation channel that catches the low frequency components, which also represent the shape of the given profile. In this study, Haar wavelet is used as the primary mother wavelet used in the wavelet transformation.

3.2.2 B-Spline Approximation

Mortenson [0] shows a (K-1) degree of B-Spline curve in general form as shown in equation (5).

$$\mathbf{C}(\boldsymbol{t}) = \sum_{\boldsymbol{i}=\mathbf{0}}^{\boldsymbol{n}} \boldsymbol{P_i}\mathbf{N}_{\boldsymbol{i,K}}(\boldsymbol{t}) \tag{5}$$

where P_i are the control points, and $N_{i,K}(t)$ are the (K-1)th degree of basis polynomials. The i th basis function $N_{i,k}(t)$ is defined by

$$N_{i,k}(t) = \frac{t-u_i}{u_{i+k-1}-u_i}N_{i,k-1}(t) + \frac{u_{i+k}-t}{u_{i+k}-u_{i+1}}N_{i+1,k-1}(t) \tag{6}$$

$$N_{i,1}(t) = \begin{cases} 1 & if\ u_i \le t < u_{i+1} \\ 0 & otherwise \end{cases} \tag{7}$$

where k is integers, i.e., k=2,…,K. In this study, we applied the cubic B-spline, such that K is equal to 4. The matrix form of cubic B-Spline for each curve segment used in Chang and Yadama (2010) can be specified as equation (8)

$$\boldsymbol{C_i(t)} = \frac{\mathbf{1}}{\mathbf{6}}[\boldsymbol{t}^{\mathbf{3}}\ \boldsymbol{t}^{\mathbf{2}}\ \boldsymbol{t}^{\mathbf{1}}\ \mathbf{1}]\begin{bmatrix} -1 & 3 & -3 & 1 \\ 3 & -6 & 3 & 0 \\ -3 & 0 & 3 & 0 \\ 1 & 4 & 1 & 0 \end{bmatrix}\begin{bmatrix} p_{i-1} \\ p_i \\ p_{i+1} \\ p_{i+2} \end{bmatrix} \boldsymbol{t}\in[\mathbf{1}, \boldsymbol{n}-\mathbf{2}] \tag{8}$$

3.2.3 Chang and Yadama's Work

Chang and Yadama (2010) propose a process to monitor nonlinear profiles for identifying mean shifts or shape changes in a profile. The main idea is, first, to use discrete wavelet transform to decompose a profile by lowpass and highpass filtering according to equation (4). Then, reconstruction step reverses the process of decomposition by setting all wavelet coefficients in the detailed channels to zero. The output of this step is the shape signals without noise. Then the reconstructed signal is partitioned into various segments according to engineering knowledge. Within each segment, users choose a fix number of control points in a B-Spline model to fit the profile. Users then calculate the distance vector d that contains the MSE using the control point matrix that stores control points by each profile. After that, mean difference distance vector of each segment is computed. The Hotelling's T^2 statistics is then adopted on the vector statistics for process monitoring. Their simulation results show the proposed method is capable of detecting and diagnosing shifts in profile shape. In this study, we further extend the process monitoring to detect possible variation changes in a profile.

3.2.4 Levene Transformation

The Levene transformation is one component of the Levene test which is used to detect difference in variability among data sets in the field of analysis of variance when the normality assumption is not obtained. In Levene's (1960) work, the original variable is subtracted from sample mean. The absolute value of this difference is then used in ANOVA for better performance in terms of higher detecting power and lower false alarm rate. Further, Brown and Forsythe (1974) compared 10% trimmed mean and median as the estimators of location in place of the sample mean. Their results show trimmed mean and median form have similar detecting power when a distribution is asymmetric (long-tail distribution) but are superior to the sample mean method. In this study, the modified Levene transformation with median is considered and shown in equation (9)

$$z_{ij} = \left| x_{ij} - \mu_{med,j} \right| \tag{9}$$

where i is the index of profiles, j is the jth point in a profile, x_{ij} is the j^{th} data point of i^{th} profile, and $\mu_{med,j}$ is the median value at j^{th} point among all phase I profiles.

3.3 The Proposed Methodology

The proposed method is described in this section. In this study, we assume the target profiles are known. Therefore, the procedure for phase II process monitoring is described as follows.

3.3.1 Phase II Process

Step 1. Initialize the number of level l for DWT to decompose profiles and the number of knots k for B-Spline.

Step 2. Decompose each original profile of the process using DWT, such that, a series of scale coefficients represents the shape (or mean) channel while variance channel is a series of wavelets coefficients. Note that the number of data points for each decomposed channel will be reduced to $m/2^l$, where m is the number of data points of the original profile.

Step 3a. Reconstruct each decomposed shape channel. The decomposed shape channels are reconstructed by setting wavelet coefficients to zero in each level, so that the number of data point of the reconstructed shape channel (denote as RS channel) will be identical to that of the original profile.

Step 3b. Reconstruct each decomposed variance channel. The decomposed variance channels are reconstructed by setting scale coefficients to zero in each level, so that the number of data points of the reconstructed variance channel (denote as RV channel) will have the same number as that in the original profile.

Step 3b.1 Apply the Levene transformation shown in equation (9) to each point at knot location in the RV channel. Denote the modified Levene transformed variance channel as LV channel.

Step 4. Apply B-spline to fit through RV and LV channel for each profile, and then calculate the mean square error D from various knot locations. Note that the mean profile was target profile. The equation of D is shown in equation (10).

$$\boldsymbol{D} = \frac{\sum_{i=1}^{k}(S_i-\mu_i)^2}{k} \tag{10}$$

where i is the index of knot, k is the number of knots, and S_i is the corresponding value of the channel at location of knot. Denote the mean square error D of RS channel as D_{RS}, and that of LV channel as D_{LV}.

Step 5. Plot D_{RS} and D_{LV} to its respective EWMA chart with its proper mean μ, standard deviation σ, upper control limit UCL, and lower control limit LCL. In this study we assume these parameters are known but they can be easily established from a phase I analysis.

3.4 Experimental Design

To examine the performance of the proposed method in terms of correct classification rate and misclassification rate, three types of profile considered in this study are shape change only, variance change only, and mixture situations. We first simulated 125 profiles of phase I process to establish EWMA chart parameters. Next, in the phase II process, the first 25 profiles are generated from the in-control process followed by the next of 25 profiles that represent an out-of-control process. In other words, the simulated process always shifts at 26th profile in mean or variance, or both in each replication. A total of 1000 replications are tallied. Specific details on the simulated profiles are shown in the next section.

$$f(x) = \left[\sqrt{2} \left(\frac{1 + 2\cos^2 \frac{x}{2}}{1 + 2\cos^2 x} \right)^{\frac{1}{2}} \cos^2 \frac{x}{2} \right]^2 \qquad , -\pi \le x \le 0 \tag{11}$$

3.4.1 Profile Function

The simulated true profile was a simple gradient step profile, which the maximal value of the profile was 2, while the minimal value was 0. Each profile consists 512 points and was generated from equation (11) as shown in Figure 3.1 (a). The simulated phase I profile was generated by *f(x)+e*, where *e~N*(0*,* 0.1^2) as shown in Figure 3.1 (b).

Figure 3.1 (a) Simple profile without noise; (b) Simple profile with noise which follows normal distribution with mean 0 and stand deviation 0.1; (c) Three different types of magnitude change; (c) Three types of phase shift.

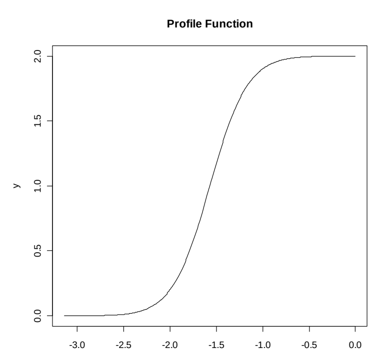

(a)

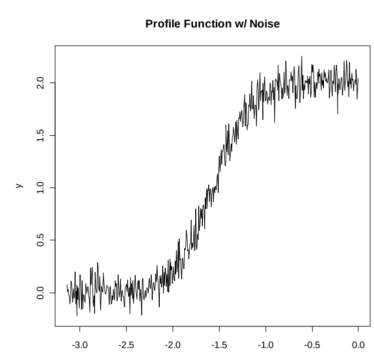

(b)

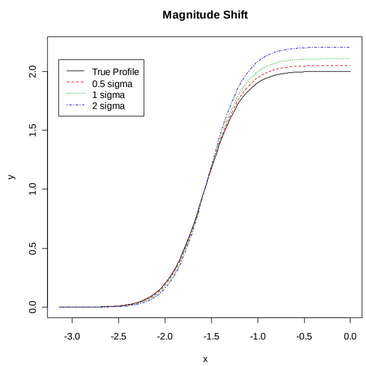

(c)

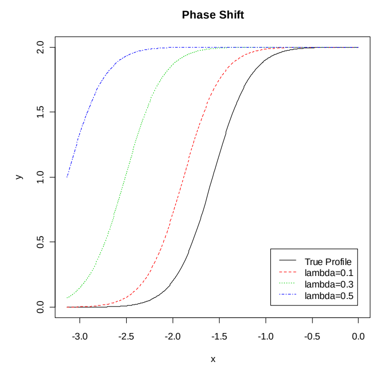

(d)

3.4.2 Types of Shape Change

There are two types of shape changes simulated in this study—magnitude change and phase shift change. Each type of these factors consists of three situations. In magnitude change, three different types of magnitude would be investigated in this study, i.e., δ=0.5σ, σ, and 2σ, where δ is the absolute value of maximum value subtract to minimum value of the true profile. Figure 3.1 (c) shows three different types of magnitude change for the simulated profile. In Figure 3.1 (c), solid line represents the true profile; dash line represents 0.5σ magnitude shape changed profile; dot line and dash-dot line are σ and 2σ magnitude shape changed profiles, respectively.

The other type of shape change called phase shift change was investigated in this study, as well. Three different lengths of phase shift change were examined. In this experiment, all simulated profiles have the same shape but shifted backward in three different ratios. The ratio λ is defined as length of shift divided by overall length of the true profile. Figure 3.1 (d) shows three different phase-shifted profiles and the true profile, in which the solid line represents the true profile, the dash line represents λ=0.1, the dot line is λ=0.3, and the dash-dot line means λ=0.5 for the profile.

3.4.3 Variance Change

In this study, the proposed method is also designed to detect variance change during the process monitoring. It is necessary to examine the capability of the proposed method in detecting variance change in a process. Two types of variance change will be investigated in this experiment— variance changed in the entire profile and in the bottom half of a profile as shown in Figure 3.2 (a) and (b), respectively. For variance changed in bottom half of a profile, the first 25 profiles were simulated as in-control profiles, while the rest 25 profiles were out-of-control profiles which error term were generated from N(0, σ2), where σ=0.15, 0.5, and 1. As for variance changed in the overall profile, the simulated change magnitudes are similar to the bottom half of the previous case.

3.4.4 Mixture

The mixture of both shape and variance changes is aimed to test whether the proposed method is capable of identifying proper scenarios. In each profile, the combinations of two types of shape change and two types of variance change are considered. Since shape and variance change consists of three treatments, the mixture factor has 36 combinations, i.e., 2 types of shape as well as variance change in which each type of change consists 3 magnitudes. Figure 3.2 shows an example of magnitude shape change and variance change on half part of the profile, where the magnitude of shift is 0.2 while variation is shifted from 0.1 to 0.5.

Figure 3.2 (a) Variance changed in the entire profile, (b) Variance changed in half of profile, and (c) An example of mixture change—magnitude shape change with variance changed on the half of a profile.

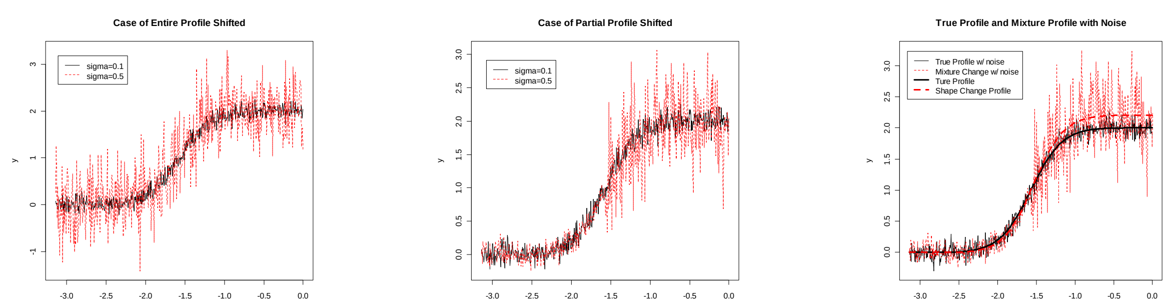

(a) (b) (c)

3.5 Simulation Results and Discussion

In this study, the performance statistics include correct classification rate and misclassification rate for shape change only, variation change only, and mixture situation. One thousand replications are used for each case. The higher the correct classification rates the better the proposed method works.

3.5.1 Case of Shape Change Only

The simulation results for the case of shape change only are shown in Table 3-1. In this scenario, the simulated profiles were designed in shape change only starting at 26th profile in the process. The simulation results show that the proposed method successfully identified the shape change in shape channel with rate of 1, while the proposed method does not provide an out-of-control signal from the variance channel 89.2%. In other words, the misclassification rate due to this additional EWMA chart for detecting variance changes is 0.108.

Table 3-1 Simulation results for the case of shape change only.

<table>
<tr><td colspan="2">Case</td><td>correct.shape</td><td>correct.var</td></tr>
<tr><td rowspan="3">Phase Shift only</td><td>λ=0.1</td><td>1</td><td>0.9</td></tr>
<tr><td>λ=0.3</td><td>1</td><td>0.889</td></tr>
<tr><td>λ=0.5</td><td>1</td><td>0.901</td></tr>
<tr><td rowspan="3">Magnitude shift only</td><td>0.5σ</td><td>1</td><td>0.885</td></tr>
<tr><td>1σ</td><td>1</td><td>0.878</td></tr>
<tr><td>2σ</td><td>1</td><td>0.897</td></tr>
<tr><td colspan="2">Avg.</td><td>1</td><td>0.892</td></tr>
</table>

3.5.2 Case of Variation Change Only

In this scenario, the process involved only variance change starting at 26th profile in the process. The proposed method was able to successfully identify variation change in the variance channel with 100% accuracy. However, the EWMA chart associated with the shape channel also indicate that the process is out of control. This situation is very similar to the practice of univairate control chart where X-bar and R chart are used simultaneously. When both X-bar and R chart indicates that the process is out of control, we should look into the causes of process variation first before concluding that the process mean shift has taken place, simultaneously.

3.5.3 Case of Mixture Situations

The mixture situations contained 36 combinations in which shape and variation change were occurred simultaneously. The proposed method identified correctly in all 36 combinations, i.e., the proposed framework is capable to identify the mixture scenario, so that the process involved both shape and variation change can be detected simultaneously.

3.6 Conclusions and Future Study

This study proposed a framework to monitor profile shape and variance changes simultaneously. According to the simulation results, the proposed two-channel monitoring framework are able to detect scenarios when profiles exhibit shape change only and both shape and variation changes. Similar to the classic univariate control charting monitoring, the proposed method would indicate that both shape and variance changes in a profile while in fact only variance changes exist. We suggest that the causes due to variation changes should be examined first. On the other hand, if the proposed system indicates that a process experiences shape change only. The performance statistics suggest that the shape change is the most likely cause for the out-of-control situation. For future study, we would like to (1) develop a plotting statistic(s) to distinguish shape changes from variation changes more effectively; (2) extend this study to multiple segments; and (3) extend this framework to multiple profile cases.

References

Bernadette, G. and Jonathan, N., (2005), " Analysing the Results of a Designed Experiment when the Response is a Curve: Methodology and Application in Metal Injection Moulding." *Quality and Reliability Engineering International*. 21, pp. 509-520.

Brill, R. V., (2001), "A Case Study for Control Charting a Product Quality Measure That is a Continuous Function Over Time". Presentation at the 45thAnnual Fall Technical Conference, Toronto, Ontario.

Brown, M.B. and Forsythe, A.B., (1974), "Robust test for the equality of variance." *Journal of the American Statistical Association,* 69, 364-367.

Chang, S.I. and Yadama, S. (2010). Statistical Process control for Monitoring Non-linear Profiles using Wavelet Filtering and B-Spline Approximation, *International Journal of Production Research*, 48(4):1049-1068.

Chang, T.C., and Gan, F.F. (2006), "Monitoring Linearity of Measurement Gauges." *Journal of Statistical Computation and Simulation,* v.76, pp. 889-911.

Daubechies, I., (1988), "Orthonormal bases of compactly supported wavelets." *Comm. in Pure and Applied Math.*, 41(7):909-996.

Gardner, M.M.; Lu, J. –C; Gyurcsik, R. S.; Wortman, J. J.; Hornung, G. E.; Heinisch, H.H.; Rying, E. A.; Rao, S.; Davis, J.C.; and Mozumder, P. K., (1997), "Equipment Fault

Detection Using Spatial Signatures". *IEEE Transactions on Components, Packaging, and Manufacturing Technology—Part C* 20, 295-304.

Gilbert, S. and Truong, N., (1997), *Wavelets and Filter Banks*. Wellesley, MA: Wellesley-Cambridge Press.

Graps, A., (1995), "An introduction to wavelets." *IEEE Computational Science and Engineering*, pp. 50-61.

Jin, J. and Shi, J., (2001), "Automatic Feature Extraction of Waveform Signals for In-Process diagnostic Performance Improvement." *Journal of Intelligent Manufacturing* 12, pp.257-268.

Kang, L. and Albin, S. L., (2000), "On-Line Monitoring When the Process Yields a Linear Profile." *Journal of quality Technology*, 32, 418-426.

Kim, K., Mahmoud, M. A., and Woodall, W. H., (2003), "On the Monitoring of Linear Profiles." *Journal of Quality Technology,* 3, 317-328.

Levene, H., (1960), "Robust Tests for Equality of Variances", In: I. Olkin, S.G. Ghurye, W. Hoeffding, W.G. Madow and H.B. Mann (Eds) *Contributions to Probability and Statistics* (Stanford: Stanford University Press) pp. 278-292

Mahmoud M. A. and Woodall, W. H., (2004), "Phase I Analysis of Linear Profiles With Calibration Applications." *Technometrics,* 46, 380-391.

Mallat, S., (1989), "A theory for multiresolution signal decomposition: the wavelet representation." *IEEE Trans. on Pattern Analysis and Machine Intell*, 11(7):674-693.

Mortenson, M. E., C., (2006), *Geometric Modeling.* New York, NY: Industrial Press Inc.

Walker, E. and Wright, S.P., (2002), "Comparing curves using additive models." *Journal of Quality Technology, 34*(1):118-129.

Williams, J.D., Woodall, W.H., Birch, J.B., (2007), "Statistical monitoring of nonlinear product and process quality profiles." *Quality and Reliability Engineering International*, 23, pp. 925-941.

Chapter 4 Monitoring Waveform Profiles with No Gold Standard Reference

Paper Title:

CASE STUDIES: Monitoring Waveform Profiles with No Gold Standard Reference

Submit to:

Journal of Quality Technology

Author's Name:

Shih-Hsiung Chou[1], Dr. Shing I Chang[1], Dr. Tzong-Ru Tsai[2], Dr. Dennis K.J. Lin[3], and Dr. Yu-Siang Lin[4]

Authors' Affiliations:

1. Department of Industrial and Manufacturing Systems Engineering, Kansas State University, USA
2. Department of Statistics, Tamkang University, New Taipei City, Taiwan
3. Department of Statistics, Pennsylvania State University, USA
4. Department of Industrial Management, National Taiwan University of Science and Technology, Taipei, Taiwan

Abstract

Problem: Condensation water temperature profiles are collected from a curing process for high-pressure hose products. The shape of those profiles resembles sine waves with diminishing amplitudes. A gold standard wave profile does not exist. Instead some wave profiles with various frequency and amplitudes are deemed normal for the water release operation. To the best of our knowledge, the current practice and research on SPC do not provide a solution for monitoring wave profiles of this kind.

Approach: The proposed SPC implementation framework first converts waveform profiles from the time domain to the frequency domain. Then a set of phase I *IX* control charts is constructed based on a Partition Around Medoids (PAM) clustering method. A Support Vector Machine (SVM) classifier is then used to label a new profile to its associated group for phase II

monitoring so that the *IX* chart associated with a homogeneous group can provide better process monitoring.

Results: Comparing with other widely used profile analysis techniques, such as, wavelet transformation (WT), principle component analysis (PCA), and B-spline fitting (BS) in the time domain, the proposed SPC implementation in the frequency domain works well during phase I control charting with low false alarm rates. It also outperforms the other methods in phase II control charting in term of high detection rate of abnormal profiles.

Keywords: Individual Control Chart; PAM clustering method; Support Vector Machine.

4.1 Process Description

High-pressure hoses are made out of rubber material with layers of metal wraps. Rubber products often require a curing process called vulcanization as the final step to activate cross-linking reaction so that the tensile strength of finished rubber is stronger (Hoster et al., 2009). In a curing process, reels of un-vulcanized hose are loaded into a sealed autoclave or vulcanizer whose in-chamber temperature and various valves are controlled by a programmable logical controller (PLC). Once all reels are loaded, the heat-up stage of curing process is enabled. The PLC monitors the chamber temperature and controls the steam valve to heat up the chamber until the temperature is reaching to a fixed target temperature, says, 500 °F. Once the target temperature is reached, the PLC will activate the curing stage to maintain the target temperature for a fixed number of time units, e.g., 480. Due to the confidential agreement with the process owner, the curing recipe (i.e., 500 °F and 480 time units) is a process setting for illustration purpose only. The final stage of the curing process is called cool-down stage to decrease the chamber temperature. For more details of curing process please see Figure 4.1 and Chang *et al.* (2012).

This study focuses on an additional control of water valve during the curing stage (the second stage shown in Figure 1) of a curing process. During the curing stage, condensation water accumulates at the bottom of the chamber. A water valve is installed at the end of the water releasing pipe for releasing condensation water. If this valve fails to open, the water would keep accumulating at the bottom of a vulcanizer, and cause cosmetic or functional damage of hoses. On the other hand, if the water valve fails to close, the chamber temperature would be difficult to maintain and result in energy wastes.

Figure 4.2 shows a schematic diagram of a vulcanizer with accumulated condensation water and the location of valves. A thermocouple is mounted at the end of condensation water releasing pipe (before the condensation water valve) to read the condensation water temperature. One typical condensation water temperature profile is shown in Figure 4.3. Note that once the condensation water temperature is decreased to a certain degree, the PLC will open the condensation water valve for a period of time to release water, and then the water temperature is climbing rapidly until the condensation water valve is closed. This mechanism results in the waveform shape of the condensation water profile. Since the company produces different kind of high-pressure hose products, they load different reels of hose products into the vulcanizer at the same time according to production orders. Reels in the vulcanizer may contain different amount of rubber material or different layers of metal wraps on hoses. It is not a surprise that the condensation water temperature profiles do not have a gold standard.

The condensation water temperature is recorded by a thermocouple located close to the water valve as shown in Figure 4.2. It is also a suitable indicator of the operation of condensation water valve because it can be used to detect abnormal situations, such as, malfunction condensation water valve or thermocouple. However, the current detection method relies on visual inspection, i.e., through a quick glance of the water-temperature print out. If a profile contains enough number of waves, it is deemed as a normal profile. For example, the condensation water temperature profile shown in Figure 4.3 is considered good because it contains 22 waves. It is a challenge to develop a non-subjective, systematic process control strategy for experienced and new engineers or operators. Figure 4.4 shows three other examples of in-control waveform profiles.

Figure 4.1 Steps of curing process for high-pressure hose products.

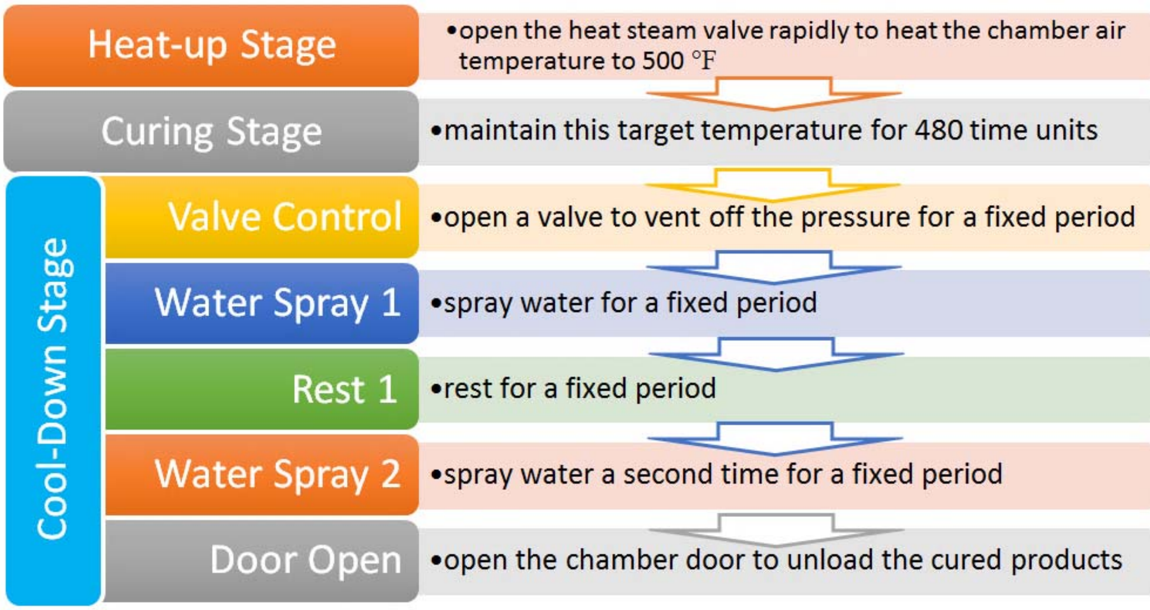

Figure 4.2 A schematic diagram of vulcanizer.

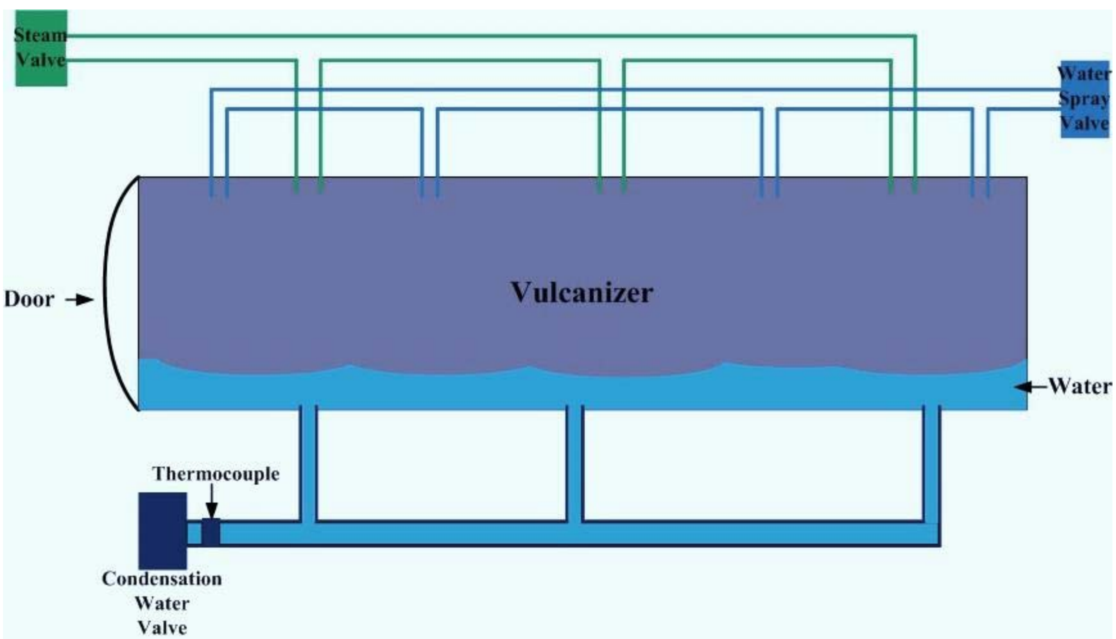

Figure 4.3 An example of condensation water temperature profile.

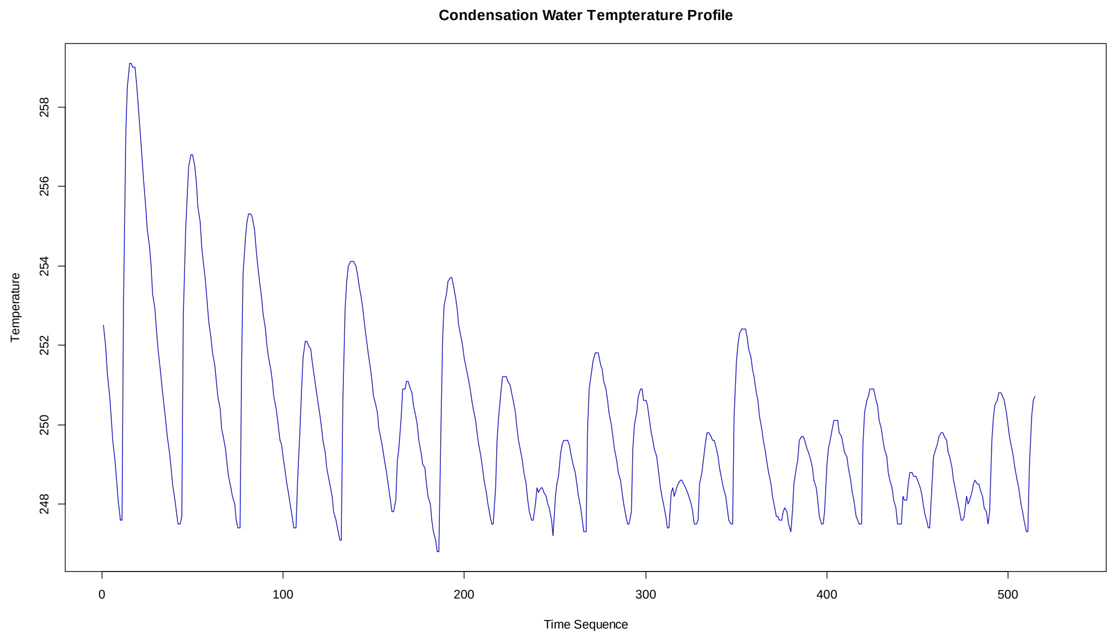

Figure 4.4 Example of three in-control condensation water profiles.

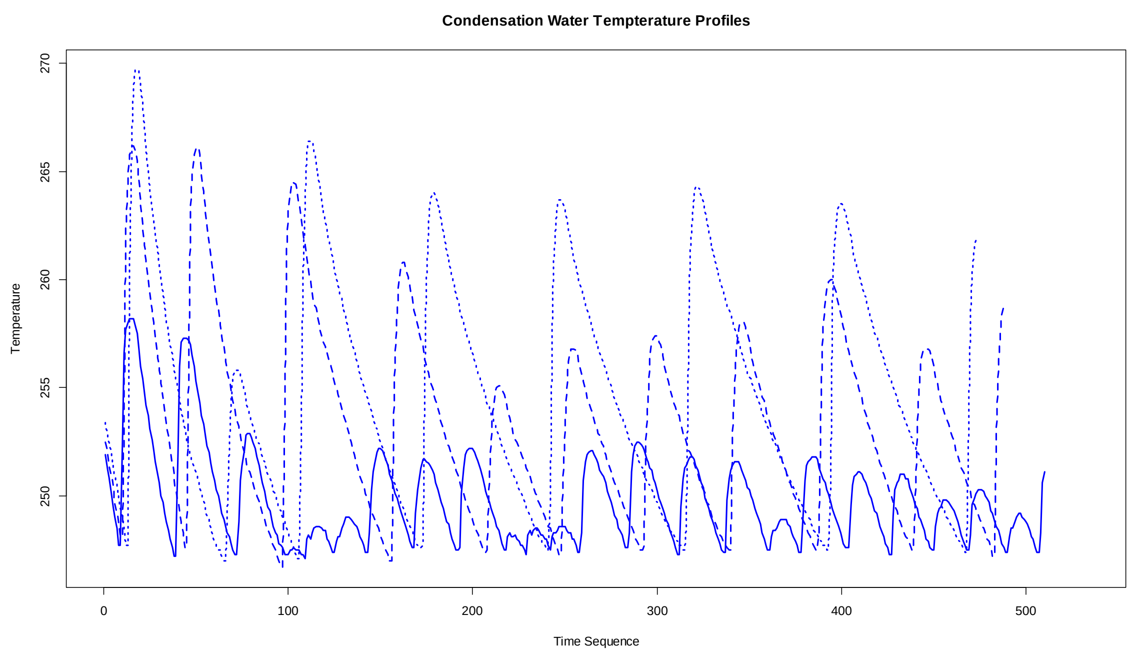

Current Profile analysis techniques can be simply characterized into two categories, linear and nonlinear profiles in regard to profile shape structure. Many studies monitored parameters of the linear regression model, such as, intercept or slope parameter. For example, Kang and Albin (2000) monitored slope and intercept with the Hotelling's T^2 control chart as first method to detect abnormal profiles, and they also proposed the second method which monitored average residuals between sample profiles and reference profile followed by EWMA and R chart. Kim *et al.* (2003) proposed three univariate EWMA charts which monitoring slope, intercept, and the variance of deviation between samples and regression line simultaneously.

Many techniques in nonlinear profile analysis can be found in Woodall (2007) and Noorossana et al. (2011). Woodall (2007) classified nonlinear profile analysis into four categories—applying multiple and polynomial regression (Zou et al., 2007; Kazemzadeh et al. 2008; Mahmoud 2008), applying nonlinear regression models (Ding et al., 2006; Williams et al., 2007; Shiau et al., 2009; Chang and Yadama 2010; Chen and Nembhard 2011), the use of mixed models (Jensen et al., 2008; Jensen and Birch, 2009; Qiu et al., 2010; Paynabar and Jin, 2011), and the use of wavelets (Reis and Saraiva, 2006; Zhou et al., 2007; Chicken et al., 2009). The wave profiles studied here cannot be easily classified into any one of these four categories of nonlinear profile analysis.

Although the above-mentioned methods are successful in dealing with the situations in their problem domains, those techniques deal with profiles that contain specific shape with a standard or model profile that can be predefined or estimated. In addition, none of these methods are suitable for waveform shape profile. Since the quality engineers are interested in if water-releasing cycle is under a statistical control, this study develops a general SPC implementation framework to monitor waveform shape profiles when no gold standard profile can be established. In the next section, we will describe how the wave profiles are collected.

4.2 Data Collection

In this case study, 146 condensation water temperature profiles were deemed good by the company's quality engineers and our best judgments, i.e., in control because of their frequent temperature oscillations. Most importantly these profiles were collected from the production batches where high-pressure hose products, the condensation water valve, and the condensation water thermocouples were all in good conditions. No cosmetic or malfunction hose was found in those production batches. Each wave profile can be presented as a vector as shown in equation

(1) where n is number of profiles and p_i is number of data points within i^{th} profile. These profiles (n=146 in this case) will be used to construct the phase I control charts.

$$W_{ji} = [w_{11}, w_{12}, \dots, w_{ji}, \dots, w_{pi,n}], i = 1,2,3, \dots, n, j = 1,2,3, \dots, p_i \quad \textbf{(1)}$$

The proposed framework is robust in that it strives to achieve the lowest false alarm rate and highest accuracy rate. The accuracy rate is a function of sensitivity and specificity defined in equation (19), (20), and (21) in the latter section. An experiment is also conducted to examine various well known clustering methods and dimension reduction methods that are often applied to profile analysis with promising results. Then, the best method is chosen based on the criteria of false alarm rates and accuracy rates. In this case study, thirty nine new condensation water temperature profiles were collected as phase II data to test the proposed framework.

4.2.1 The Proposed Framework

The proposed framework is shown in Figure 4.5 that demonstrates the monitoring the condensation water temperature profiles during the curing stage of vulcanization process. In phase I, the original waveform profiles in time domain is transformed to frequency domain using the Fast Fourier Transformation (FFT), which is a logical choice for dealing with wave signals. Then, a clustering method will be applied to the frequency domain profiles. This step will group frequency-domain signals into homogeneous clusters. Once all profiles have been clustered to their associated group, the dimension reduction method will be applied to all profiles so that the number of dimension for each profile will be reduced to less than 10 dimensions for user to use univariate or multivariate control charts as Montgomery (2009) suggested. A control chart for each cluster is then to be constructed based on members of the cluster. Note that the information of the clusters and their associated membership will be utilized as a training dataset for training a classifier model in phase II. Once the classifier has been trained, it will be applied to the phase II process to determine which group a new profile in frequency domain belongs to. For example, if a new waveform profile is assigned to cluster *k* by the classifier, then the parameters constructed in phase I, such as, mean, standard deviation, and control limits, can be obtained for phase II process monitoring. If the control chart indicates that an out-of-control signal occurs, the profile which contributed to this out-of-control signal will be considered an abnormal profile. More detail of the FFT, clustering method, dimension reduction method, and the classifier component will be introduced in the latter section.

Figure 4.5 The proposed framework for condensation water temperature monitoring.

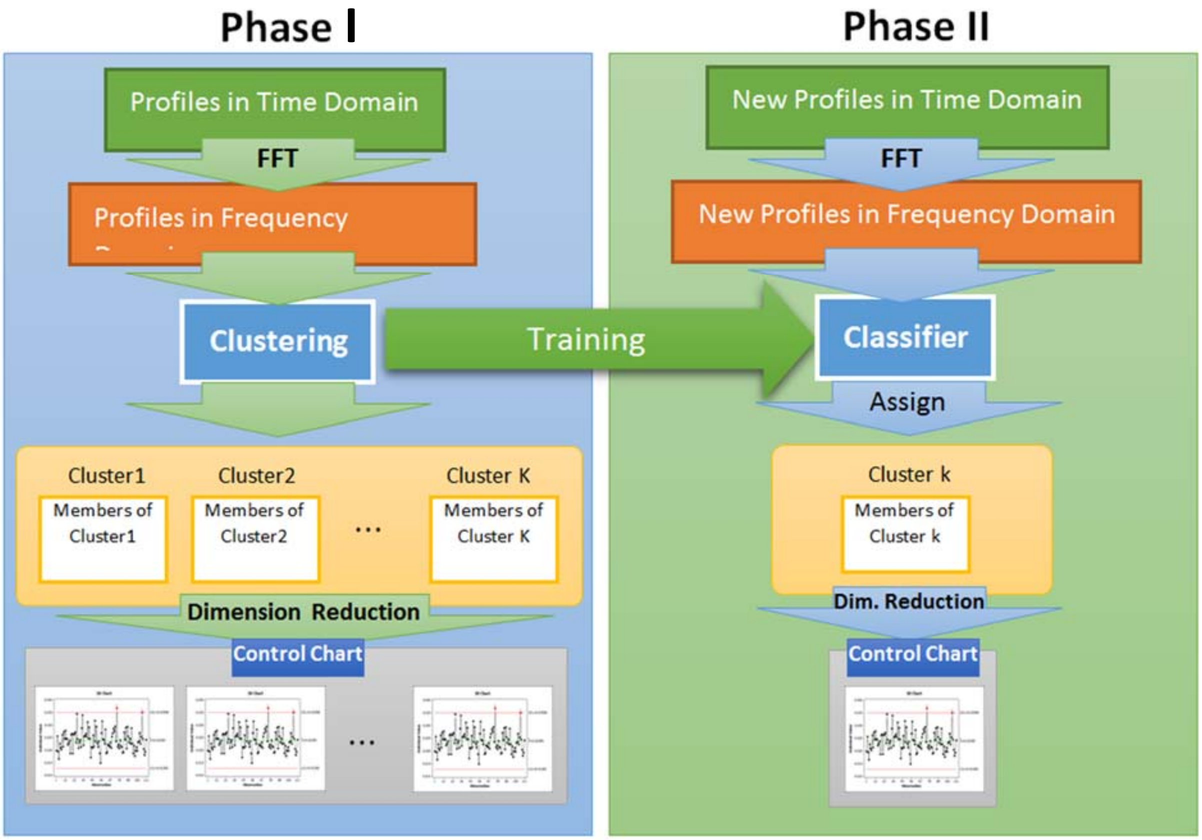

There are many candidate methods that may be appropriate for the clustering and dimension reduction functions shown in Figure 4.5. We will not introduce the detailed mechanism of all techniques we examined in this study. Instead, we will only introduce the methods recommended in this study. We will also discuss why these methods are applied and how we expect the results to be. The proposed framework will be still valid when new or more advanced clustering techniques and dimension reduction methods are introduced in the future. Quality engineers may also choose the other methods that they are more familiar with due to the availability of the computational software and package available to them.

4.2.2 Fast Fourier Transformation Component

Fast Fourier Transformation (FFT) developed by Cooley and Tukey (1965) is the most well-known algorithm to calculate discrete Fourier Transformation (DFT) for converting a signal from time domain to frequency. Both R and Matlab software contain the FFT function called "fft" without having to import any package or toolbox loaded in advance. In this study, the fft function from Matlab is applied is because it can specify the number of output data points after transformation. Note that, since the FFT-transformed profile is a symmetric shape, i.e., the shape in the right hand side is mirrored from the left hand side shape, it is suggested to specify the number of output data points to be dyadic, i.e., the power of 2. Therefore, only half of the number of data points that converted by fft function of Matlab will be used to further analysis. Since a typical condensation water temperature profile consists of 480 data points, the next power of 2 is 512 data points. Therefore, in each FFT-transformed condensation water temperature profile, the number of data points is 256. The output vector of fft function can be defined as equation (2) where p_f is the size of the FFT-transformed vector which is specified to 256. For more detail of the usage of fft function, one can refer to Matlab's online document at http://www.mathworks.com/help/matlab/ref/fft.html. For those who would like to develop their own FFT program, Smith (2002) provided a pseudocode.

$$W_{ji}^{f} = \left[w_{11}^{f}, w_{12}^{f}, \dots, w_{ji}^{f}, \dots, w_{pf,n}^{f}\right], i = 1,2,3, \dots, n;\ j = 1,2,3, \dots, p_f \quad \textbf{(2)}$$

We convert the condensation water temperature profiles from the time domain to the frequency domain in that the original waveform profiles are too complicated to be directly applied to the existing SPC profile monitoring methods as reviewed earlier. Figure 4.6 shows an example of the in-control profile 15 and its Fourier transformed profile. Although we can observe that the majority frequency of the profile 15 is 0.00091 Hz, there are other frequencies between 0 Hz and 0.01 Hz that cannot be ignored. After the FFT transformation, we can now treat the FFT transformed profiles as the other regular profile analysis problems except that we still need to address the issue of diverse frequency domain profiles in the next section.

Figure 4.6 Condensation water temperature profile 15 in (a) time domain and (b) frequency domain.

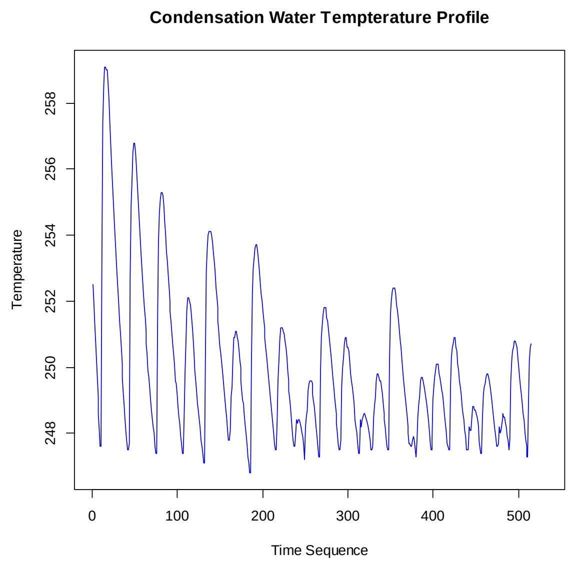

(a)

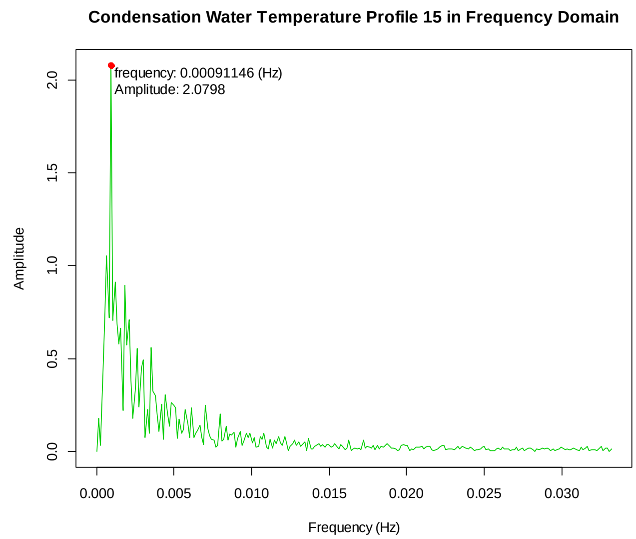

(b)

4.2.3 Clustering Component

Even though the in-control FFT transformed profiles are potential representations of the original time domain profiles, they are not homogeneous. For example, the in-control profile 5 and 15 in frequency domain has different profile shape in frequency domain as shown in Figure 4.7. Profile 5 has two majority frequencies while profile 15 only has one peak with gradient decline between 0.0025 Hz and 0.01 Hz. Therefore, we proposed to cluster the in-control FFT transformed profiles into homogeneous groups.

Figure 4.7 Profile 5 and 15 in frequency domain.

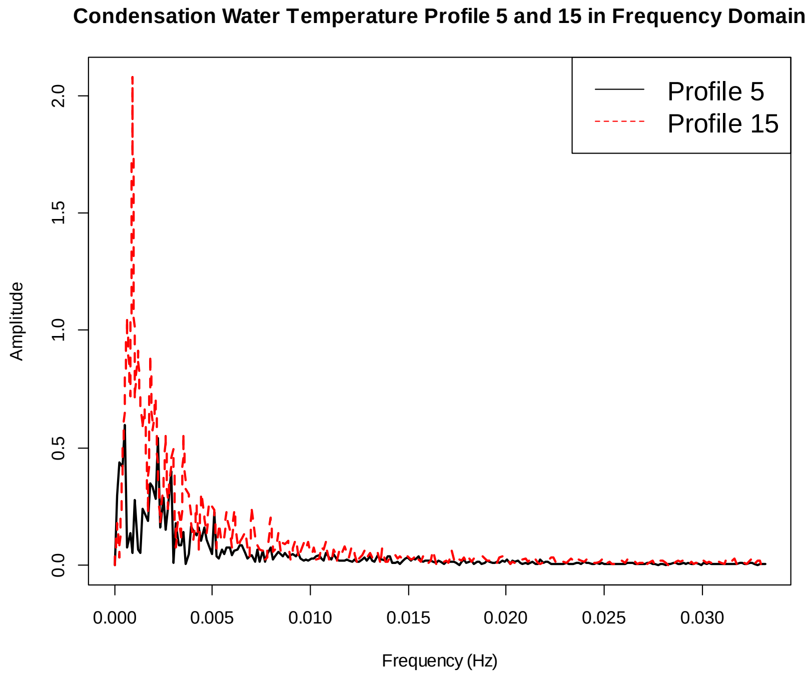

The purpose of a clustering method is to group a set of frequency domain members as similar as possible within a group, and those members can be distinguished from the other groups. In this study, we examine several widely used clustering analysis methods to the FFT transformed profiles such that members within the same group can be more homogeneous for subsequent profile analysis.

Table 4-1 shows the selected clustering methods examined in this study. Those well-developed methods including hierarchical clustering, mclust, K-means, Partition Around Medoids, fuzzy clustering, and fuzzy C-means are candidates for performance comparison (Leisch and Gruen, 2013). These clustering methods were used to group 146 in-control FFT transformed profiles as defined in equation (2). Then, the variance ratio criterion (VRC) is used as the clustering methods evaluation criterion (Mooi and Sarstedt, 2011) as shown in equation (3).

$$VRC = \frac{SS_B/(K-1)}{SS_W/(n-K)} \quad \textbf{(3)}$$

where K is the number of clusters, n is total number of profiles to be clustered, SS_B is the sum of the squares between clusters, and SS_W is the sum of the squares within the clusters. Note that, the larger the value of VRC, the better the performance of the clustering method.

According to Table 4-1, the largest VRC among all clustering methods is PAM. Note that, PAM requires the prior knowledge of the number of clusters. Users can either determine the number of clusters by using Hierarchical Clustering (hclust) or using mclust method, in which the prior knowledge of the number of clusters is not required. For more information regarding to clustering analysis methods in R please refer to Leisch and Gruen (2013).

Table 4-1 Clustering methods examined in this study.

Clustering Method	R Package	Function	SS_W	SS_B	*VRC*
Hierarchical Clustering	stat or cluster	hclust()	171.949	71.604	29.774
mclust	mclust	Mclust()	179.856	63.698	25.323
K-means	stats	kmeans()	156.309	87.245	39.909
PAM	cluster	pam()	164.266	101.880	**44.345**
Fuzzy clustering	cluster	fanny()	166.989	76.564	32.782
Fuzzy C-Means	e1071	cmeans()	158.9717	37.172	16.719

Partition Around Medoids (PAM)

The Partition Around Medoids clustering algorithm proposed by Kaufman and Rousseeuw (2005) is the first known algorithm of k-medoids clustering method (Han and Pei, 2006). Unlike a k-means algorithm that calculates the mean value of the cluster (centroid) as representative object of the cluster, a k-medoids algorithm uses the actual data point to represent the cluster. The objective of PAM is to minimize the cost function, i.e., sum of dissimilarities between given data points and the medoids as shown in equation (4). Note that, the measurement of dissimilarity between objects can be calculated by Euclidean distance or Manhattan distance as described in Kaufman and Rousseeuw (2005). A PAM cost function *F* is defined as:

$$F = \sum_{j}^{K} \sum_{W^f \in C_j} d(W^f, m_j) \tag{4}$$

where *K* is the number of clusters, W^f defined in equation (2) is a FFT-transformed profile assigned in cluster C_j, m_j is the medoid of C_j, which is also a vector of size p_f, and $d(W^f, m_j)$ is the function of dissimilarity between FFT-transformed profile W^f and medoid m_j. The algorithm of PAM is shown in Figure 4.8. The output of PAM is the FFT-transformed profile with its class label.

Figure 4.8 PAM algorithm.

```
Randomly select K FFT-Transformed profiles as medoids of the clusters
Repeat
    Assign each non-medoid FFT-Transformed profile to the nearest
    medoid using the dissimilarity function
    For each medoid m
        For each non-medoid FFT-Transformed profile W^f
            Swap m and W^f then calculate F
    Determine the new set of K medoids with the lowest F
Until no change in the medoid.
```

4.2.4 Classifier Component

In data mining, classification analysis constructs a model or classifier to predict the categorical labels. There are two steps in the classification analysis, training phase (or learning phase) and classification step. Training phase builds a classifier by learning from a given training dataset with class labels predetermined, while the classification step classifies the new data without a given class label to one of the associated classes (Han et al., 2006). In Figure 4.5, a classifier is needed to identify a new profile's membership. However, it needs to be trained first during the phase I process. The training dataset is generated from a clustering method, whose output contains the attributes of FFT-transformed profiles along with class labels. Then, the proposed classifier is constructed by learning from the trained data. Once the classifier is trained, it assigns a profile to an appropriate cluster for phase II process monitoring. The classifier used in this study is the support vector machine (SVM) classifier.

The SVM classification method has become an indispensable classifier in machine learning or pattern recognition field. SVM is adopted as the proposed phase II classifier in that it is one of the most competitive classification methods. Meyer et al (2003) confirmed that the SVM is the best classifier among 16 popular classifiers. Details of the theory and application of SVM may be found in Cortes and Vapnik (1995) and Campbell and Ying (2011).

The main idea of SVM classifier is mapping input variables into higher dimensional space using a kernel function to distinguish non-linearly separable datasets. The choice of a kernel function may result in different accuracy rates in the same problem domain. Many kernel functions have been embedded in packages of R. For example, linear, polynomial, Gaussian radial basis function kernel (RBF), and sigmoid kernel function. We will apply the svm() function in the e1071 R package to various training and test datasets. We will also examine the following kernel functions for the best performance in term of the accuracy rate in phase II process:

Linear Kernel:	$K(u,v) = u'v$	(5)
Polynomial Kernel of degree h:	$K(u,v) = (u'v + \phi)^h$	(6)
Gaussian Radial Basis Function Kernel (RBF):	$K(u,v) = e^{-\kappa\|u-v\|^2}$	(7)
Sigmoid Kernel:	$K(u,v) = \tanh(\kappa u'v + c)$	(8)

Note that u and v are both p-dimensional frequency domain profiles, and φ, h, κ, and c are all parameters that determined by users. In this study, all parameters we used are all default values from the R function svm() in the package e1071, i.e., φ=0, h=3, κ=1/p, and c=0. For more details in adjusting kernel function, please refer to Karatzoglou et al. (2006).

4.2.5 Dimension Reduction Component

Montgomery (2009) suggested that the maximum number of dimensions for a multivariate control chart should be no larger than ten. When the quality characteristic is defined as all observations in a profile, the dimensions may be in hundreds or thousands. In this case study, the FFT-transformed profile still contains 256 data points. In other words, the number of dimensions for each profile is 256. No multivariate control chart can handle such a large dimension effectively. Therefore, various dimension reduction methods have been applied to profile analysis. They include: (1) wavelet transformation (Reis and Saraiva, 2006; Zhou et al., 2007; Chicken et al., 2009); (2) Principal Component Analysis (Ding et al., 2006; Noorossana et al., 2008; Shiau et al., 2009); (3) B-Spline Fitting (Walker and Wright, 2002; Williams et al., 2007; Chang and Yadama, 2010).

Choosing an appropriate dimension reduction method, we need to consider the balance between computational cost and performance. The Euclidian distance method (ED) seems to be a good candidate. Not only this approach reduces the number of dimensions to one, but also the steps of calculating the Euclidian distance between two profiles are simpler than those of the other dimension reduction methods. In this study, we will compare the proposed method to the other methods. All methods studied and their associated R packages used in this study are listed as follows: (1) discrete wavelet transformation: dwt() in wavelets package; (2) principal component analysis: prcomp() in stats package; (3) cubic B-spline: ns() in splines package; (4) Euclidian distance: dist() in stats package. Since a multivariate control chart, e.g., Hotelling's T^2 or MEWMA, is only effective in handling the number of dimension of less than ten, the number of dimensions reduced by wavelet transformation is specified to eight (or less), while the maximum number of dimension that reduced by PCA is no larger than ten.

4.2.6 Control Chart Component

In the proposed SPC framework, a control chart plays the role of decision making. Both multivariate and univariate control charts with individual observation can be used. If the dimensionality of profiles is reduced to one, individual X control chart (*IX* chart) can be obtained. On the other hand, when the number of dimensions is larger than one after running the dimensional reduction method, the Hotelling's T^2 control chart with individual observations can then be used. We can substitute the *IX* chart with either a EWMA or a CUSUM chart, and the Hotelling's T^2 control chart with a MEWMA chart depending on the magnitude of the expected shifts. Montgomery (2009) provides details of both control charts.

To establish the individual control chart based on the independent observations x_i, $i = 1,2,\cdots n_k$, n_k is the number of observations in k^{th} cluster. In this study, since the B-spline and Euclidian distance dimension reduction method will reduce the number of dimensions to one, the *IX* control chart is applied to the transformed datasets. The I*X* control chart parameters are formulated as follows:

$$\mathrm{UCL}_k = \bar{x}_k + 3\overline{\mathrm{MR}}_k/d_2, \tag{9}$$

$$\mathrm{CL}_k = \bar{x}_k \tag{10}$$

$$\mathrm{LCL}_k = \bar{x}_k - 3\overline{\mathrm{MR}}_k/d_2, \tag{11}$$

where k represents kth cluster $\bar{x}_k$ is the average of individual observations while $\overline{MR}_k$ is the average of moving ranges of consecutive observations of k^{th} cluster, specifically, $\overline{\mathrm{MR}}_k = \sum_{i=2}^{n_k} |x_{ik} - x_{(i-1)k}|/(n_k - 1)$, and $d_2 = 1.128$. UCL_k, CL_k, and LCL_k are represented upper control, central line, and lower control limit of k^{th} cluster.

Moreover, PCA and wavelet dimension reduction methods result larger than one dimension. Therefore, the Hotellng's T^2 control chart with individual observations is obtained. To construct the Hotelling's T^2 control chart with individual observations (Tracy et al., 1992), one can follow the formula:

$$T_{ik}^2 = (x-\bar{x})_i' S_k^{-1} (x-\bar{x})_i \quad (12)$$

$$\mathrm{UCL}_k = \frac{p(n_k+1)(n_k-1)}{n_k^2 - n_k p} F_{\alpha,p,n_k-p} \quad (13)$$

$$\mathrm{UCL}_k = \frac{(n_k-1)^2}{n_k} \beta_{\alpha,p/2,(n_k-p-1)/2} \quad (14)$$

$$\mathrm{LCL}=0 \quad (15)$$

$$\mathrm{S}_k = \frac{V'V}{2(n_k-1)} \quad (16)$$

$$V_k = \left[v_{1k}' \; v_{2k}' \; \cdots \; v_{(n_k-1)k}'\right]' \quad (17)$$

$$v_{ik} = x_{(i+1)k} - x_{ik} \quad (18)$$

The statistics T_{ik}^2 of the i^{th} observation in k^{th} cluster is shown in equation (12), where S_k is calculated by using the equation (16). Moreover, S_k estimates the variance-covariance matrix better than that of using the conventional approach if there was no trend, cycle, etc., in the process. If the process was totally random, the variance-covariance structure determined by equation (16) and the conventional approach would have no difference (Holmes and Mergen, 1993). The UCL_k in equation (13) should be chosen when the control chart monitors phase II process, while equation (14) shows the UCL in the phase I process. Note that, n_k is number of profiles in k^{th} cluster, p is number of dimensions, and α is the confidence level in equation (13) and (14). LCL in both phase I and phase II is zero.

4.3 Experimental Design

In order to optimize the proposed SPC implementation framework, we conduct an experiment as shown in Figure 4.9. In this experiment, we use 146 in-control condensation water temperature profiles that were collected over two months in 2011 from the hose production manufacturing process to construct phase I process. Note that those 146 in-control data will be the training data for SVM classifier for phase II process if the clustering method is applied to the phase I process. We also collected extra 39 profiles in different months in 2011 in which 6 of those were abnormal profiles identified by quality engineers' and our judgments. Those abnormal profiles are profile 16, 24, 26, 27, 37, and 39 as shown in Figure 4.10, which are superimposed on overall 146 in-control phase I profiles. According to Figure 4.10, the abnormal profile 16, 24, and 27 have unusual period of time that the condensation water valve was kept closed after 200 time units. Profile 26 indicated that the valve was kept closed between 200 and 390 time units. The profile 37 is an obvious failure run of the hoses manufacturing process while the profile 39 indicates that the water valve opened and closed too frequently comparing to a normal pattern.

Moreover, since the proposed framework consists of a clustering/classification method, we investigate the performance in terms of accuracy rate with and without applying clustering/classification. The clustering method used in the proposed framework is PAM due to its highest VRC value based on the phase I data described in the above section. PAM is used to determine the clusters and their memberships which are then used as the training data for a SVM classifier. Because different kernel function in SVM classifier may result in different accuracy rates, therefore, four popular kernel functions specified in Figure 4.9 will be investigated in this experiment so that we can optimize the proposed framework. The performance criteria used in this experiment, false alarm rates and accuracy rate, are introduced in the next section.

Figure 4.9 The experimental design of the proposed SPC implementation framework for the condensation water temperature profiles.

Data

- Phase I (training data) 146 in-control waveform profiles
- Phase II (testing data) 39 waveform profiles

Domain

- Frequency domain

Clustering

- Include clustering method (PAM)
- Exclude clustering method

SVM Classifier Kernel Function (if clustering method is applied)

- Linear kernel function (LK)
- Polynomial kernel function (PK)
- Gaussian radial basis function kernel (RBF)
- Sigmoid kernel (SK)

Dimension Reduction

- Discrete Wavelet Transformation (DWT)
- Principle Component Analysis (PCA)
- B-spline (BS)
- Euclidian Distance (ED)

Control Chart

- IX chart or Hotelling's T^2 control chart

Performance Comparison

- False alarm rate (in phase I process)
- Accuracy rate (in phase II process)

Figure 4.10 Six abnormal condensation water temperature profiles in phase II process (thick solid line: abnormal profiles; thin dot lines: overall 146 in-control profiles).

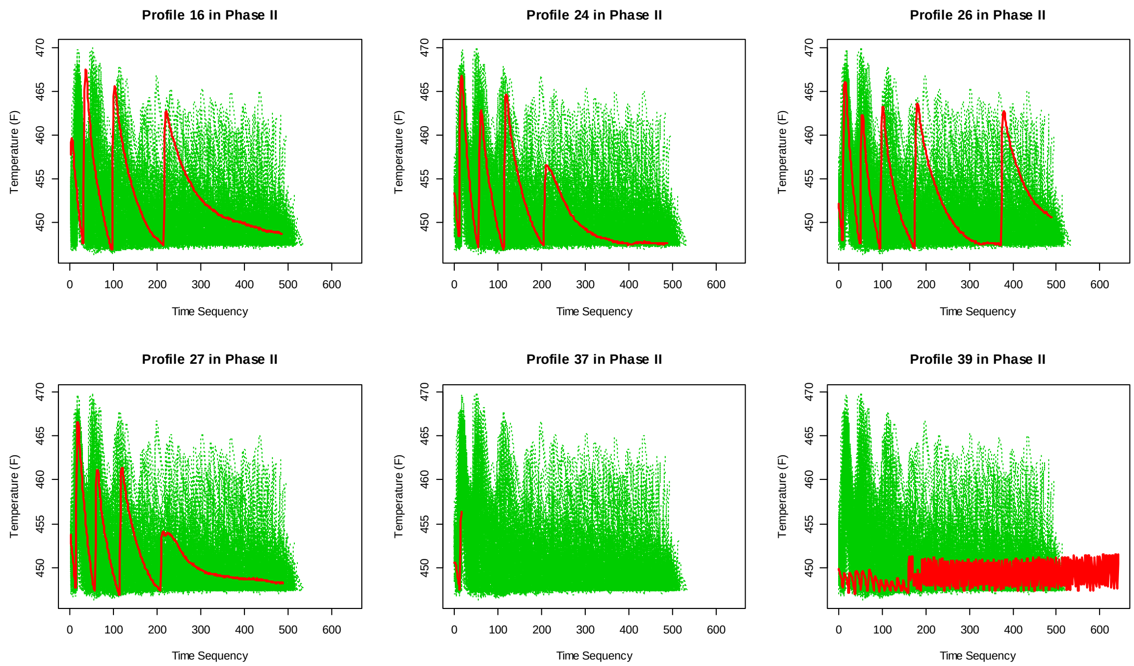

4.4 Performance Comparison

We use false alarm rates to evaluate the proposed framework in a phase I process, and the accuracy rate in a phase II process in this study. The accuracy rate can be calculated from the information listed in a confusion matrix as shown in Figure 4.11 that is often used in the machine learning field. The true positives (TP) are the number of in-control observations assigned to the in-control group, while the true negatives (TN) are out-of-control observations classified as the out-of-control group. If in-control observations are assigned to the out-of-control group, they are called false negatives (FN). On the other hand, when out-of-control observations are classified to the in-control group, they are called false positives (FP). Moreover, according Han et al. (2006), the accuracy rate can be defined in equation (19). The accuracy is a function of sensitivity and specificity defined in equations (20) and (21), respectively. Sensitivity and specificity are known as true positive rate and true negative rate, i.e., the proportion of positive tuples and negative tuples are all correctly identified. The accuracy rate is a good indicator of optimizing the proposed framework because it provides overall performance criteria, such as, sensitivity and specificity, in one value.

Figure 4.11 A confusion matrix for positive and negative tuples (adapted from Han et al., 2006).

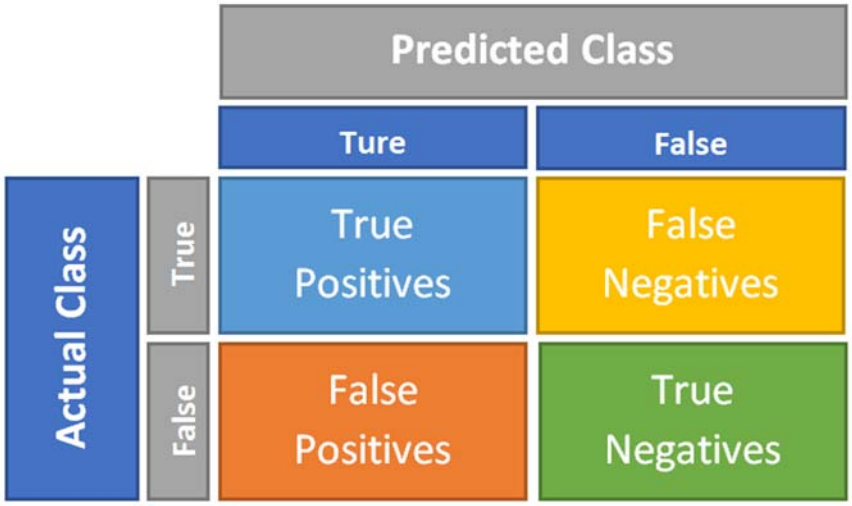

$$accuracy = sensitivity \frac{(TP + FN)}{(TP + FN + FP + TN)} + specificity \frac{(FP + TN)}{(TP + FN + FP + TN)} \quad (19)$$

$$sensitivity = \frac{TP}{(TP + FN)} \quad (20)$$

$$specificity = \frac{TN}{(FP + TN)} \quad (21)$$

4.5 Analyses and Interpretations

In this section, the performance results of the experiment expressed in above section will be shown and discussed. We will discuss the results in the two phases of process monitoring, i.e., phase I process and phase II process.

4.5.1 Phase I Process

In the phase I process, we examined the performance of four dimension reduction methods on frequency domain with and without applying a clustering method based on 146 in-control condensation water temperature profiles collected from the hoses manufacturing process. The performance results of the experiment for phase I process are shown in Table 4-2 in ascending order of the false alarm rate. From Table 4-2, the analysis in the frequency domain dominates the top three spots. Specifically, the cubic B-spline method shows the lowest false alarm rate as well as smallest number of false alarm with and without applying clustering method among all dimension reduction methods. Moreover, according to the bar chart of the four dimension reduction methods shown in Figure 4.12, B-spline and Euclidian distance method performs better (i.e. with smaller average false alarm rates) than other methods in phase I process. In fact, both BS and ED methods show very competitive results in frequency domain with or without applying the clustering method to the waveform profiles in phase I process as shown in Table 4-2. We examine the top three methods that result the first three lowest false alarm rate in phase I data, i.e., FFT+BS, FFT+PAM+BS, and FFT+PAM+ED. Note that, the BS method we used in the experiment is modified from one segment method of Chang and Yadama (2010). Specifically, the output of the BS is calculated by sum of absolute value of deviation between the cubic B-spline fitting curve of the FFT-transformed profile and the mean profile of the cluster. The mean profile of each cluster is also generated by cubic-B-spline fitting. Therefore, the dimensionality of the problem is reduced from 256 to one.

Table 4-2 Performance results of the experiment for phase I data.

clustering	dim. Reduction	# of false alarm	False alarm rate
w/o	BS	0	0.0000
w/	BS	1	0.0068
w/	ED	2	0.0137
w/o	ED	5	0.0342
w/o	DWT	11	0.0753
w/o	PCA	16	0.1096
w/	DWT	19	0.1301
w/	PCA	28	0.1918

w/: with clustering method; w/o: without clustering method; WT: wavelet transformation; PCA: principle component analysis; BS: cubic b-spline; ED: Euclidian distance.

Figure 4.13, Figure 4.14, and Figure 4.15 show the *IX* charts for these three methods. Although Figure 4.14 and Figure 4.15 shows three out-of-control points in total in the IX chart, it is a reasonable step to remove those out-of-control points from the *IX* chart during constructing phase I process control chart. After those three points were removed from the cluster 1 in Figure 4.14 and Figure 4.15, the results of *IX* charts of cluster 1 by using FFT+PAM+BS and FFT+PAM+ED show that both methods are ready for phase II monitoring since no point is outside the control limits as shown in Figure 4.16. Note that FFT+BS in Figure 4.13 only uses one control chart for phase II monitoring because no clustering method is used to assigned profiles into homogeneous groups.

Figure 4.12 Bar chart of the four dimension reduction methods and their average false alarm rates.

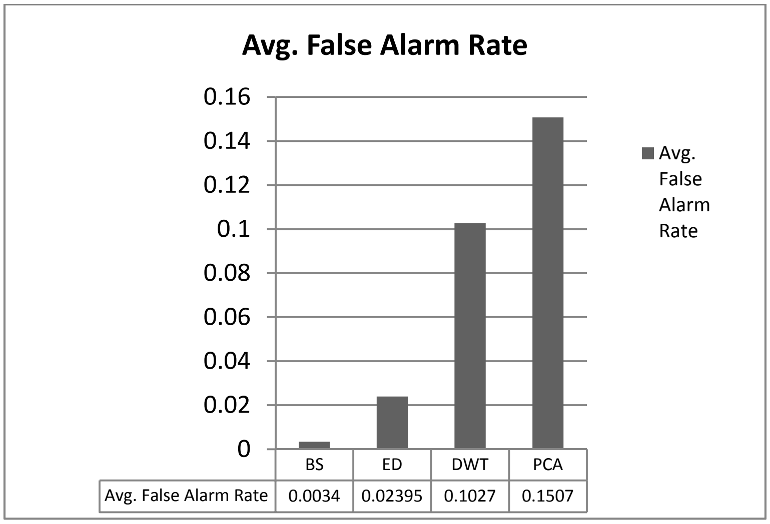

Figure 4.13 The IX chart of 146 in-control waveform profiles in phase I process using FFT+BS method.

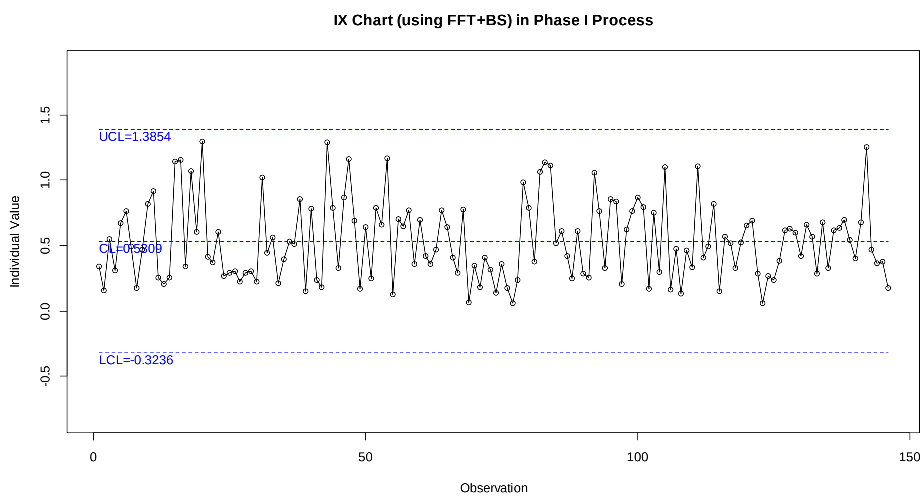

Figure 4.14 The IX charts of 146 in-control waveform profiles in phase I process for each cluster using FFT+PAM+BS method.

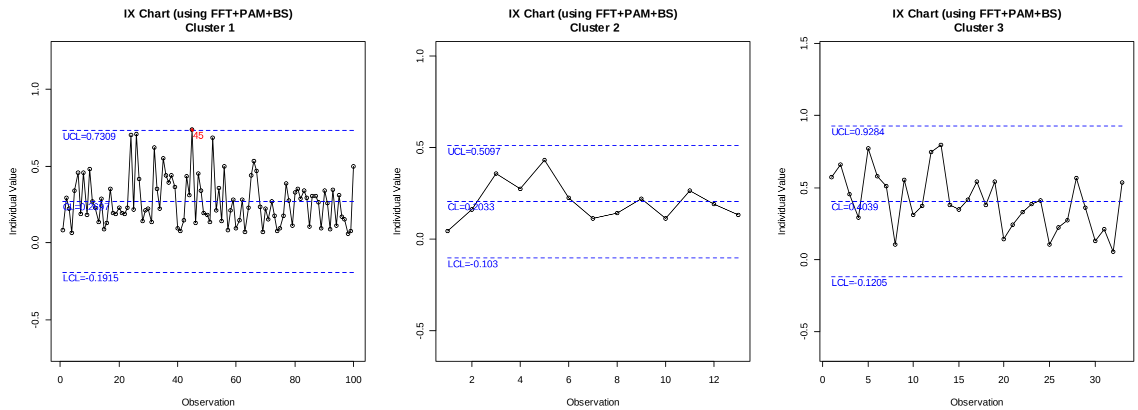

Figure 4.15 The IX charts of 146 in-control waveform profiles in phase I process for each cluster using FFT+PAM+ED

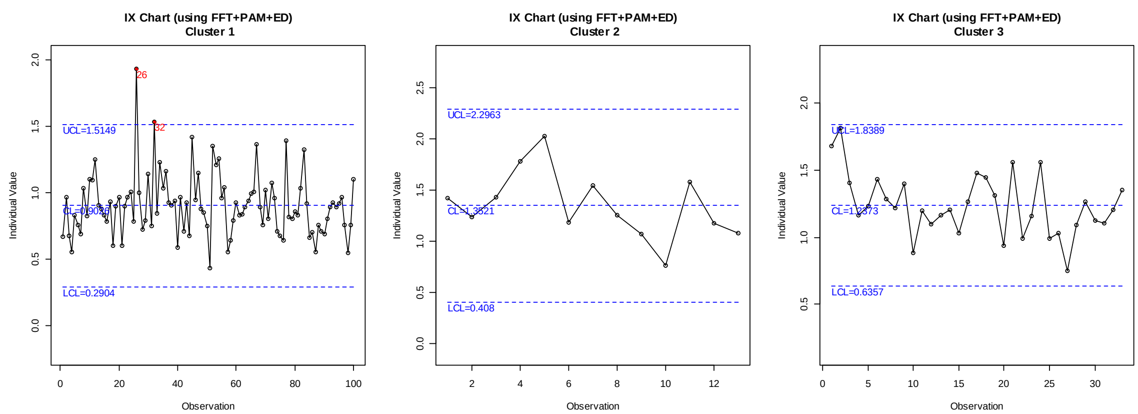

Figure 4.16 The IX charts of Cluster 1 using FFT+PAM+BS and FFT+PAM+ED with out-of-control points removed in constructing phase I process.

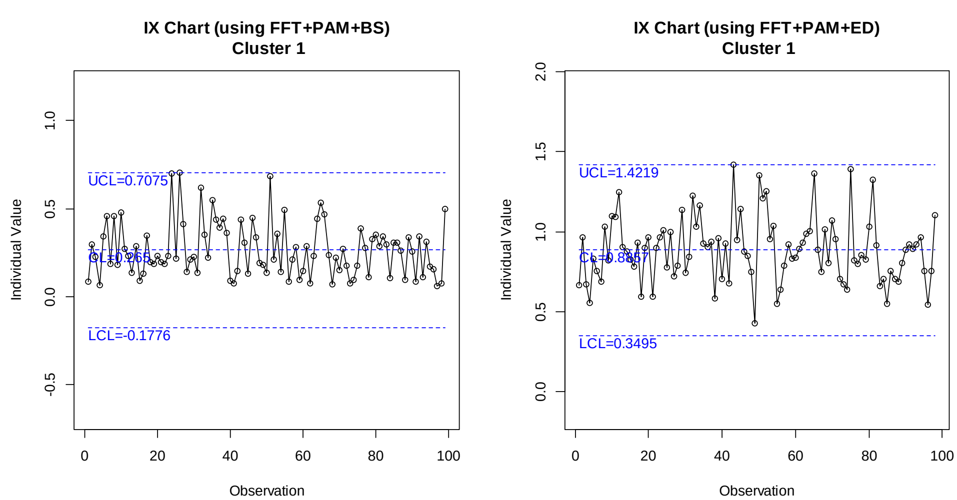

4.5.2 Phase II Process

Phase II data contains 39 condensation water temperature profiles, and 6 of which are recognized as abnormal waveform profiles by quality engineers and our judgments as shown in Figure 4.10. The performance results of the experiment for phase II data are shown in Table 4-3 in the descending order of the accuracy rate defined in equation (19). In Table 4-3, the method that combines the SVM classifier with RBF kernel function and Euclidian distance has the best performance due to its largest accuracy rate among all methods studied. Moreover, the first two highest accuracy rates that were applied SVM classifier with Euclidian distance dimension reduction method on frequency domain to the phase II data provide sensitivity rate of 1. In other words, they can identify all in-control profiles correctly, that is, no profile has been falsely detected as out of control in the phase II process using those methods. Even though the specificity rates that provided by SVM_{RBF}+ED and $SVM_{sigmoid}$+ED are not the highest rate, their overall performance scores in terms of accuracy rates are higher than the other methods.

Although the FFT+BS shows the lowest false alarm rate in phase I process, its specificity rate is 0.33 and the overall performance in terms of accuracy rate is 0.87, which is ranked in the 6th place. In other words, the proposed SPC implementation framework that applies FFT and clustering/classification to the waveform profile analysis can not only provide a solid phase I process control chart but also construct competitive phase II process control chart than other methods examined in this study. Therefore, based on the sensitivity rate of 1, specificity rate of 0.83, and the overall performance in terms of accuracy rate of 0.97, we recommend the combination of the FFT, the clustering (PAM)/classification (SVM with RBF kernel function) method, and the dimension reduction approach (ED).

Table 4-3 Performance results of the experiment for phase II data

Classifier	Dim. Reduct.	kernel	TP	TN	FP	FN	Sensitivity	Specificity	Accuracy
w/	ED	RBF	33	5	1	0	1.0000	0.8333	**0.9744**
w/	ED	sigmoid	33	4	2	0	1.0000	0.6667	0.9487
w/o	WT	NaN	31	5	1	2	0.9394	0.8333	0.9231
w/	PCA	RBF	30	5	1	3	0.9091	0.8333	0.8974
w/	PCA	sigmoid	30	5	1	3	0.9091	0.8333	0.8974
w/	ED	linear	33	2	4	0	1.0000	0.3333	0.8974
w/o	BS	NaN	32	2	4	1	0.9697	0.3333	0.8718
w/	PCA	linear	30	3	3	3	0.9091	0.5000	0.8462
w/	PCA	poly	30	3	3	3	0.9091	0.5000	0.8462
w/o	PCA	NaN	32	1	5	1	0.9697	0.1667	0.8462
w/o	ED	NaN	33	0	6	0	1.0000	0.0000	0.8462
w/	BS	linear	26	6	0	7	0.7879	1.0000	0.8205
w/	BS	RBF	26	6	0	7	0.7879	1.0000	0.8205
w/	BS	sigmoid	26	6	0	7	0.7879	1.0000	0.8205
w/	BS	poly	24	6	0	9	0.7273	1.0000	0.7692
w/	ED	poly	25	5	1	8	0.7576	0.8333	0.7692
w/	WT	poly	24	1	5	9	0.7273	0.1667	0.6410
w/	WT	RBF	23	1	5	10	0.6970	0.1667	0.6154
w/	WT	sigmoid	23	1	5	10	0.6970	0.1667	0.6154
w/	WT	linear	23	0	6	10	0.6970	0.0000	0.5897

w/: with clustering method; w/o: without clustering method; WT: wavelet transformation; PCA: principle component analysis; BS: cubic b-spline; ED: Euclidian distance; linear: linear kernel function; RBF: RBF kernel function; poly: Polynomial kernel function; sigmoid: sigmoid kernel function.

4.6 Conclusions and Recommendations

Profile monitoring using SPC has been studied in manufacturing process in recent years. Many researches provided successful approaches in their problem domain. However, no study has been found in the monitoring of process stability when the profile shape is a waveform without a gold standard. Since waveform profiles generated from a manufacturing process may consist of various magnitudes and frequencies, the process monitoring problem becomes more challenging due to the homogeneity issue. In this study, we propose a SPC implementation framework that consists of FFT and the clustering/classification method as well as the dimension reduction approach to monitor waveform profiles. The proposed framework is capable of identifying abnormal wave profiles with minimal false alarms based on both phase I and phase II data sets.

We compared the proposed method to a few widely used dimension reduction techniques in profile analysis, such as, wavelet transformation, principle component analysis, and B-spline transformation. We also considered applying clustering/classification method on frequency domain. The phase I and phase II datasets in the experiment are from the condensation water temperature profiles that collected from the curing process of the high-pressure hoses. According to Table 4-2, the proposed framework in phase I (FFT+PAM+ED) constructs a solid phase I process control chart with competitive performance in terms of false alarm rates after removing abnormal data points. In addition, as shown in Table 4-3, the proposed framework in phase II (FFT+PAM+SVM_{RBF}+ED) dominates other famous profile analysis techniques with respect to the accuracy rate. In summary, we recommend the use of FFT+PAM+ED in constructing phase I process, and FFT+SVM_{RBF}+ED in phase II.

Although the proposed method provides robust results than the other profile analysis techniques in this problem domain, we are interested in online monitoring of these condensation water temperature profiles because operators can examine the condensation water valve during the process rather than wait until the entire process is finished.

Reference

Campbell, C. and Ying, Y. (2011). *Learning with Support Vector Machines*: Morgan & Claypool.

Chang, T.C., Gan, F.F. (2006). Monitoring Linearity of Measurement Gauges. *Journal of Statistical Computation and Simulation*, 76(10): 889-911.

Chang, S.I., Tsai, T.R., Lin, D.K.J., Chou, S.H., and Lin, Y.S. (2012). Statistical Process Control for Monitoring Nonlinear Profiles: A Six Sigma Project on Curing Process, *Quality Engineering*, 24:251-263.

Chang, S.I. and Yadama, S. (2010). Statistical Process control for Monitoring Non-linear Profiles using Wavelet Filtering and B-Spline Approximation, *International Journal of Production Research*, 48(4):1049-1068.

Chicken, E., Pignatiello, Jr., J., and Simpson, J.R. (2009). Statistical Process Monitoring of Nonlinear Profiles Using Wavelets, *Journal of Quality Technology,* 41(2): 198-212.

Chen, S. and Nembhard, H.B., (2011). A High-dimensional Control Chart for Profile Monitoring, *Quality and Reliability Engineering International*, 27(4): 451-464.

Cooley, J.W. and Tukey, J.W. (1965). An Algorithm for the Machine Calculation of Complex Fourier Series, *Mathematics Computation*, 19:297-301.

Cortes, C. and Vapnik, V. (1995). Support-vector Network, *Machine Learning*, 20:273-297.

Ding, Y., Zeng, L., and Zhou, S. (2006). Phase I Analysis for Monitoring Nonlinear Profiles in Manufacturing Processes, *Journal of Quality Technology*, 38(3): 199-216.

Fraley, C. and Raftery, A. (2002). Model-based Clustering, Discriminant Analysis, and Density Estimation, *Journal of the American Statistical Association,* 97:611 – 631.

Han, J., Kamber, M., and Pei, J. (2006). *Data Mining, Second Edition: Concepts and Techniques*: Elsevier Science.

Holmes, D.S. and Mergen, A.E. (1993). Improving the Performance of the T2 Control Chart, *Quality Engineering*, 5(4):619-625.

Hoster, B., Jaunich, M., and Stark, W. (2009). Monitoring of the Vulcanisation Process by Ultrasound during Injection Moulding," ndt.net, 14(9):1-9.

Jensen, W.A. and Birch, J.B. (2009). Profile Monitoring Via Nonlinear Mixed Models, *Journal of Quality Technology* 41(1):18-34.

Jensen, W.A., Birch, J.B., and Woodall, W.H. (2008). Monitoring Correlation within Linear Profiles using Mixed Models, *Journal of Quality Technology*, 40(2):167-183.

Jin, J., and Shi, J. (1999). Feature-Preserving Data Compression of Stamping Tonnage Information Using Wavelets, *Technometrics* 41(4): 327–339.

Karatzoglou, A., Meyer, D., and Hornik, K. (2006). Support Vector Machines in R, *Journal of Statistical Software*, 15(9):1-28.

Kaufman, L., & Rousseeuw, P. J. (2005). *Finding groups in data: An introduction to cluster analysis.* New York: Wiley.

Kazemzadeh, R.B., Noorossana, R., Amiri, A. (2008). Phase I Monitoring of Polynomial Profiles, *Communications in Statistics—Theory and Methods*, 37(10):1671-1686.

Kang, L.; Albin, S.L. (2000). On-Line Monitoring when the Process Yields a Linear Profile, *Journal of Quality Technology*, 32(4): 418-426.

Kim, K., Mahmoud, M.A. and Woodall, W.H. (2003). On the Monitoring of Linear Profiles, *Journal of Quality Technology*, 35:317-328.

Leisch, F. and Gruen, B. (2013). Cluster Analysis & Finite Mixture Models. In *CRAN Task View*. Retrieved 2/28/2013, from http://cran.at.r-project.org/web/views/Cluster.html.

Lowry, C.A., W.H. Woodall, C.W. Champ, and S.E. Rigdon (1992). A Multivariate Exponentially Weighted Moving Average Control Chart, *Technometrics*, 34(1): 46-53.

Mahmoud, M.A. (2008). Phase I Analysis of Multiple Regression Linear Profiles, *Communications in Statistics - Simulation and Computation*, 37(10):2106-2130.

Mason, R.L., Tracy, N.D., and Young, J.C. (2001). A Practical Approach for Interpreting Multivariate T2 Control Chart Signals, *Journal of Quality Technology*, 29 (4):396 – 406.

Meyer, D. Leisch, F., and Hornik, K. (2003). The Support Vector Machine under Test, *Neurocomputing*, 55:169-186

Montgomery, D.C. (2009). *Introduction to statistical quality control.* New York, NY: John Wiley & Sons.

Mooi, E.A., & Sarstedt, M. (2011). *A Concise Guide to Market Research: The Process, Data, and Methods Using IBM SPSS Statistics*: Springer.

Noorossana, R., Amiri, A., and Soleimani, P. (2008). On the Monitoring of Autocorrelated Linear profiles, *Communications in Statistics-Theory and Methods*, 37(3):425-442.

Noorossana, R., Saghaei, A., and Amiri, A. (2011). *Statistical Analysis of Profile Monitoring,* Hoboken, New Jersey: John Wiley & Sons, Inc.

Paynabar, K. and Jin, J. (2011). Characterization of Non-linear Profiles Variations using Mixed-effect Models and Wavelets, *IIE Transactions*, 43(4):275-290.

Qiu, P., Zou, C. and Wang, Z. (2010). Nonparametric Profile Monitoring by Mixed Effects Modeling, *Technometrics,* 52(3):265-277.

Reis, M.S., SARAIVA, P.M. (2006). Multiscale Statistical Process Control of Paper Surface Profiles, *Quality Technology and Quantitative Management*, 3(3): 263-282.

Shiau, J.J.H., Huang, H.L., Lin, S.H., and Tsai, M.Y. (2009). Monitoring Nonlinear Profiles with Random Effects by Nonparametric Regression, *Communications in Statistics-Theory and Methods*, 38(10):1664-1679.

Smith, S.W. (2002). *The Scientist & Engineer's Guide to Digital Signal Processing.* California Technical Publishing.

Tracy, N., Young, J., and Mason, R. (1992). Multivariate Control Charts for Individual Observations, *Journal of Quality Technology*, 24(2):88-95.

Walker, E. and Wright, S.P. (2002). Comparing Curves Using Additive Models, *Journal of Quality Technology*, 34(1): 118-129.

Williams, J. D., Woodall, W.H., and Birch, J.B. (2007). Statistical Monitoring of Nonlinear Product and Process Quality Profiles, *Quality & Reliability Engineering International*, 23(7):925-941.

Woodall, W.H. (2007). Current Research on Profile monitoring, *Produção* 17(3): 420-425.

Zhou, S.Y., Sun, B.C., and Shi, J.J. (2006). An SPC Monitoring System for Cycle-based Waveform Signals using Haar Transform. *IEEE Transactions on Automation Science and Engineering*, 3(1), 60- 72.

Zou, C.,Tsung, F., and Wang, Z. (2007). Monitoring General Linear Profiles Using Multivariate Exponentially Weighted Moving Average Schemes, *Technometrics*, 49(4):395-408.

Chapter 5 On Monitoring of Multiple Non-linear Profiles

Paper Title:

On Monitoring of Multiple Non-linear Profiles

Published in:

International Journal of Production Research (16 Dec 2013 published online)

Author's Name:

Shih-Hsiung Chou[1], Dr. Shing I Chang[1], and Dr. Tzong-Ru Tsai[2]

Authors' Affiliations:

1. Department of Industrial and Manufacturing Systems Engineering, Kansas State University, USA
2. Department of Statistics, Tamkang University, New Taipei City, Taiwan.

Abstract

Most state-of-the-art profile monitoring methods involve studies of one profile. However, a process may contain several sensors or probes that generate multiple profiles over time. Quality characteristics presented in multiple profiles may be related multiple aspects of product or process quality. Existing charting methods for simultaneous monitoring of each multiple profile may result in higher false alarm rates. Or worse, they cannot correctly detect potential profile relationship changes. In this study, we propose two approaches to detect process shifts in multiple nonlinear profiles. A simulation study was conducted to evaluate the performance of the proposed approaches in terms of average run length under different process shift scenarios. Pros and cons of the proposed methods are discussed. A guideline for choosing the proposed methods is introduced. In addition, a hybrid method combining the salient points of both approaches is explored. Finally, a real-world data set from a vulcanization process is used to demonstrate the implementation of the proposed methods.

Keywords: Big Data, Profile Analysis, Multiple Profiles Analysis, Multivariate SPC, Multivariate EWMA.

5.1 Introduction

Quality characteristics represented as profiles have been studied in recent quality monitoring literature in recent years. For examples, Jin and Shi (1999) examined the stamping tonnage data over time within a cycle. Kang and Albin (2000) introduced a calibration issue during the etch step of a semiconductor manufacturing process. Walker and Wright (2002) studied the density of wood board over a section. Chang and Gan (2006) showed the monitoring stability of a calibration process in order to assure its accuracy. Paynabar and Jin (2011) presented pressing force profile signals in a valve seat assembly operation. Chang et al. (2012) investigated the temperature profile from a curing process for high-pressure hose products. These studies only consider one profile type in their respective applications.

Taking the advantage of information technology, engineers no longer measure the quality characteristics by hands but through automatic data sensors. This paradigm shift has resulted in a tremendous amount of data. For example, Jin and Shi (1999) reported that one tonnage sensor within a sampling interval could collect 1500 data points for each part, and the database would store 2.88×10^6 data points for 30 presses in 16 hours of production. Although modern database management systems can handle and store those huge datasets, it is very difficult for conventional multivariate statistical process control techniques, such as, Multivariate Hotelling's T^2 control chart, to deal with big data and multiple types of profiles simultaneously.

Profile analysis can be simply characterized into two categories, linear and nonlinear profiles according to the shape complexity of a profile of interest. With respect to linear profile applications, model parameters are the subjects of monitoring because linear profiles are easy to be presented by, for example, a simple linear regression model. Many studies monitored either intercept or slope parameter of the calculated simple linear regression model or monitoring both. For example, Kang and Albin (2000) proposed two approaches, the first one monitored slope and intercept with the Hotelling's T^2 control chart, while the second one monitored average residuals between sample profiles and reference profile followed by exponentially weighted moving average (EWMA) chart and R chart. Kim *et al.* (2003) showed their method of three univariate

EWMA charts monitoring slope, intercept, and the variance of deviation between samples and regression line performs better than EWMA/*R* chart in terms of average run length (ARL).

Studies in nonlinear profile analysis can be categorized into four types— applying multiple and polynomial regression (Zou et al., 2007; Kazemzadeh et al. 2008; Mahmoud 2008), applying nonlinear regression models (Ding et al., 2006; Williams et al., 2007; Shiau et al., 2009; Chang and Yadama 2010; Chen and Nembhard 2011;), use of mixed models (Jensen et al., 2008; Jensen and Birch, 2009; Qiu et al., 2010; Paynabar and Jin, 2011), and use of wavelets (Reis and Saraiva, 2006; Zhou et al., 2007; Chicken et al., 2009). For more detail of those methods to monitor the process stability can be found in Woodall (2007) and Noorossana *et al.* (2011).

The studies mentioned above only consider one profile type for process monitoring. However, data points that collected in a process or system may be characterized by two or more profiles. Noorossana *et al.* (2010) investigated a calibration application between desired force and the real force produced by 1600-ton hydraulic press machine. The machine consists of a set of cylinders, pistons and hydraulic pipe controlled by a programmable logic controller (PLC) for input and output factors adjustment. The input variable known as the desired force or nominal force is given by a motor placed on the top of machine so that four real forces or the response variables collected from four cylinders of the press can be measured by a PLC. Since four response variables can be considered as correlated linear profiles, Noorossana *et al.* (2010) proposed a multivariate simple linear profile method to deal with this problem. Specifically, all linear profiles are of the same type but for each press cylinder. Their method cannot monitor multiple correlated nonlinear profiles of different types that measure different process characteristics.

An example of multiple correlated nonlinear profiles can be found in a curing process of high-pressure hose products. According to Chang et al.'s (2012) study, the high-pressure hose products are covered layers of rubber and metal wires, which are loaded and cured in a heated chamber called an autoclave or vulcanizer, equipped with several sensors in different locations for monitoring air temperature, condensation water temperature, and chamber pressure. Although the key factor of curing process is the air temperature, the other profiles, such as, chamber pressure profiles, monitored simultaneously also play important roles in the curing process. Note that, high chamber pressure will increase the speed of reaching target air temperature. Also, a sealed chamber helps air temperature climb quickly and stably to the setup temperature point. On the other hand, a leaking vulcanizer requires more energy consumption to maintain the same temperature during the curing stage. Therefore, it is easier for quality engineers to monitor the pressure profile using statistical process control (SPC) tool for saving energy.

Chang *et al.* (2012) only investigated the air temperature profile of the curing process. When this process is out of control, it is very difficult for quality engineers to pinpoint the root cause. It is possible that the chamber is not airtight but both temperature and pressure maintain their target values. However, the relationship between the temperature and pressure profiles may have changed. In this study, both air temperature and pressure profiles are considered simultaneously. This example provides an illustration of how the proposed framework addresses multiple profile process monitoring in general. This paradigm motivates us to develop a novel approach for simultaneous monitoring of multiple correlated nonlinear profiles. A two-profile simulation study is conducted to evaluate the performance of the proposed charting methods.

Figure 5.1 shows overall air temperature and pressure profiles that generated from a typical curing process. It may be possible to construct an underlining physics equation between the air temperature and pressure so that the quality characteristics can then be transformed from profiles to parameters as variables used in multivariate control chart. However, this underlining equation is not easy to be formulated, and it cannot be generalized for all applications. In other words, this equation (if it can be formulated) can only be used in this curing process application. In addition, according to Figure 5.1, it is obvious that the temperature and pressure profile are correlated, and yet, it is hard to define such a correlation between profiles in general. Although monitoring those profile types using multiple multivariate control charts independently provides a solution, high false alarm rate and low detecting power is the major concern given that profiles are correlated to each other. This study provides a general SPC framework for multiple correlated linear or nonlinear profiles.

The focus of this study is the development of a proper process monitoring strategy for monitoring multiple correlated nonlinear profiles. This study examines two alternative solutions, in which profiles are first fitted by B-splines according to Chang and Yadama's method (2010). Then the deviations of the observed profile from the fitted profile are recorded to generate a vector of plotting statistics. A multivariate EWMA (MEWMA) control chart is then used for process monitoring. The first proposed method converts absolute deviations at each profile into a summary statistic. The second proposed method contains several numbers for each profile because a profile is segmented into p sections where $p>1$, where p is a constant to be determined from engineering knowledge or the complexity of a profile. Each section is represented by a summary absolute deviation statistic. A two-profile simulation study is conducted to characterize property of the proposed approaches in terms of ARL. We will also discuss the pros and cons of both approaches, and how we combine the salient features of both methods into a hybrid approach. The proposed hybrid method combines method I and method II, which monitors each section or segment by a MEWMA control chart. Multiple (p) MEWMA charts need to be maintained for the proposed hybrid method. A real-world data set from a curing process is used to demonstrate the implementation of the proposed methods.

The organization of this study is the following. First, the modified Chang and Yadama's (2010) method is briefly summarized, as well as the MEWMA procedure, followed by the proposed methods. Second, the experimental design of the simulation is introduced for testing the robustness of the proposed methods. Third, the ARL property for all proposed methods is introduced. Finally, the discussion and conclusion will be drawn in this section.

Figure 5.1 Overall air temperature and pressure profiles from the curing process of high-pressure hose products.

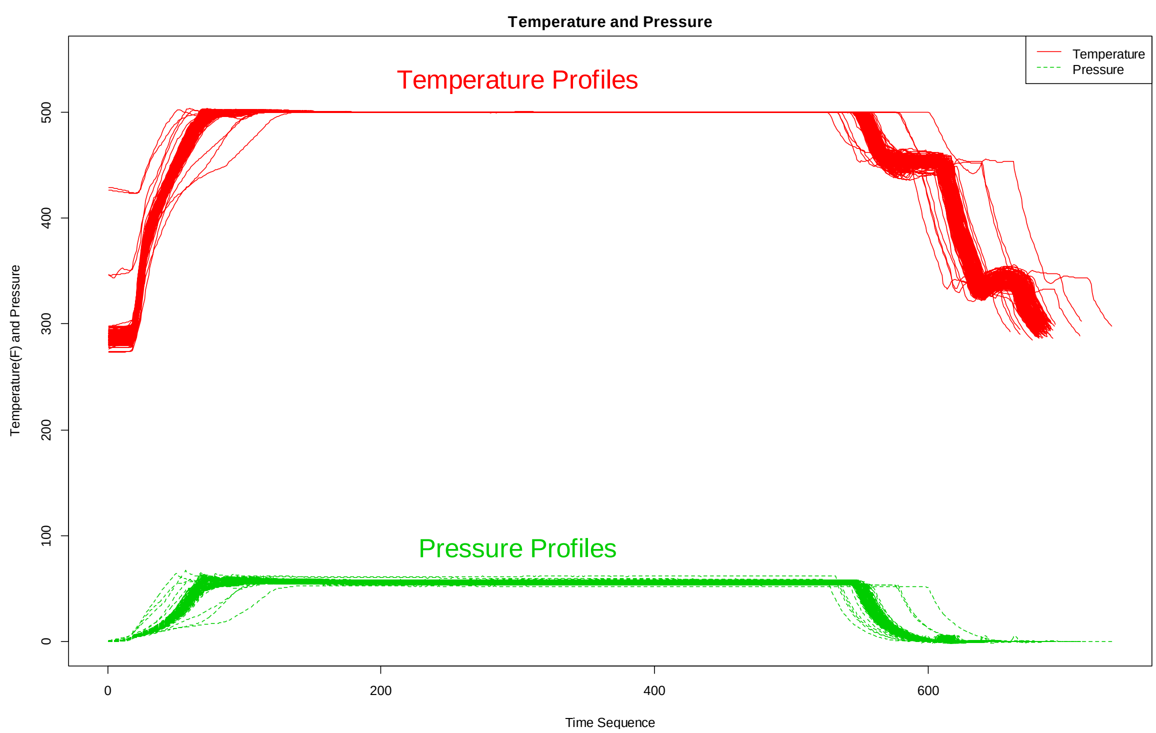

5.2 The Proposed Methods

In this study, two methods, method I and method II, are proposed to monitor the stability of the process whose quality characteristics are multiple profiles. Both methods consist of one multivariate control chart for all profiles and share the common modelling treatment, i.e., the modified Chang and Yadama's method (see Chang and Yadama's, 2010). Therefore, this section summarizes the original Chang and Yadama's method followed by the modified version. Then, the MEWMA procedure is presented. Finally, the proposed method I and II are shown in the last part of this section.

5.2.1 Modified Chang and Yadama's Method

Chang and Yadama (2010) proposed a control charting framework to monitor non-linear profiles in detecting shape changes. They proposed single segment and multiple segments approach for monitoring one profile. We will only introduce their multiple segments approach in this study because this approach provides more details of fault location for diagnosis purposes. The procedure of their proposed multiple segments approach is shown in Figure 5.2. Note that D_{ij} in Step 5 can be presented as equation (1) where $\overline{x}_{jk}$ is the mean profile of segment *k* that can be calculated by using B-spline fitting. Moreover, the MTY decomposition method shown in Step 7 can be found in Mason, Tracy, and Young's (2001) study for interpreting T^2 control chart signals.

$$D_{ij} = \frac{\sum_{k=1}^{c} |x_{ijk} - \overline{x}_{jk}|}{c}, \qquad i = 1,2,\dots,n; \;\; j = 1,2,\dots,p, \tag{1}$$

where $|\cdot|$ represents absolute value; *n* is the number of profiles and *i* is the index of profile; *p* is the number of segments of a profile and *j* is index of the segment; *c* is the number of control points within each segment so that a B-spline can be fit to each segment, and *k* is the index of control point. All numbers of *n*, *p* and *c* are known or well defined according to the manufacturing process and the complexity of a profile. The default *c* is equal to 16 according to Chang and Yadama's study (2010).

Figure 5.2 Procedure of Chang and Yadama's Method.

Procedure of Chang and Yadama's Method
Step 1: Apply Discrete Wavelet Transformation (DWT) to the given profile to the desired level, so that the DWT coefficients can be obtained.
Step 2: Reconstruct the DWT coefficients to original domain in two sets, signal of mean and signal of variance.
Step 3: Partition the mean signal into p segments.
Step 4: Apply B-spline with c control points to each segment, so that a control point matrix of order $n \times c \cdot p$ is constructed, where n is the profile replicates.
Step 5: The mean distance difference vector $Y_i = [D_{i1}, D_{i2}, \ldots, D_{ip}]$ is calculated, in which is associated with the control point matrix.
Step 6: To monitor the profile stability, the Hotelling's T^2 statistics on Y_i are calculated using the mean distance difference vectors.
Step 7: If process is in-control, go to Step 5; otherwise the MTY decomposition method is used for identifying the responsible T^2 components.

For the curing example in this study, since the curing process is control by the PLC, the within profile variance is very small. In other words, noises in each profile are very small. Therefore, we do not consider the use of the discrete wavelet transformation (or DWT) method for modeling the variance profiles as originally proposed in steps 1 and 2 in Chang and Yadama (2010). Moreover, according to Chang and Chou's (2009) study, the B-spline fitting is sufficient without applying the DWT to the Chang and Yadama's method when the monitoring of the profile shape change is the only consideration. Therefore, the B-spline fitting technique is applied to construct the proposed control charts. In addition to these changes, a MEWMA control chart is selected to be the charting tool due to its sensitivity and flexibility. In addition, the MTY decomposition method can be replaced by Chang and Chou's (2010) marginal cumulative sum (or CUSUM) glyphs because of its benefits of visualization and capability of dealing with high dimensional dataset of up to 20. The procedure of modified Chang and Yadama's method is shown in Figure 5.3. The MEWMA control chart is introduced in the next section.

Figure 5.3 Procedure of Modified Chang and Yadama's Method

Procedure of the Modified Chang and Yadama's Method
Step 1: Partition the mean signal into p segments.
Step 2: Apply B-spline with c control points to each segment, so that a control point matrix of order $n \times c \cdot p$ is constructed, where n is the number of profiles.
Step 3: The mean distance difference vector $Y_i = [D_{i1}, D_{i2}, \ldots, D_{ip}]$ is calculated, in which is associated with the control point matrix.
Step 4 To monitor the profile stability, the MEWMA statistics are calculated using the mean distance difference vectors.
Step 5: If process is in-control, go to Step 3; otherwise marginal CUSUM glyphs method is used for identifying the responsible T^2 components.

5.2.2 Multivariate EWMA Control Chart

The charting technique based on MEWMA is introduced in this section. The MEWMA was first developed by Lowry et al. (1992). It is the extension version of the EWMA for solving multivariate quality control problem. The procedure of MEWMA is presented as follows. The MEWMA statistics T^2 of the i^{th} observation is shown in equation (2), where Z_i is the extension form of univariate EWMA as shown in equation (3). Note that $0 \leq \lambda \leq 1$ and Z_0=0. The selection of chart parameters, λ and H, can be found in Prabhu and Runger's (1997). The variance-covariance matrix of Z's, Σ_{Z_i}, can be calculated using equation (4), where Σ is a variance-covariance matrix, which is either known or can be estimated from a phase I control charting procedure with m individual observations according to equations (5), (6), and (7). Moreover, Σ, shown in the equation (5) performs better than that of using the conventional approach if there was no trend, cycle, etc., in the process. If the process was totally random, the variance-covariance structure determined by equation (5) and the conventional approach would have no difference (Holmes and Mergen, 1993).

$$T_i^2 = Z_i^{'}\Sigma_{Z_i}^{-1}Z_i \tag{2}$$

$$Z_i=\lambda(x_i)+(1-\lambda)Z_{i-1} \tag{3}$$

$$\Sigma_{Z_i} = \frac{\lambda}{2-\lambda}[1-(1-\lambda)^{2i}]\Sigma \tag{4}$$

$$\Sigma = \frac{V'V}{2(m-1)} \tag{5}$$

$$V = [v_1' \; v \; \cdots \; v_{m-1}']' \tag{6}$$

$$v_i = x_{i+1} - x_i \tag{7}$$

Method I: One Chart for All Profiles and One Segment per Profile

The first method proposed in this study is straightforward. We first apply the Step 1 to Step 5 of the modified Chang and Yadama's method in Figure 3 with one segment to each profile so that multiple profiles become a vector with each element representing one profile. As shown in equation (8), given a set of profiles, X_i is the i^{th} observation and m is the number of types of profile and D_j can be calculated by using equation (1) with the number of segment of 1. For example, if the number of multiple profiles is two types with 512 data points in a profile, such as, temperature and pressure profiles of curing process of high-pressure hose products in this study, the number of types of profile m is equal to two. Therefore, the X_i is transformed from a matrix of size 2×512 into a 2×1 matrix. After Step 1 to Step 5 in Figure 3 is applied, the input variables expressed as equation (8) will be input into the MEWMA. Then a process will be stopped if any out-of-control signal takes place.

$$X_i = [D_1\ D_2 \dots D_j]_i',$$
where i is the index of observations and j=1,2,…,m (8)

Method II: One Chart for All Profiles and Multiple Segments per Profile

The second approach in this study is similar to the method I except that the number of segments of each type of profile p is greater than 1. The number of segments p is defined by users' pre-knowledge about the process of interest. In our real world case, the curing process of high-pressure hose product, and the p is equal to three because the quality engineers in the PH cooperate specified the process consists of three stages. Users can also segment the profile based on the section of interests. The choice of p is a balance of diagnostic need and computational resources. Once the number of the segments is determined by quality engineers, the procedure of the method II and method I are identical. The input variables are specified in equation (9), where X_i represents the i^{th} observation, k is the index of segment, and j is the index of profile. The advantage of using segmentation is that the quality engineers can gain more details of fault locations when a diagnosis is needed. In other words, the segmentation method is sensitive to partial profile shape changes. The main drawback of method II is that the type I error of the MEWMA will increase when the number of segments increases. For example, if the process consists of 5 profiles with 4 segments each, the vector X_i will contain 20 elements while the one segment approach only has 5 elements in the vector.

$$X_i = [D_{11}, D_{12}, \dots, D_{kj}]_i'$$
where k=1,2,…,p; j=1,2,…,m; i is the index of observations. (9)

5.3 A Simulation Study

In order to study the performance of the proposed methods, all charts are established with in-control ARL approximately 200, denoted by ARL_0=200. Moreover, the out-of-control ARL is denoted by ARL_1 in the simulation study. ARL_1 is used to evaluate the charting performance of the proposed approaches at the same false alarm rate. The simulation study conducts two correlated four-parameter logistic curves. The curve equation is adapted from Jensen and Birch (2009). They used this curve in their simulation study for generating ARL property and then applied this property to the real world case. Note that, their study only consider one type of profile. In this study, the curve equation will be extended to multiple profiles case. Specifically, in each sample, two correlated profiles are studied simultaneously. Equation (10) shows the operated function in this simulation study. Note that the coefficients in the equation (10), A=5, B=8, C=0.6, and D=0, are as same as the setup in Jensen and Birch's (2009) study. Further, to simulate the correlated multiple non-linear profiles, it is assumed that the parameters between profiles are generated from independently and identically multivariate normal distribution from one observation to another. If the parameters a and b are said to be generated from independently and identically multivariate normal distribution with mean vector μ and variance-covariance matrix Σ, it is denoted as $(a,b)' \sim NM(\mu, \Sigma)'$. The equation of simulated multiple correlated non-linear profiles is shown in equation (11) of which coefficients follow the following distribution: $(a_{0i}, b_{0i})' \sim MN(\mu_0, \Sigma_0)'$, $(a_{1i}, b_{1i})' \sim MN(\mu_1, \Sigma_1)'$, and $(e_{1i}, e_{1i})' \sim MN(\mu_e, \Sigma_e)'$. Specific setup for the parameters of multivariate normal distribution is given in equation (12). Note that equation (10) determines the shape of two multiple correlated profiles in the simulation study. Following the profile property of the high-pressure hose products in the curing example, in which the noises within each profile are very small, and the variance-covariance matrix of error terms in equation (11) is denoted as Σ_e specified by equation (12). An example of 25-pair in-control multiple correlated nonlinear profiles generated by equation (11) is shown in Figure 5.4.

$$y_{ij} = A + \frac{D-A}{1+\left(\frac{x_{ij}}{C_i}\right)^{B_i}} + \epsilon_{ij} \text{ for } i = 1,2,3,\dots,m; j = 1,2,3,\dots,n_i \tag{10}$$

$$\begin{cases} f_{ij} = a_{0i} + a_{1i}y_{ij} + e_{1i} \\ g_{ij} = b_{0i} + b_{1i}y_{ij} + e_{2i} \end{cases} \tag{11}$$

$$\begin{aligned} &\mu_0 = (10,-5)', \mu_1 = (10,3)', \Sigma_0 = \begin{pmatrix} 1 & \rho \\ \rho & 1 \end{pmatrix}, \Sigma_1 = \begin{pmatrix} 0.1^2 & 0.01\rho \\ 0.01\rho & 0.1^2 \end{pmatrix}, \text{and} \\ &\mu_e = (0,0)', \Sigma_e = \begin{pmatrix} 0.1^2 & 0.01\rho \\ 0.01\rho & 0.1^2 \end{pmatrix} \text{where } \rho \text{ is correlation parameter.} \end{aligned} \tag{12}$$

Figure 5.4 **An example of 25-pair in-control profiles.**

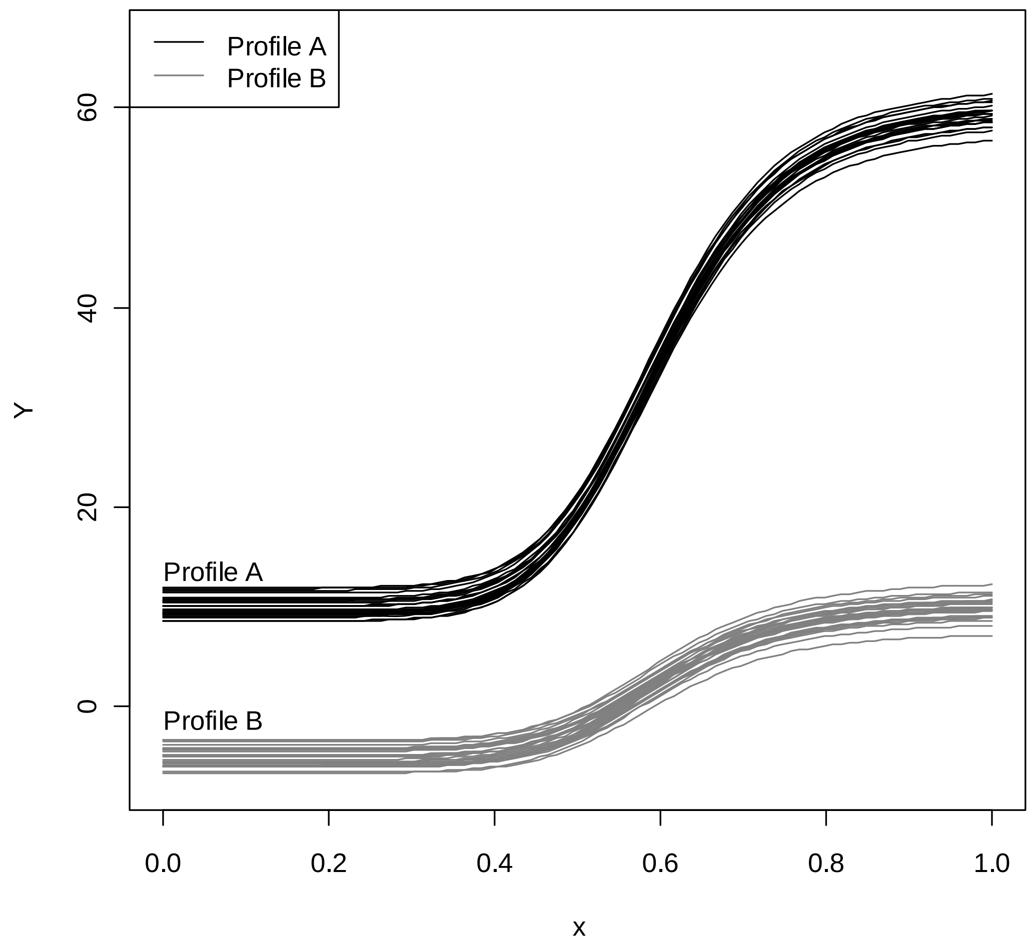

5.4 Experimental Design

To test the robustness of the proposed methods, profiles shifted in shape is considered in this simulation study with various testing factors. Figure 5.5 shows the experimental design of the simulation study. In this research, only shape changes are considered due to the shape change could be caused by a number of factor combinations. Given two types of profiles, Profile A and Profile B, possible factor combinations include two categories and five scenarios for the profile shapes changes are given according the scheme in Figure 5.5 for the simulation study.

In addition to shifted types, correlations between profiles and shift sizes are also considered in this simulation study. For the factor of correlation between profiles, there are three attributes to be tested, i.e., low (ρ=0.3), moderate (ρ=0.5), and high correlated (ρ=0.9). As for shift sizes, three magnitudes: small, medium, and large shift, are considered in this simulation study. The in-control ARL is fixed at approximately 200 for method I and method II. Therefore, there are total 45 cases to be tested for the proposed methods. Detailed parameter settings for the simulation study are discussed as follows:

Figure 5.5 Design of experiment of simulation study

Methods:

- Method I and II.

Shifted Types:

- Only one type of profiles changed:
  - Entire profile changed: only profile A changed (Scenario 1).
  - Partial profile changed: only profile B changed (Scenario 2).
- Both type of profiles changed:
  - Entire profile changed: both profile A and profile B changed (Scenario 3).
  - Partial profile changed: both profile A and profile B changed (Scenario 4).
  - Mixture changed: entire profile changed on profile A and partial profile changed on profile B (Scenario 5).

Correlation between profiles:

- ρ=0.3, 0.5, and 0.9

Shift size:

- Small, Medium, and Large shift

Performance:

- Average Run Length with in-control ARL of approximately 200.

5.4.1 Only the shape of either profile A or B is shifted

Scenario 1: The shape of profile A shifts entirely and the shape of profile B unchanged

In this scenario, the shape of profile A is vertically shifted away from the reference profile. With respect to the real world case, the curing process for high-pressure hose products, it is possible that the temperature profiles are shifted and go above the reference profile if the PLC or a thermocouple malfunctions, but the chamber is still airtight so that the pressure profiles are in control. This scenario may result in defective hose products due to overheating in the chamber. In this simulation study, we consider whether the shape of profile A is shifted entirely and go above the reference profile or not. Note that coefficient a_0 in equation (11) controls the vertical magnitudes change of profile A. Small shift is defined as the magnitude of a_0 from 10 to 12; medium shift is magnitude of a_0 from 10 to 14; and the large shift scenario is magnitude of a_0 from 10 to 16. Figure 5.6 (a) shows the profiles in scenario 1 where the shape of profile A exhibits a large shift. Twenty-five in-control profiles and another 25 shifted profiles with correlation ρ=0.5 are superimposed on top of each other.

Scenario 2: The shape of profile B shifts partially and the shape of profile A unchanged

In this scenario, we alter b_1 in equation (11) to change the partial shape of profile B. Scenario 2 examines whether the proposed method is capable of detecting a leaking chamber during the operation process. As described in scenario 1, scenario 2 also considers three different correlations between profiles. Figure 5.6 (b) shows the graphics of scenario 2 profiles with large shift magnitudes along with ρ=0.5. From Figure 5.6 (b), profile B changes at the middle of the profile. The magnitude of small shift in the simulation model is b_1 changed from 3 to 3.5. For medium shift, b_1 is changed from 3 to 4, while b_1 changed from 3 to 4.5 represents large shift in this simulation study.

5.4.2 Shapes of both profiles are shifted

Scenario 3: Shapes of both profiles A and B are shifted entirely

This scenario simulates the case both shapes of profiles A and B are changed entirely. Since the parameters a_0 and b_0 control vertical shifts in equation (11), a_0 is altered to change the shape of profile A higher than the reference profile, and b_0 is manipulated to make the entire profile B shift below the reference profile. The setting of correlations for scenario 3 is the same as that in the scenario 1 and 2, but the magnitudes of shift sizes are different from the former settings and given as follows: (1) small shift: a_0 shifted from 10 to 12 and b_0 shifted from -5 to -3; (2) medium shift: a_0 shifted from 10 to 14 and b_0 shifted from -5 to -1; and (3) large shift: a_0 shifted from 10 to 16 and b_0 shifted from -5 to 1. The superimposed profiles A and B with large shifted for scenario 3 is shown in Figure 5.6 6 (c). Scenario 3 intends to simulate the case where both temperature and pressure profiles are changed, especially when malfunctions take place in both thermocouples and pressure sensors or the door of vulcanizer is not sealed.

Scenario 4: Shapes of both profiles A and B are partially changed

Scenario 4 examines the case when shapes of both profiles are partially changed. In this case, profiles A and B are all in control before the middle point of the process, but both profile A and profile B are shifted after the middle point. Figure 5.6 6 (d) shows the overall profiles of A and B including shifted profiles with large shifted magnitude. The shift size in this scenario is as the follows: (1) small magnitude size of shift is simulated by altering a_1 from 10 to 10.5 and b_1 from 3 to 3.5; (2) medium shift is generated by changing a_1 from 10 to 11 and b_1 from 3 to 4; (3)

large shift is created by changing the parameters a_1 and b_1 from 10 to 11.5 and 3 to 4.5, respectively. The correlations setting for each profiles in this scenario is the same as scenario 1 as well.

Scenario 5: Shape of profile A is shifted entirely and the shape of profile B is shifted partially

The parameter settings for the profiles in scenario 5 are given as following: (1) small shift: a_0 shifted from 10 to 12 and b_1 shifted from 3 to 3.5; (2) medium shift: a_0 shifted from 10 to 14 and b_1 shifted from 3 to 4; (3) large shift: a_0 shifted from 10 to 16 and b_1 shifted from 3 to 4.5. Specifically, we examine if the proposed method is capable of detecting changes when the shape of temperature profile A is shifted entirely but the pressure profile B is changed after half of the process. Figure 5.6 (e) shows the superimposed profile A and profile B with large shift magnitude.

Figure 5.6 Scenarios of simulation study, (a) entire Profile A shifted only; (b) partial Profile B shifted only; (c) both Profile A and Profile B shifted entirely; (d) both Profile A and Profile B changed partially; (e) entire Profile A changed and partial Profile B changed.

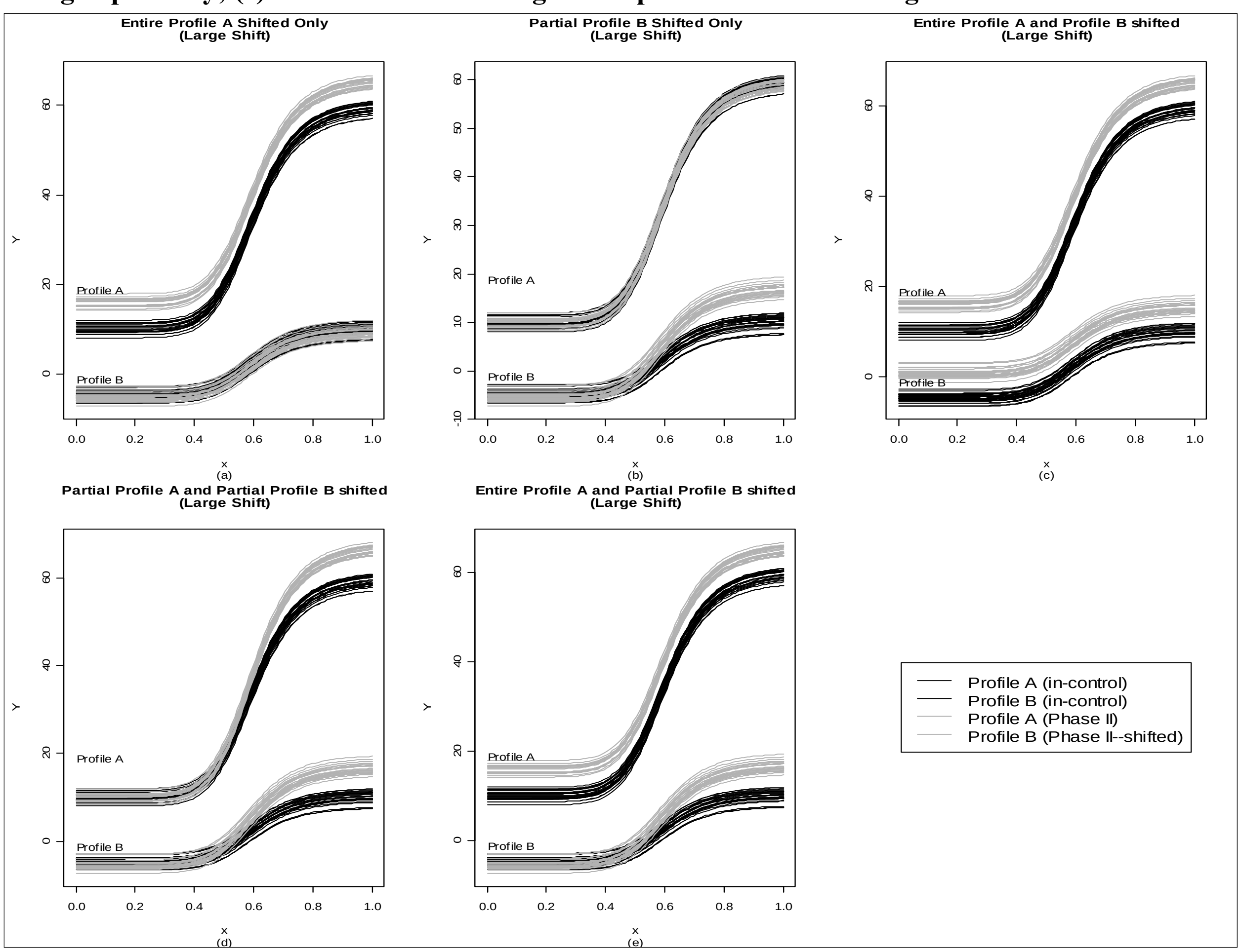

5.5 Simulation Results and Discussion

Simulations according to the scenarios 1 to 5 described in the previous section are conducted. The property of method I and method II is characterized by both in-control and out-of-control ARL values. We fixed the in-control ARL_0=200 for both methods. The out-of-control ARL, denoted by ARL_1, is the smaller the better. The smallest ARL_1 of both methods for all scenarios are shown in Table 5-1, which can also be used for MEWMA design since λ and H are readily available. In Table 5-1, the values of ARL_1 of both methods are close to each other when the correlation coefficient, ρ, is low or moderate. However, once ρ is high, the ARL_1 is dramatically decreased in all scenarios. For example, the ARL_1 for the case of small shift of scenario 2 is 36.349 when ρ=0.3, but it decreases to 19.901 when ρ=0.9. This crucial result confirms the research hypothesis that highly correlated profiles enhance detection power. This result also justifies the merit of the use of multivariate control charts to monitor all profiles simultaneously rather than monitoring one profile at a time.

Table 5-1 The smallest ARL_1 method I method II under different correlation structures in all scenarios.

		ρ=0.3		ρ=0.5		ρ=0.9	
		Method I	**Method II**	**Method I**	**Method II**	**Method I**	**Method II**
Scenario	Shift Size	λ=0.1 H=14.03	λ=0.1 H=25.90	λ=0.1 H=14.49	λ=0.1 H=28.28	λ=0.1 H=14.49	λ=0.1 H=33.01
1	Small	**2.981**	3.994	**2.922**	4.140	**1.695**	2.103
	Medium	**1.480**	1.827	**1.468**	1.873	**1.205**	1.259
	Large	**1.101**	1.233	**1.107**	1.253	**1.061**	1.081
2	Small	36.349	**2.477**	37.816	**2.562**	19.901	**1.706**
	Medium	18.203	**1.480**	18.407	**1.555**	9.160	**1.069**
	Large	10.474	**1.136**	10.470	**1.171**	5.333	**1.018**
3	Small	**1.753**	2.369	**1.753**	2.604	**1.513**	1.914
	Medium	**1.070**	1.195	**1.055**	1.244	**1.006**	1.260
	Large	**1.001**	1.006	**1.000**	1.006	**1.000**	1.001
4	Small	18.390	**1.385**	20.123	**1.552**	25.526	**2.181**
	Medium	9.389	**1.054**	10.341	**1.131**	13.240	**1.471**
	Large	5.696	**1.003**	6.339	**1.015**	8.163	**1.173**
5	Small	2.907	**1.730**	2.968	**1.791**	2.048	**1.151**
	Medium	1.476	**1.101**	1.497	**1.120**	1.208	**1.039**
	Large	1.103	**1.004**	1.110	**1.006**	1.044	**1.006**

Moreover, method I performs better (i.e. smaller ARL1 values) in scenario 1 and scenario 3 comparing to method II, while the method II has lower ARL_1 in scenario 2, 4 and 5 than method I. In summary, when the shape of a profile change entirely, such as, scenario 1 and 3, method I is recommended. Otherwise, method II is recommended for the other cases, such as, scenarios 2, 4, and 5, where profiles shift partially. In practice, one may not know whether a profile may shift entirely or partially. It is up to the quality engineers to collect process data and identify the majority of the scenarios during a phase I study. Details of the proposed methods property, ARL_0 and ARL_1, for all five scenarios in the simulation study are shown in Table A5.1and Table A5.2 in the Appendix.

We suggest the following strategy for users to implement the proposed methods. First, users should determine whether segmentations of profiles are appropriate or not. Second, they should also examine whether a linear model or nonlinear model can be used to fit the entire profile or a segment of a profile. For example, the shape of temperature profiles in the curing process consists of three stages the heat-up stage, the curing stage and the cool-down stage. If users need to know at what stage a profile may be out of control, then profiles need to be divided into three segments. A linear model is adequate for the curing stage since the profile shape in this stage is a straight line. However, nonlinear models are needed to fit the warm-up stage and the cool-down stage. If users are confident in their process is stable and they only intent to know whether the process is in-control or not, method I is capable of fulfilling this need with its simplicity. Nonlinear models should be used to fit the entire temperature and pressure profiles.
If the number of segments times the number of profile types is larger than 10, the conventional multivariate control chart may lose its effectiveness (Montgomery, 2009) such that the proposed methods work worse than the nominal performance. To deal with this issue, users can combine method I and method II together. In other words, users can apply the hybrid method to separate process monitoring into stages if the process stages are well defined. Each stage can be treated as one complete profile period and method I can be applied to each stage. For instance, if the process can be divided into three segments, users can construct three multivariate control charts for the process. Note that each multivariate control chart is associated to each stage. The advantage of this method is that users can monitor the process and diagnose a potential problem at the end of a stage instead of the end of a process. This hybrid method maintains the effectiveness of the multivariate control chart.

In summary, the charting frameworks of method I, method II, and the hybrid method are summarized here for any general multiple profiles problem with p profiles and m segments. We assume that all profiles can be segmented at the same locations. For method I, one MEWMA chart is maintained with the plotting statistics of a $p \times 1$ vector. Each element of this vector represents an average sum of deviations of a profile from its nominal profile. Method II also maintains one MEWMA chart but with the plotting statistics of a $mp \times 1$vector. Each element of this vector is the average sum of deviation of a segment instead of a profile. Finally, the hybrid method maintains m EWMA charts with the plotting statistics of a $p \times 1$vector. Each element of this vector is the average sum of deviation of a segment. All segments are from their respective profiles. Each MEWMA is used during a particular segment only.

5.6 A Case Study: a Curing Process of High-Pressure Hose Products

In this section, the proposed charting framework for monitoring multiple nonlinear correlated profiles is applied to a curing process that consists of temperature and pressure profiles for high-pressure hose products. PH Corporation seeking opportunities for improvement provides 154 air temperature and pressure profiles of phase I data. All 154 profiles are superimposed in Figure 5.1. Also, based on the PLC setting for temperature, each profile was divided into three segments, the heat-up stage, curing stage~~,~~ and cool-down stage. Therefore, p=3 is given for method II in the process. Since two kinds of profiles are involved, m=2 in equation (9).

Those 154 profiles are prepared for phase I control charting. In Figure 5.1, it is easy to visually identify some out-of-control profiles due to their shapes are significantly different from the major group. Figure 5.7 shows all abnormal profiles, characterized by solid lines, as well as in-control profiles, shown in shadow. Note that the abnormal profiles are excluded from the phase I control charting. Figure 5.8 shows the MEWMA control charts on the cleaned data set using (a) method I and (b) method II. From these figures, we observe that all data points are in control with its associated control limit H. Therefore, the control limit H, mean vector, and variance-covariance matrix generated from method I and method II are used in phase II process for further process monitoring.

The issue of losing effectiveness using the multivariate control chart caused by the number of input variables larger than 10 may happen when the number of segments and number of profile types are large. To deal with this problem, the hybrid method is used to construct~~s~~ three MEWMA charts for heat-up, curing, and cool-down stage, respectively. Figure 5.9 shows the phase I MEWMA control charts for these three stages using the hybrid methods. Note that, since the number of profile types in each control chart is two, users can use the same control limit H as in method I, i.e., H=14.03. By using this hybrid method, users can not only diagnose which stage is responsible for the out-of-control signal, but also examine the stability at the end of the stage instead of at end of the entire process. For example, if the MEWMA control chart in the heat-up stage signal for out-of-control, operators can determine to stop the curing process or not, and start to diagnose potential causes at the end of that heat-up stage rather than at the end of the curing process. Early detection of process faults provides energy savings and assures product quality.

Figure 5.7 Abnormal (a) temperature profiles and (b) pressure profiles superimposed on in-control profiles.

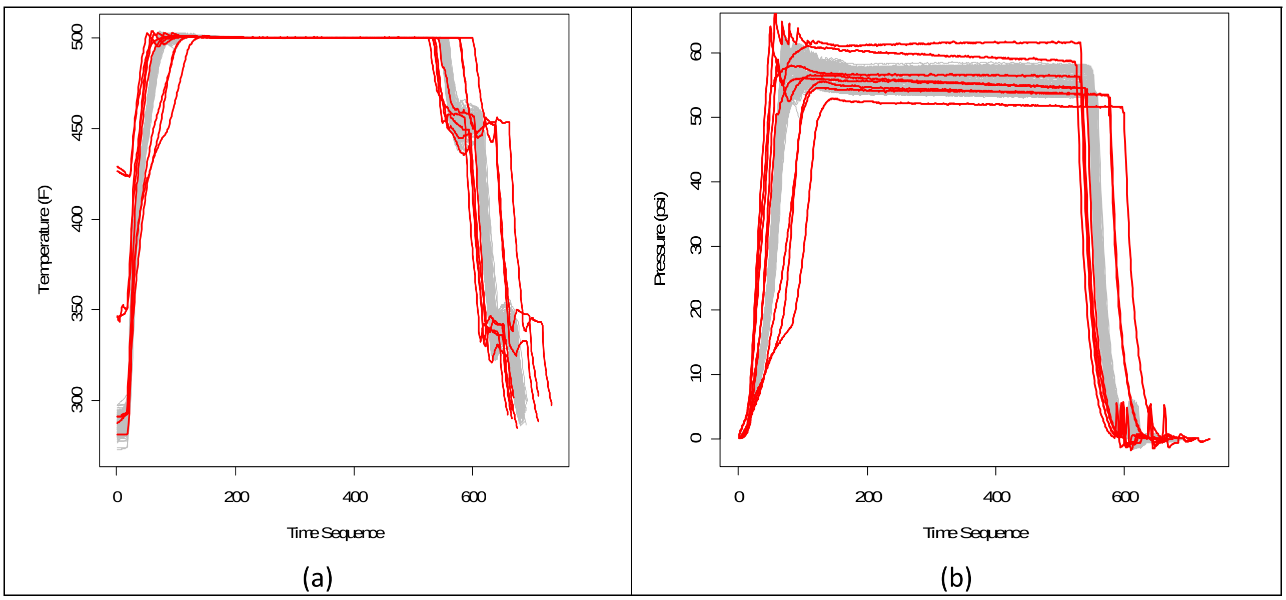

Figure 5.8 **The phase I process MEWMA control charts of curing process of high-pressure hose products using (a) method I and (b) method II.**

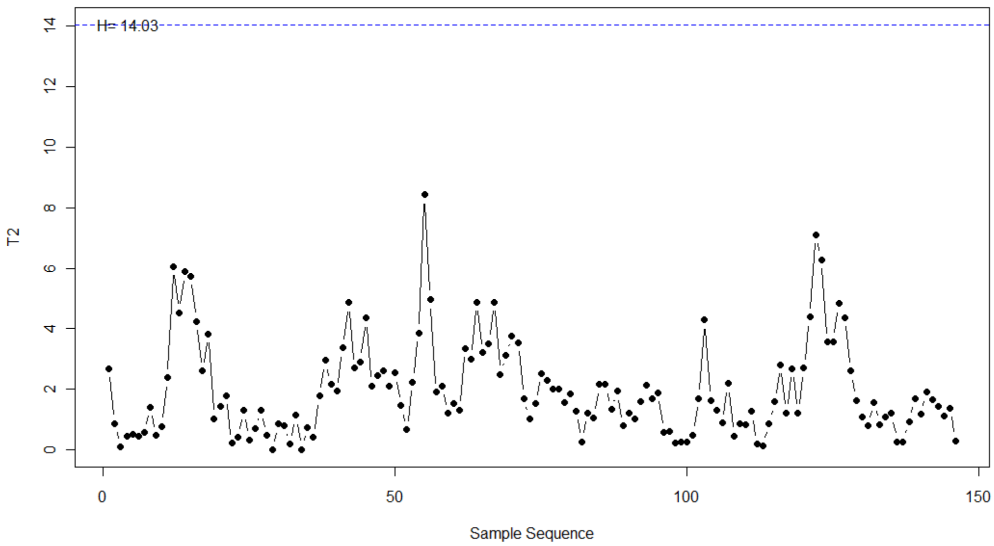

(a)

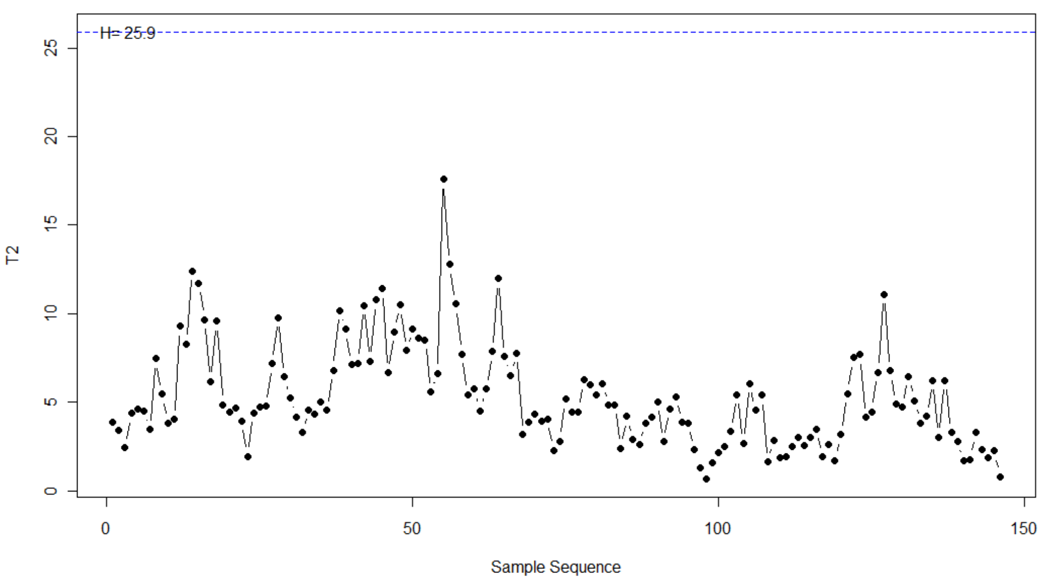

(b)

Figure 5.9 **Phase I control charts of the curing process using the hybrid method.**

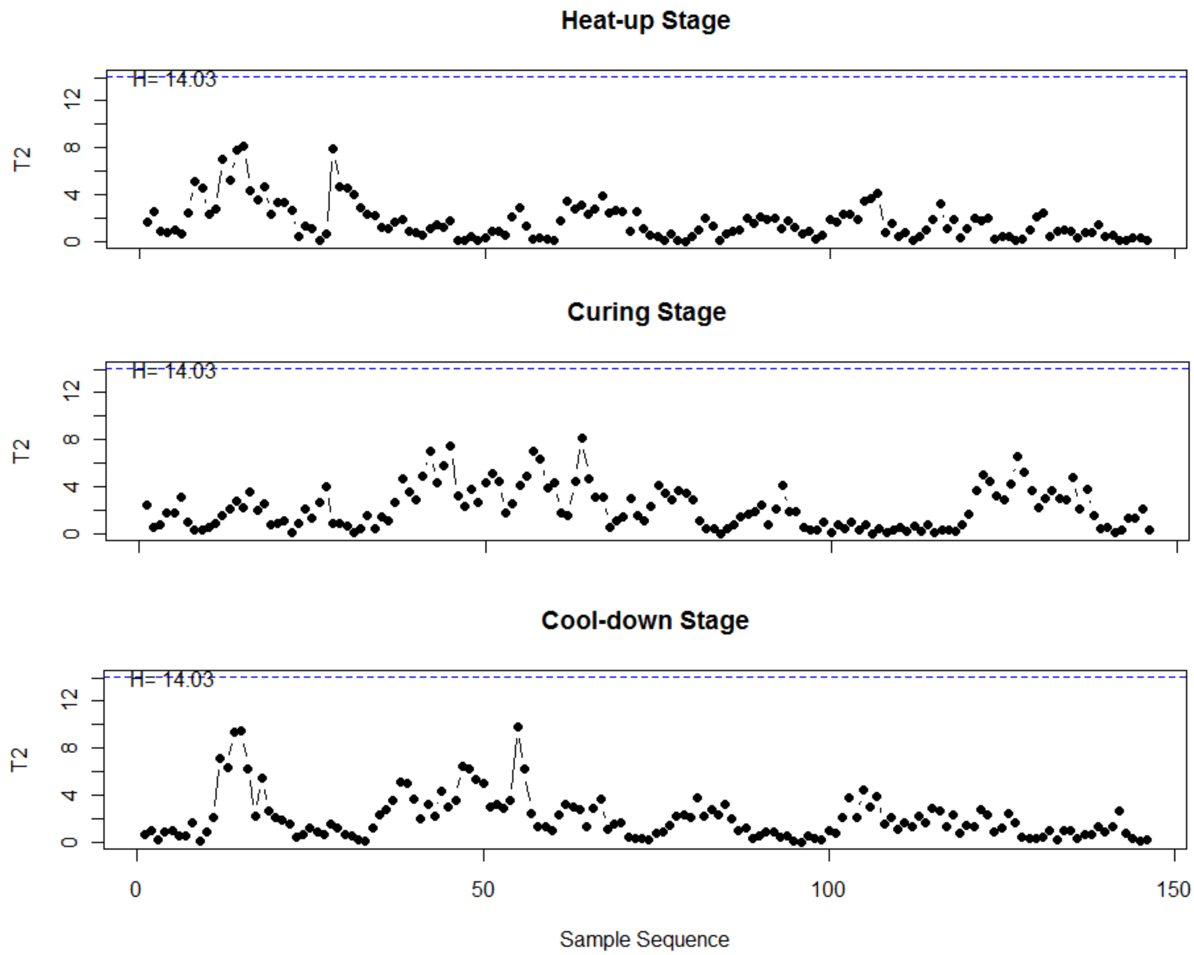

5.7 Conclusion and Future Study

Most profile analysis research up to date deals with the monitoring of single profile, but applications, such as, the hydraulic press machine and the curing process of high-pressure hose products, contain multiple correlated profiles for process monitoring. Although the monitoring of each type of profiles independently may be considered as an approach for detecting abnormal ones, high false alarm and low detecting power may be a consequence when given profiles are highly correlated. This study aims to tackle this problem by providing a framework for the process monitoring when the process consists of multiple linear or nonlinear correlated profiles. The proposed method I applies the modified Chang and Yadama's method that extends one profile process monitoring method (with *m* segments) to a multiple profile solution (each profile representing a segment). The proposed method II divides each profile into p segments first, and then applies the modified Chang and Yadama's method to each segment. Therefore, the multiple-profile problem can be considered as a multivariate statistical process control problem with the number of input variables $m \times p$. According to the simulation study, the method I has better performance in terms of out-of-control ARL values when the shape of profiles is changed entirely in the process, and method II is more sensitive when the process experiences partial profiles changes.

Additionally, the simulation results show that when profiles are highly correlated, the detecting power of the proposed method is much better than those cases with lower correlations. In a real-world case study, both method I and method II are capable of constructing the phase I process control chart if the product of the number of segments and the number of profile types is smaller than 10. The hybrid method that combines method I and method II are also investigated to provide quality engineers a broader view of diagnosis and maintains the effectiveness of detecting power. Moreover, since the proposed methods are sharing the common treatment of Chang and Yadama's (2010) method, they can handle the different shapes from other applications as long as profiles in the process have their own desired shapes with gold reference profiles existed. For example, the shape of temperature and pressure profiles generated from a curing process of high-pressure hose products follow their respective shapes, and the proposed methods all construct the phase I control chart without generating any false alarm signals.

Although the proposed methods show capability of dealing with multiple nonlinear profiles on monitoring products' quality perspective, they have some limitations. First, although the method I is capable of detecting entire shape shifted scenario, it lack of diagnosis ability when the process goes out-of-control. Second, even though the method II provides quality engineers more information in regards to diagnostic purpose, it will be less efficient if the number of segments times the profile types is over 10. Finally, the hybrid method takes care of those disadvantages that provided by the method I and method II, but it will be distract if there are too many segments have been defined. The future study of profile analysis should be extended to cover all the disadvantages of the proposed methods and to be applied for more complicated data sets, such as, the data sets of images and spatial surface.

Reference

Chang, S.I. and Chou, S.H., 2009. A Study of Using Wavelet Transformation and B-Spline Approximation for Nonlinear Profiles Monitoring, Proceedings of the 2009 Industrial Engineering Research Conference (IERC), 1567-1572, Miami, Florida, May 30-June 03.

Chang, S.I. and Chou, S.H., 2010. A Visualization Decision Support Tool for Multivariate SPC Diagnosis Using Marginal CUSUM Glyphs, *Quality Engineering*, 22(3):182-198.

Chang, T. C., Gan, F. F., 2006. Monitoring Linearity of Measurement Gauges. *Journal of Statistical Computation and Simulation*, 76(10):889-911.

Chang, S.I., Tsai, T.R., Lin, D.K.J., Chou, S.H., and Lin, Y.S., 2012. Statistical Process Control for Monitoring Nonlinear Profiles: A Six Sigma Project on Curing Process, *Quality Engineering*, 24(2):251-263.

Chang, S.I. and Yadama, S., 2010. Statistical Process control for Monitoring Non-linear Profiles using Wavelet Filtering and B-Spline Approximation, *International Journal of Production Research*, 48(4):1049-1068.

Chicken, E. Pignatiello, Jr., J., andSimpson, J.R., 2009. Statistical Process Monitoring of Nonlinear Profiles Using Wavelets, *Journal of Quality Technology,* 41(2), 198-212.

Chen, S. and Nembhard, H.B., 2011. A High-dimensional Control Chart for Profile Monitoring, *Quality and Reliability Engineering International*, 27(4):451-464.

Ding, Y., Zeng, L., and Zhou, S., 2006. Phase I Analysis for Monitoring Nonlinear Profiles in Manufacturing Processes, *Journal of Quality Technology*, 38(3), 199-216.

Holmes, D. S. and Mergen, A. E., 1993. Improving the Performance of the T2 Control Chart, *Quality Engineering*, 5(4):619-625.

Jensen, W.A. and Birch, J.B., 2009. Profile Monitoring Via Nonlinear Mixed Models, *Journal of Quality Technology* 41(1):18-34.

Jensen, W.A., Birch, J.B., and Woodall, W.H., 2008. Monitoring Correlation within Linear Profiles using Mixed Models, *Journal of Quality Technology*, 40(2):167-183.

Jin, J., and Shi, J., 1999. Feature-Preserving Data Compression of Stamping Tonnage Information Using Wavelets, *Technometrics* 41(4):327–339.

Kazemzadeh, R.B., Noorossana, R., Amiri, A., 2008. Phase I Monitoring of Polynomial Profiles, *Communications in Statistics—Theory and Methods*, 37(10):1671-1686.

Kang, L.; Albin, S. L., 2000. On-Line Monitoring when the Process Yields a Linear Profile, *Journal of Quality Technology*, 32(4):418-426.

Kim, K., Mahmoud, M. A. and Woodall, W. H., 2003. On the Monitoring of Linear Profiles, *Journal of Quality Technology*, 35:317-328.

Lowry, C.A., Woodall, W.H., Champ, C.W., and Rigdon, S.E., 1992. A Multivariate Exponentially Weighted Moving Average Control Chart, *Technometrics*, 34(1):46-53.

Mahmoud, M. A., 2008. Phase I Analysis of Multiple Regression Linear Profiles, *Communications in Statistics - Simulation and Computation*, 37(10):2106-2130.

Mason, R.L., Tracy, N.D., and Young, J.C., 2001. A Practical Approach for Interpreting Multivariate T2 Control Chart Signals, *Journal of Quality Technology*, 29 (4):396 – 406.

Montgomery, D. C., 2009. *Introduction to statistical quality control.* New York, NY: John Wiley & Sons.

Noorossana, R., Amiri, A., and Soleimani, P., 2008. On the Monitoring of Autocorrelated Linear profiles, *Communications in Statistics-Theory and Methods*, 37(3):425-442.

Noorossana, R, Eyvazian, M., Vaghefi, A., 2010. Phase II Monitoring of Multivariate Simple Linear Profiles, *Computers & Industrial Engineering,* 58(4):563-570.

Noorossana, R., Saghaei, A., and Amiri, A., 2011. *Statistical Analysis of Profile Monitoring,* Hoboken, New Jersey: John Wiley & Sons, Inc.

Paynabar, K. and Jin, J., 2011. Characterization of Non-linear Profiles Variations using Mixed-effect Models and Wavelets, *IIE Transactions*, 43(4):275-290.

Prabhu, S.S. and Runger, G.C., 1997. Designing a Multivariate EWMA Control Chart, *Journal of Quality Technology*, 29(1):8-15.

Qiu, P., Zou, C. and Wang, Z., 2010. Nonparametric Profile Monitoring by Mixed Effects Modeling, *Technometrics,* Vol. 52(3):265-277.

Reis, M.S., SARAIVA, P.M., 2006. Multiscale Statistical Process Control of Paper Surface Profiles, *Quality Technology and Quantitative Management*, 3(3):263-282.

Shiau, J.J.H., Huang, H.L., Lin, S.H., and Tsai, M.Y., 2009. Monitoring Nonlinear Profiles with Random Effects by Nonparametric Regression, *Communications in Statistics-Theory and Methods*, 38(10):1664-1679.

Walker, E. and Wright, S. P., 2002. Comparing Curves Using Additive Models, *Journal of Quality Technology*, 34(1):118-129.

Williams, J. D., Woodall, W. H., and Birch, J. B., 2007. Statistical Monitoring of Nonlinear Product and Process Quality Profiles, *Quality & Reliability Engineering International*, 23(7):925-941.

Woodall, W.H., 2007. Current Research on Profile monitoring, *Produção* 17(3):420-425.

Zou, C.,Tsung, F., and Wang, Z., 2007. Monitoring General Linear Profiles Using Multivariate Exponentially Weighted Moving Average Schemes, *Technometrics*, 49(4):395-408.

Appendix

Table A5.1 The average run length of method I with three different correlation structures.

Method I									
ρ=0.3									
λ	0.1	0.2	0.3	0.4	0.5	0.6	0.7	0.8	0.9
H	14.03	15.81	16.97	17.86	18.61	19.13	19.55	19.87	19.98
ARL_0	200.170	199.925	199.809	200.167	199.617	199.829	199.840	200.167	199.809
Scen. 1 (small)	2.981	3.203	3.400	3.614	3.896	4.242	4.705	5.275	5.987
Scen. 1 (medium)	1.480	1.554	1.608	1.665	1.717	1.760	1.821	1.897	2.014
Scen. 1 (large)	1.101	1.125	1.142	1.162	1.174	1.184	1.195	1.205	1.214
Scen. 2 (small)	36.349	49.035	59.258	68.725	76.818	83.557	88.074	94.022	99.801
Scen. 2 (medium)	18.203	24.604	30.988	37.398	43.991	49.290	55.851	62.033	66.700
Scen. 2 (large)	10.474	13.208	16.867	21.015	23.316	29.945	34.551	39.603	44.195
Scen. 3 (small)	1.753	1.886	1.976	2.053	2.163	2.277	2.432	2.662	2.886
Scen. 3 (medium)	1.070	1.091	1.107	1.122	1.135	1.144	1.155	1.164	1.173
Scen. 3 (large)	1.001	1.001	1.002	1.002	1.003	1.004	1.004	1.004	1.004
Scen. 4 (samll)	18.390	23.135	27.833	32.099	36.519	40.005	43.883	47.784	51.197
Scen. 4 (medium)	9.389	11.178	13.228	15.711	18.580	21.055	23.962	27.048	29.549
Scen. 4 (large)	5.696	6.504	7.522	8.668	10.082	11.653	13.457	15.642	18.002
Scen. 5 (small)	2.907	3.135	3.301	3.493	3.743	4.047	4.386	4.935	5.499
Scen. 5 (medium)	1.476	1.545	1.594	1.641	1.696	1.732	1.785	1.864	1.953
Scen. 5 (large)	1.103	1.128	1.145	1.163	1.175	1.186	1.194	1.205	1.217
ρ=0.5									
λ	0.1	0.2	0.3	0.4	0.5	0.6	0.7	0.8	0.9
H	14.49	16.26	17.55	18.52	19.28	19.83	20.3	20.57	20.72
ARL_0	199.870	199.829	200.106	200.249	199.916	199.809	200.152	200.166	199.870
Scen. 1 (small)	2.922	3.163	3.369	3.571	3.834	4.165	4.638	5.218	5.852
Scen. 1 (medium)	1.468	1.541	1.592	1.646	1.701	1.748	1.811	1.886	1.983
Scen. 1 (large)	1.107	1.132	1.155	1.172	1.185	1.198	1.210	1.221	1.238
Scen. 2 (small)	37.816	49.977	61.750	71.478	80.470	86.518	92.114	96.633	102.777
Scen. 2 (medium)	18.407	24.791	32.102	39.083	45.808	51.963	58.493	64.189	69.712
Scen. 2 (large)	10.470	13.175	17.043	21.470	26.123	31.187	36.361	41.304	46.366
Scen. 3 (small)	1.753	1.891	2.002	2.115	2.255	2.419	2.654	2.930	3.265
Scen. 3 (medium)	1.055	1.079	1.096	1.111	1.125	1.134	1.148	1.160	1.171
Scen. 3 (large)	1.000	1.000	1.001	1.001	1.001	1.001	1.001	1.001	1.001
Scen. 4 (samll)	20.123	25.168	30.797	35.059	40.091	43.785	47.510	51.021	55.109
Scen. 4 (medium)	10.341	12.377	14.897	17.851	20.570	23.577	26.695	29.542	32.576
Scen. 4 (large)	6.339	7.271	8.485	9.909	11.521	13.280	15.450	17.942	20.349
Scen. 5 (small)	2.968	3.192	3.398	3.596	3.857	4.185	4.604	5.130	5.797
Scen. 5 (medium)	1.497	1.569	1.623	1.677	1.727	1.770	1.837	1.913	2.026

Scen. 5 (large)	1.110	1.135	1.154	1.174	1.186	1.194	1.210	1.220	1.236
				ρ=0.9					
lambda	0.1	0.2	0.3	0.4	0.5	0.6	0.7	0.8	0.9
H	14.49	15.95	16.99	17.81	18.4	18.9	19.16	19.38	19.43
ARL_0	199.995	199.809	199.743	199.731	199.840	200.167	200.167	200.152	200.098
Scen. 1 (small)	1.695	1.741	1.767	1.792	1.814	1.825	1.843	1.869	1.881
Scen. 1 (medium)	1.205	1.219	1.229	1.236	1.244	1.250	1.253	1.259	1.261
Scen. 1 (large)	1.061	1.067	1.073	1.076	1.078	1.082	1.084	1.085	1.085
Scen. 2 (small)	19.901	24.360	29.931	35.278	41.769	48.012	53.213	58.377	62.349
Scen. 2 (medium)	9.160	10.493	12.289	14.643	17.444	20.958	24.490	28.552	32.204
Scen. 2 (large)	5.333	5.852	6.479	7.379	8.526	10.127	11.763	13.906	16.345
Scen. 3 (small)	1.513	1.590	1.652	1.713	1.762	1.827	1.888	1.941	1.972
Scen. 3 (medium)	1.006	1.020	1.038	1.049	1.062	1.073	1.081	1.088	1.091
Scen. 3 (large)	1.000	1.000	1.000	1.000	1.000	1.000	1.000	1.000	1.000
Scen. 4 (samll)	25.526	31.831	37.762	43.219	48.015	52.195	55.907	59.355	62.502
Scen. 4 (medium)	13.240	16.166	19.269	22.902	26.093	29.443	32.566	35.929	39.076
Scen. 4 (large)	8.163	9.380	10.997	12.814	14.774	17.386	19.817	22.445	25.021
Scen. 5 (small)	2.048	2.136	2.196	2.258	2.326	2.405	2.481	2.603	2.747
Scen. 5 (medium)	1.208	1.233	1.246	1.258	1.269	1.275	1.283	1.294	1.300
Scen. 5 (large)	1.044	1.051	1.054	1.058	1.060	1.062	1.062	1.064	1.064

Table A5.2 The average run length of method II with three different correlation structures.

				Method II					
				ρ=0.3					
λ	0.1	0.2	0.3	0.4	0.5	0.6	0.7	0.8	0.9
H	25.9	30.85	35.68	40.12	44.13	47.45	50.14	52.09	53.3
ARL_0	199.958	199.829	199.809	199.967	200.173	199.989	199.905	199.910	200.157
Scen. 1 (small)	3.994	4.754	5.920	7.896	11.420	17.129	26.333	39.057	55.486
Scen. 1 (medium)	1.827	2.076	2.350	2.655	3.075	3.673	4.565	6.151	8.515
Scen. 1 (large)	1.233	1.323	1.426	1.538	1.668	1.789	1.966	2.217	2.549
Scen. 2 (small)	2.477	2.812	3.152	3.583	4.008	4.425	4.776	5.004	5.128
Scen. 2 (medium)	1.480	1.659	1.828	1.995	2.169	2.378	2.592	2.823	3.011
Scen. 2 (large)	1.136	1.229	1.331	1.431	1.524	1.619	1.726	1.873	2.035
Scen. 3 (small)	2.369	2.807	3.319	4.021	5.273	7.464	11.209	17.554	27.241
Scen. 3 (medium)	1.195	1.297	1.417	1.552	1.696	1.848	2.044	2.332	2.833
Scen. 3 (large)	1.006	1.015	1.031	1.057	1.083	1.105	1.132	1.153	1.175
Scen. 4 (samll)	1.385	1.544	1.672	1.821	1.964	2.101	2.241	2.368	2.470
Scen. 4 (medium)	1.054	1.099	1.155	1.209	1.262	1.319	1.371	1.416	1.463
Scen. 4 (large)	1.003	1.009	1.016	1.029	1.044	1.063	1.083	1.107	1.111
Scen. 5 (small)	1.730	1.964	2.198	2.440	2.740	3.050	3.459	3.829	4.169

Scen. 5 (medium)	1.101	1.166	1.247	1.323	1.403	1.476	1.560	1.648	1.752
Scen. 5 (large)	1.004	1.010	1.021	1.037	1.053	1.068	1.085	1.100	1.113
ρ=0.5									
λ	0.1	0.2	0.3	0.4	0.5	0.6	0.7	0.8	0.9
H	28.28	34.4	40.14	45.58	50.21	54.05	56.94	59.14	60.46
ARL0	200.002	199.826	199.918	199.918	200.157	199.890	200.026	200.261	200.009
Scen. 1 (small)	4.140	5.068	6.520	9.160	13.793	22.487	36.628	55.881	78.656
Scen. 1 (medium)	1.873	2.185	2.487	2.860	3.376	4.108	5.312	7.541	10.969
Scen. 1 (large)	1.253	1.363	1.477	1.615	1.760	1.917	2.143	2.431	2.876
Scen. 2 (small)	2.562	2.946	3.353	3.806	4.288	4.704	5.004	5.217	5.377
Scen. 2 (medium)	1.555	1.753	1.937	2.134	2.326	2.542	2.799	3.039	3.189
Scen. 2 (large)	1.171	1.296	1.421	1.524	1.632	1.751	1.894	2.062	2.246
Scen. 3 (small)	2.604	3.188	3.963	5.355	8.145	13.603	23.815	39.324	60.158
Scen. 3 (medium)	1.244	1.412	1.593	1.786	2.009	2.284	2.727	3.555	5.149
Scen. 3 (large)	1.006	1.020	1.051	1.092	1.140	1.194	1.242	1.294	1.352
Scen. 4 (samll)	1.552	1.727	1.910	2.078	2.243	2.385	2.536	2.684	2.778
Scen. 4 (medium)	1.131	1.206	1.280	1.371	1.438	1.505	1.577	1.644	1.710
Scen. 4 (large)	1.015	1.033	1.061	1.102	1.141	1.177	1.204	1.231	1.263
Scen. 5 (small)	1.791	2.059	2.315	2.584	2.927	3.329	3.785	4.211	4.630
Scen. 5 (medium)	1.120	1.204	1.296	1.384	1.481	1.567	1.661	1.774	1.910
Scen. 5 (large)	1.006	1.016	1.030	1.050	1.070	1.093	1.113	1.133	1.151
ρ=0.9									
lambda	0.1	0.2	0.3	0.4	0.5	0.6	0.7	0.8	0.9
H	33.01	42.39	51.24	58.85	65.58	71.08	75.29	78.35	79.98
ARL_0	199.989	199.850	200.026	200.289	199.826	199.936	200.164	199.826	199.826
Scen. 1 (small)	2.103	2.590	3.096	3.683	4.451	5.813	8.575	13.740	23.184
Scen. 1 (medium)	1.259	1.352	1.463	1.582	1.705	1.825	1.968	2.143	2.359
Scen. 1 (large)	1.081	1.118	1.157	1.188	1.214	1.234	1.261	1.286	1.303
Scen. 2 (small)	1.706	2.172	2.520	2.906	3.377	4.022	4.677	5.181	5.428
Scen. 2 (medium)	1.069	1.187	1.377	1.567	1.749	1.891	2.056	2.335	2.686
Scen. 2 (large)	1.018	1.029	1.049	1.081	1.133	1.193	1.259	1.308	1.350
Scen. 3 (small)	1.914	2.386	2.934	3.507	4.032	4.585	5.046	5.445	5.723
Scen. 3 (medium)	1.260	1.453	1.673	1.897	2.208	2.610	3.038	3.462	3.849
Scen. 3 (large)	1.001	1.035	1.151	1.297	1.409	1.500	1.617	1.826	2.137
Scen. 4 (samll)	2.181	2.479	2.773	3.091	3.366	3.569	3.665	3.737	3.777
Scen. 4 (medium)	1.471	1.660	1.842	1.998	2.151	2.312	2.433	2.520	2.556
Scen. 4 (large)	1.173	1.308	1.436	1.538	1.640	1.751	1.881	2.010	2.116
Scen. 5 (small)	1.151	1.269	1.459	1.643	1.808	1.984	2.187	2.464	2.876
Scen. 5 (medium)	1.039	1.052	1.065	1.075	1.084	1.093	1.099	1.104	1.109
Scen. 5 (large)	1.006	1.012	1.015	1.018	1.022	1.025	1.026	1.028	1.029

Chapter 6 Optimizing Cellulosic Biomass Pellets Quality via Multiple Temperature Profiles using PCA and Desirability Functions

Paper Title:

Optimizing Cellulosic Biomass Pellets Quality via Multiple Temperature Profiles using PCA and Desirability Functions.

Submit to:

International Journal of Experimental Design and Process Optimisation

Author's Name:

Shih-Hsiung Chou, Shing I Chang, Qi Zhang, Penfei Zhang, and Z.J. Pei

Authors' Affiliations:

Department of Industrial and Manufacturing Systems Engineering, Kansas State University, USA.

Abstract

Cellulosic biomass pelleting using ultrasonic vibration-assisted machine is an alternative to manufacturing biomass pellets. Both density and durability of the biomass pellets are critical quality characteristics. However, measurement of those characteristics requires destructive tests, which means pellets have to be destroyed for measurement. This study investigates an alternative for nondestructive test. Specifically, multiple temperature profiles recorded from six locations of a biomass pellets are used as surrogate response variables to density and durability. The proposed analysis method adopts the use of both the principal component analysis and desirability functions. The experimental results show that the multiple temperature profiles can be used as surrogate response factors to replace the density and durability. In addition, this study provides a predictive modeling approach for users to forecast biomass pellets' density and durability given a multiple temperature profiles.

6.1 Introduction

Biomass-based fuel ethanol has been used as an alternative to the petroleum based liquid fuels in recent years. Petroleum not only is a finite and non-renewable resource but also contributes to the greenhouse gas (GHG). Cellulosic ethanol is one of the biomass-based fuel ethanol produced by cellulosic biomass. Rubin (2008) pointed out that cellulosic biomass is often made from fibrous, woody, or wheat straw particles. The use of cellulosic-based biomass as a source to produce biofuel is beneficial in that it will not affect food and feed sources like sugar- or starch-based feedstock. In addition, Lynd (2003) reported that producing cellulosic biomass from crops may use less energy, fertilizer, and pesticide so that the soil fertility may be improved.

To produce the cellulosic ethanol, Rubin (2008) introduced the major steps in biofuel manufacturing: (1) harvest and collection; (2) transportation and handling; (3) storage; (4) pretreatment; (5) hydrolysis; and (6) fermentation. Note that the pretreatment process contributes to the lignin and crystalline destruction of cellulose so that it is easier for hydrolysis process to degrade the cellulose into its component sugars using enzyme preparations. Then, the fermentation process uses microbes to convert sugars into ethanol.

In order to produce cellulosic ethanol more efficiently, transportation, handling, and storage may play an important role in mass production of manufacturing cellulosic ethanol. Two factors has significant effects on those processes: density and durability of biomass pellets (Zhang, 2011; Zhang, 2013; Zhang et al., 2013). Both Zhang (2011) and Zhang (2013) indicated that the density will increase cellulosic ethanol yields and the durability of biomass pellets will enhance the efficiency in transportation. To increase the density and durability of the biomass pellets, pelleting methods have been considered in many studies, for example, screw extruder, a briquetting press, or a rolling machine, but extra manufacturing aids are required, such as, high-temperature steam, high pressure, and binder materials (Mani et al., 2003; Sokhansanj et al., 2005). Moreover, many researchers (Reece, 1966; Faborode, 1990; Van Dam et al., 2004, and Kaliyan et al., 2009) have provided evidence that providing high temperature during the manufacturing may result in good quality biomass pellets. However, producing high temperature steam requires more energy.

Ultrasonic vibration-assisted (UVA) pelleting is an alternative to traditional pelleting methods. It has been proven that this pelleting method can increase the density and durability of the biomass pellets significantly (Zhang, 2013 and Zhang et al., 2013). However, measurement the density and durability of the biomass pellets requires operation stoppages. Intervention from the quality engineers may slow down the production speed. Furthermore, the durability test of biomass pellets involves a destructive test.

This study explores the feasibility of a nondestructive measurement of pellet density and durability via temperature profiles recorded from six locations within a biomass pellet mold. These temperature profiles can be measured on a real-time basis so that a production line is not interrupted due to sampling.

The goal of this study is to verify that the temperature profiles collected from six locations of a pellet can be used as surrogate response variables to density and durability to reflect pellet quality. This study involves the use of two-level full factorial design within the feasible region. Further, desirability functions, developed by Derringer and Suich's (1980), are constructed based on the data collected from both experiments.

The applications of full factorial designs and desirability functions for multiple response surface methodology (Myers et al., 2009) often deal with response variables in a vector rather than profiles. In this study, the temperature profiles collected from six-locations of a biomass pellet are recorded over time in a matrix form. For example, if 180 data points are recorded every second, this matrix has a dimension of 180 x 6. Note that the conventional full factorial design and desirability functions cannot handle this problem directly. Therefore, this study applies the principal component analysis (PCA) method as a dimension reduction method to reduce the dimension from the form of a matrix to a vector so that the conventional multiple-response methods can be applied.

The organization of this paper is as follows. First, the experiment details including the setup of machine, the experimental design, and the input and output variables will be presented. After that, the proposed methodology of this study will be introduced, followed by the experimental results and discussions. At the end of this paper, conclusions will be drawn and the future study will be discussed.

6.2 Experiment Details

The main hypothesis of this study is that the temperature profiles collected from a biomass pellet can be used to measure the quality of pellets instead of using density and durability of the biomass pellet. Experiment details are presented in this section. First, the experiment setup including the components of UV-A machine and its specifications is introduced. Then, the procedure of finding the optimized input variable setting using the responses variables of density and durability is presented. After that, the optimal setting using multiple temperature profiles as responses is given. Finally, the details of input variables and measurement of response variables are introduced.

6.2.1 Experiment Setup

The UV-A biomass pelleting process has been proven to increase cellulosic ethanol yield, density of biomass pellet, and durability of pellet during transportation (Zhang and Pei, 2010; Zhang et al., 2010; Zhang, 2013). In this study, the identical UV-A biomass pelleting machine and setup from Zhang and Pei's (2010) study is applied to produce biomass pellets with the factors of pelleting pressure, ultrasonic power, and biomass weight. The schematic UV-A machine setup is shown in Figure 6.1. The UV-A can be presented in three parts, pneumatic loading system, ultrasonic generation system, and temperature measurement system. In pneumatic loading system, air pressure is generated from a 1.2 kW, 125 liter air compressor and passed through a pressure regulator to the pneumatic cylinder. The compressed air provides energy to the pneumatic cylinder to push down the pelleting tool to press the biomass in the mold. In ultrasonic generation system, the power supply converts electrical power of 60 Hz to 20 kHz providing mechanical motion energy so that the converter can generate high frequency for UV-A machine. The titanium-made pelleting tool is connected to the ultrasonic spindle to press biomass material. At the bottom of the UV-A machine are the mold and its holding system along with temperature measurement system. The mold is filled with biomass material and is setup on a fixture platform on a machine table. This setup can prevent the pelleting tool from nonalignment to the hold in the mold. Finally, in the temperature measurement system contains thermocouples, a thermometer, and a computer with data acquisition software package. Six thermocouples are inserted into the mold at six different locations as presented in Figure 6.2. Specifically, in the center axis of the pellet, temperatures at three locations will be recorded: the location of top center (TC), middle center (MC), and bottom center (BC). Meanwhile, top side (TS), middle side (MS), and bottom side (BS) are the other thermocouples for recording temperatures in the pellet. The temperature data will be collected from a thermometer and recorded by a data acquisition software package called Temp Monitor S2 (OMEGA Engineering Inc.). The ultrasonic power is turned on for 180 seconds.

Figure 6.1 The schematic UV-A machine setup.

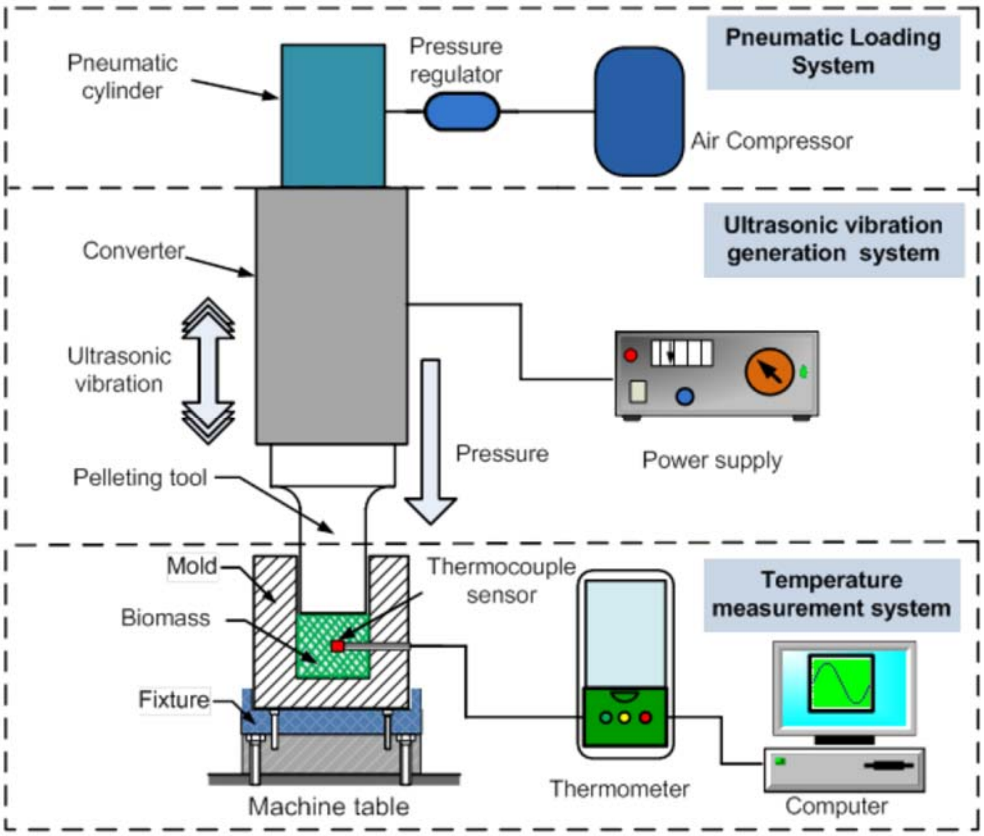

Figure 6.2 Six locations of placing thermocouples in the (a) side view and (b) top view of the mold.

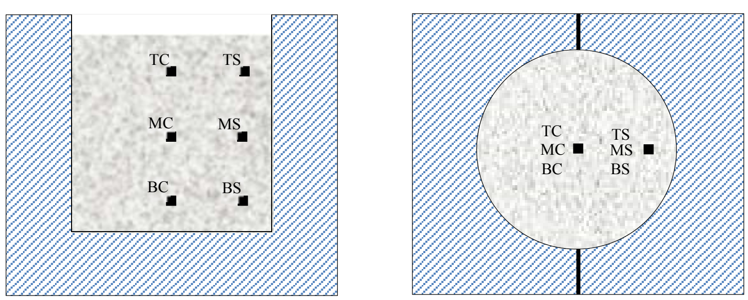

(a) Side View (b) Top View

6.2.2 Design of Experiments

There are three input variables investigated in this study: pelleting pressure, ultrasonic power, and biomass pellet weight. Those input variables are deemed as the key process variables in producing cellulosic biomass pellets (Zhang and Pei, 2010; Zhang et al., 2010; Zhang et al., 2013, Zhang, 2013). Moreover, the response variables in the experiments are pellet density, pellet durability and temperature profiles. In this study, a two-level full factorial design with four replicates of center points is used. The ranges and physical settings of the input variables in this studyare shown in Table 6-1. All the setting of input variables are identical to Zhang's study (2013). The description of the input variables and response variables are presented in following sections.

Table 6-1 Scheme of the input variables studied in the experiment.

Input Variables	*Unit*	*Levels*		
		-1(Low)	0	1(High)
Pelleting Pressure	psi	20	35	50
Ultrasonic Power	%	20	40	60
Biomass Pellet Weight	gram	1.5	2.0	2.5

6.2.3 Input Variables of the Experiment

The general format of the input variables of the experiment can be specified as equation (1):

$$X = [x_1, x_2, x_3, \dots, x_p]' \tag{1}$$

where p is the number of input variables that will be examined in the experiment. In this study, since there are three input variables to be investigated, i.e., p=3. These three variables are: pelleting pressure, ultrasonic power, and pellet weight. They will be discussed in the following sub-section.

Pelleting Pressure (PSI)

The source of the pelleting pressure (denoted as PSI) is generated by air compressor, which can be adjusted by the pressure regulator as shown in Figure 6.1. The higher pelleting pressure, the higher air pressure in the pneumatic cylinder pushes the pelleting tool. The air compressor is capable of generating the air pressure from 0 psi to 50 psi. The setting of pelleting pressure in this experiment is from 20 psi to 50 psi. The pelleting pressure is an important factor because it determines whether the pellet can be constructed or not. If the pelleting pressure is lower than 20 psi, the wheat particles cannot be formed of a pellet according to Zhang's study (2013).

Ultrasonic Power (%UVA)

The ultrasonic power (%UVA) indicates how much the electricity the power supply converting to ultrasonic vibration on biomass during the pelleting. The larger the ultrasonic power is set, the bigger vibration amplitude the converter can generate. The unit displayed on the power supply is in percentage (%). The minimum of ultrasonic power is 0% while the maximum of which is 100%. The ultrasonic power of 0% means that there is no electricity being transmitted to the converter at all. On the other hands, the ultrasonic power of 100% provides maximum power (20 kHz) to the converter. The setting of the ultrasonic power in this study is from 20% to 60%. The reason of not using 100% of ultrasonic power is because the ultrasonic machine will generate charring biomass (Feng et al., 2011 and Zhang, 2013).

Biomass Pellet Weight

The biomass pellet weight is measured by a scale from the wheat straw particles. Before running the experiment, the wheat straw particles will be weighted and inserted to the mold for making a biomass pellet. Zhang (2013) specifies the lowest value of biomass pellet weight is 1.5 gram because it was the smallest size of pellet to insert six thermocouples, while the largest value of 2.5 is due to the size of the mold.

6.2.4 Measurements of Response Variables

The response variables are outputs of evaluating the experiment. The generalization form of the response variables of experiment can be characterized as equation (2).

$$Y_i = [y_{1i}, y_{2i}, y_{3i}, \dots, y_{mi}]_i', \; i=1,2,3,\dots,n \qquad \textbf{(2)}$$

where m is the number of response variables in the experiment, i is the index of the run of experiment, and n is the number of runs of the experiment. In this study, the conventional output variables of the experiment are pellet density and durability, i.e., m=2, for assessing the quality of biomass pellets. In other words, for each run of the experiment the output is two single values that calculated by given equations that will be introduced in latter sub-sections. Moreover, Since this study applies one-block-2-level full factorial design with 4 replicates center and corner points to the experiment, the number of runs of the experiment can be determined to be 36, i.e., $p=(2^3+1)\times4=36$. In addition to those two response variables, this study obtains a surrogate response variable, multiple temperature profiles recorded from six locations of a pellet, to replace density and durability of biomass pellets. The surrogate variable that is characterized as multiple profiles data can be found in the latter sub-section as well. The general format of each run of an experiment is described as equation (3):

$$Y_i = \begin{bmatrix} t_{11i} & t_{12i} & \cdots & t_{1gi} \\ t_{21i} & t_{22i} & & t_{2gi} \\ \vdots & & \ddots & \vdots \\ t_{l1i} & t_{l2i} & \cdots & t_{lgi} \end{bmatrix}, i=1,2,3,\ldots,n \tag{3}$$

where g is the number of data points within a profile and l is the number of profiles in each run. In this study, there are six profiles will be recorded in each run of the experiment, and a thermocouple will record the temperature every second until 180 seconds. Therefore, l and g is equal to 6 and 180 in this study, respectively.

Measurement of Pellet Density

The first measurement of response variable is the in-mold density of a biomass pellet. The equation of pellet density is as equation (4):

$$Pellet\ Density = \frac{W}{H\pi\left(\frac{D}{2}\right)^2} \tag{4}$$

where W is a biomass pellet weight that measured before running UV-A machine; H is the pellet height measured when the pelleting process is finished using a digital quill; D is the pellet diameter which equals to the diameter of the mold cavity (18.6 mm), and π is a mathematical constant (3.14).

Measurement of Pellet Durability

ASAE standards S269.4 (ASAE, 2003) defines the measurement of pellet durability, which tests the ability of pellet to withstand impact from forces encountered during handling and transportation. A pellet durability tester (Seedburo Equipment, Des Plaines, IL, USA) is designed for testing the pellet durability based on ASAE standards S296.4. Biomass pellets weighted in 50 grams are loaded in the pellet durability tester tumbling for 10 minutes and followed by sieved with a U.S. No. 6 sieve. Equation (5) shows the measurement of pellet durability.

$$Pellet\ Durability = \frac{Weight\ of\ remaining\ pellets\ after\ sieving}{Weight\ of\ pellets\ before\ tumbling} \tag{5}$$

Measurement of Temperature Profiles

Temperatures within a pellet are recorded over time at six locations of the pellet as shown in Figure 6.2. The thermocouples start to record the temperatures when the pelleting process is starting. The total recording time is 180 seconds for each run of the experiment. Figure 6.3 shows the recorded temperature profiles collected from six-location of the mold with various input setting. In this study, these six temperature profiles are expected to be the surrogate response variable of the experiment to replace the density and durability of pellets during the mass production of the biomass pelleting manufacturing using the UV-A machine.

Figure 6.3 Temperature profiles recorded from six-location of the mold during the pelleting process with various input setting.

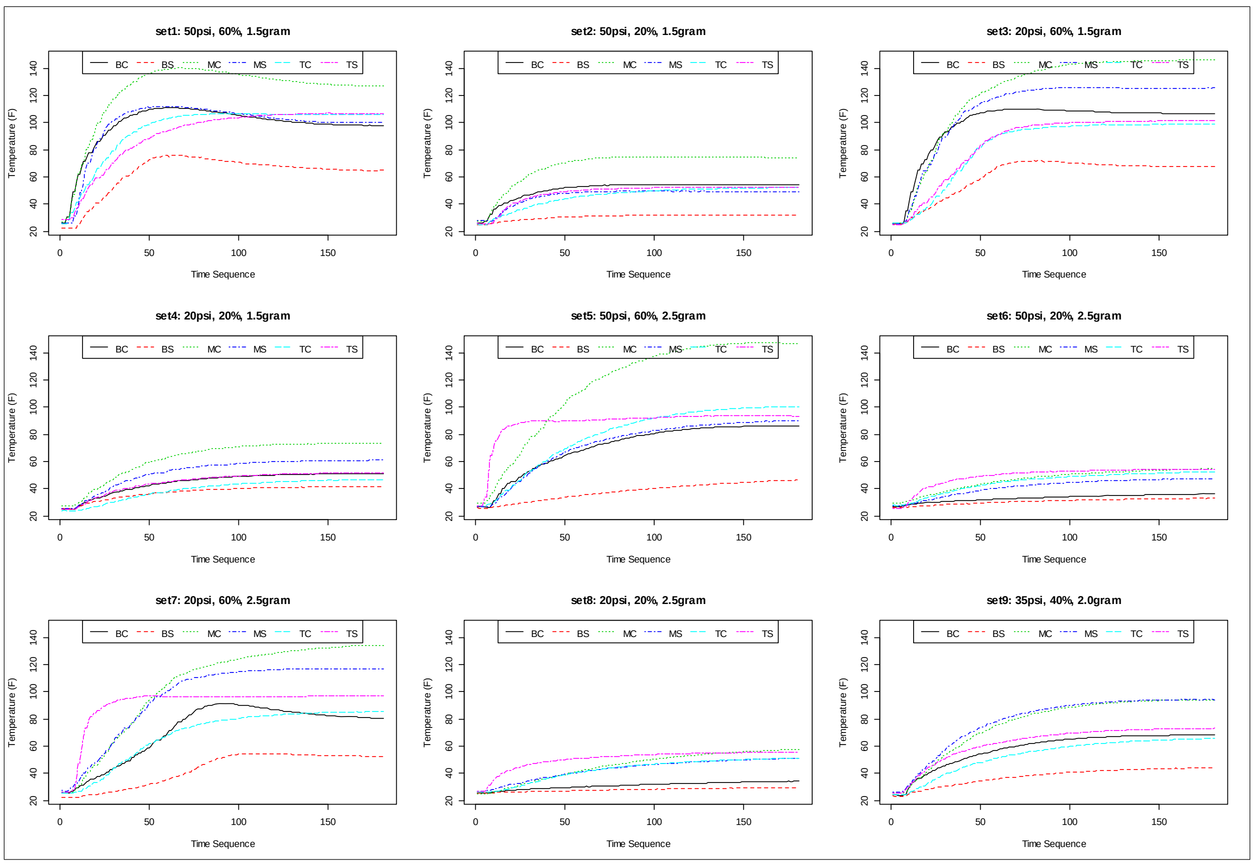

6.3 Methodology

The methodology details will be presented in this section. Most researches of full factorial design and multi-response optimization deal with the experiment results in the form of a vector as shown in equation (2). There is very little research considers the response variables of the matrix form, i.e. equation (3). As the description above, the surrogate response variables contains six profiles, so that the conventional full factorial design and multi-response optimization method cannot handle this kind of data format directly. Therefore, this study proposes the PCA as a role of dimension reduction method to dealing with high dimensionality issue in the conventional multiple-response optimization method. Note that, the PCA is well-known dimension reduction approach utilized in profile analysis (Shiau et al, 2009). Also, desirability functions method is a widely used multi-response optimization method that has been embedded in most software, such as, R, Minitab, Matlab, SAS, or JMP. Both methods will be introduced in the following section.

6.3.1 Principal Component Analysis (PCA)

The main goal of PCA is to reduce the dimensionality of the given datasets. Essentially, a principal component (PC) in this study is a particular set of linear combinations of variables. Suppose the variables are $t_1, t_2, \ldots, t_g$, the PCs will be formed as equation (6):

$$\begin{aligned} PC_1 &= \tau_{11}t_1 + \tau_{12}t_2 + \cdots + \tau_{1g}t_g \\ PC_2 &= \tau_{21}t_1 + \tau_{22}t_2 + \cdots + \tau_{2g}t_g \\ &\vdots \\ PC_g &= \tau_{g1}t_1 + \tau_{g2}t_2 + \cdots + \tau_{gg}t_g \end{aligned} \tag{6}$$

Note that τ_{ij} is the i^{th} eigenvector of variance-covariance matrix of the given dataset, which can be described in equation (7):

$$C'\Sigma C = \Lambda \tag{7}$$

where Σ is the variance-covariance of the given dataset that will be input to the PCA, C is the $g \times g$ matrix consisting of eigenvectors of Σ, and Λ is $g \times g$ diagonal matrix whose diagonal elements are eigenvalues of Σ. In this study, there are 36 runs of the experiment, and 6 profiles were collected in each run. Also, for each profile, there are 180 data points were recorded, i.e., g=180. Therefore, the size of the input dataset for the PCA is 180 ×216, and the size of the Σ, C, and Λ are all 180×180. Note that, since the conventional multi-response optimization method can only handle vector format of the given dataset as shown in equation (2), we select the first PC score to represent the temperature profiles. Therefore, the problem of multiple profiles (form of equation (3)) is simplified so that the regular multi-response optimizer can deal with the reduced form directly. Many software, such as, R, SAS, Minitab, matlab, JMP, etc., will calculate eigenvalues and eigenvectors and implement the PCA. To perform the PCA in this study, we use

R function, prcomp(), to calculate PCs of given dataset. Table 6-2 shows the summary of first five PC scores after implementing the PCA from R. From the table, the PC1 shows the proportion of variance is 0.9633, so that the PC1 can explain 96.33% of variability. Therefore, the first PC is valid representation of the entire dataset. For more detail of mathematical and statistical properties of the PCA, please refer to Jolliffe (2002).

Table 6-2 Summary of first five PC scores

	PC1	*PC2*	*PC3*	*PC4*	*PC5*
Standard Deviation	369.165	66.7852	21.5357	12.2971	7.90605
Proportion of Variance	0.9633	0.03153	0.00328	0.00107	0.00044
Cumulative Proportion	0.9633	0.99485	0.99813	0.9992	0.99964

6.3.2 Desirability Functions

The desirability functions approach developed by Derringer and Suich (1980) is one of the multi-response optimization methods. The general idea of the desirability functions approach is to maximize the overall desirability D as shown in equation (8):

$$D = (d_1 d_2 \dots d_m)^{1/m} \tag{8}$$

where m is the number of responses and d_i is the i^{th} desirability function of response y_i. Note that, d_i is updated by using the equation (9) to (11), where L is the lower limit, U is the upper limit, T is the target, and r, r_1 and r_2 are the weights. If the objective is to maximize the target T, the equation (9) is used; otherwise equation (10) is then obtained. Note that, if the target T is allocated between L and U, the equation (11) should be considered. In this study, since all responses are all the larger, the better, the equation (9) is the one to be applied to determine the optimized input variables.

$$d = \begin{cases} 0 & y < L \\ \left(\frac{y-L}{T-L}\right)^r & L \le y \le T \\ 1 & y > T \end{cases} \tag{9}$$

$$d = \begin{cases} 1 & y < T \\ \left(\frac{y-L}{T-L}\right)^r & T \le y \le U \\ 0 & y > U \end{cases} \tag{10}$$

$$d = \begin{cases} 0 & y < L \\ \left(\frac{y-L}{T-L}\right)^{r_1} & L \le y \le T \\ \left(\frac{U-y}{U-T}\right)^{r_2} & T \le y \le U \\ 1 & y > U \end{cases} \quad \textbf{(11)}$$

6.4 Experimental Results and Discussion

There are two goals in this study. The major objective is to investigate whether the temperature profiles of a biomass pellet can be the surrogate response variables to the conventional quality characteristics of interest, density and durability of biomass pellets. The second goal of this study is to find the predictive model of density and durability using the six-location temperature profiles of the biomass pellet if those profiles can be the surrogate response variables to the conventional ones.

In order to achieve the first objective of this study, a 2^3 full factorial design and the desirability functions are applied to both conventional and surrogate response factor. Figure 6.4 shows all response factors' contour plots with all the combinations of input variables. Also, the Minitab 16 output of analysis of variance for density, durability, TC, TS, MC, MS, BC, and BS versus the input variables is shown in Figure A 6-1 in the Appendix. Note that, although density, TC, TS, MC, BC, and BS shows curvature effect is existed as shown in Figure A 6-1, contour plots in Figure 6.4 show the maximum values of all response variables are allocated in the corner points of all input variables rather than in the curvature region. Therefore, extra experiments used in central composite design (CCD) is not necessary to apply to this study.

Our second goal is to further determine the optimized setting of input variables based on the given response variables, the results of desirability functions are shown in Figure 6.5 and Figure 6.6. Note that, both figures show the global solutions of the input variables' settings are PSI=50, %UVA=60, and Weight=1.5. In other words, those settings of input variables may not only result the maximum density and durability, but also maximize temperatures of biomass pellets without damaging them. Therefore, the temperature profiles of a biomass pellet can be used as the surrogate response variables to the conventional response variables, density and durability since both optimization approaches achieve the same goal.

Figure 6.4 Contour plot of density, durability, BC, BS, MC, MS, TC, and TS.

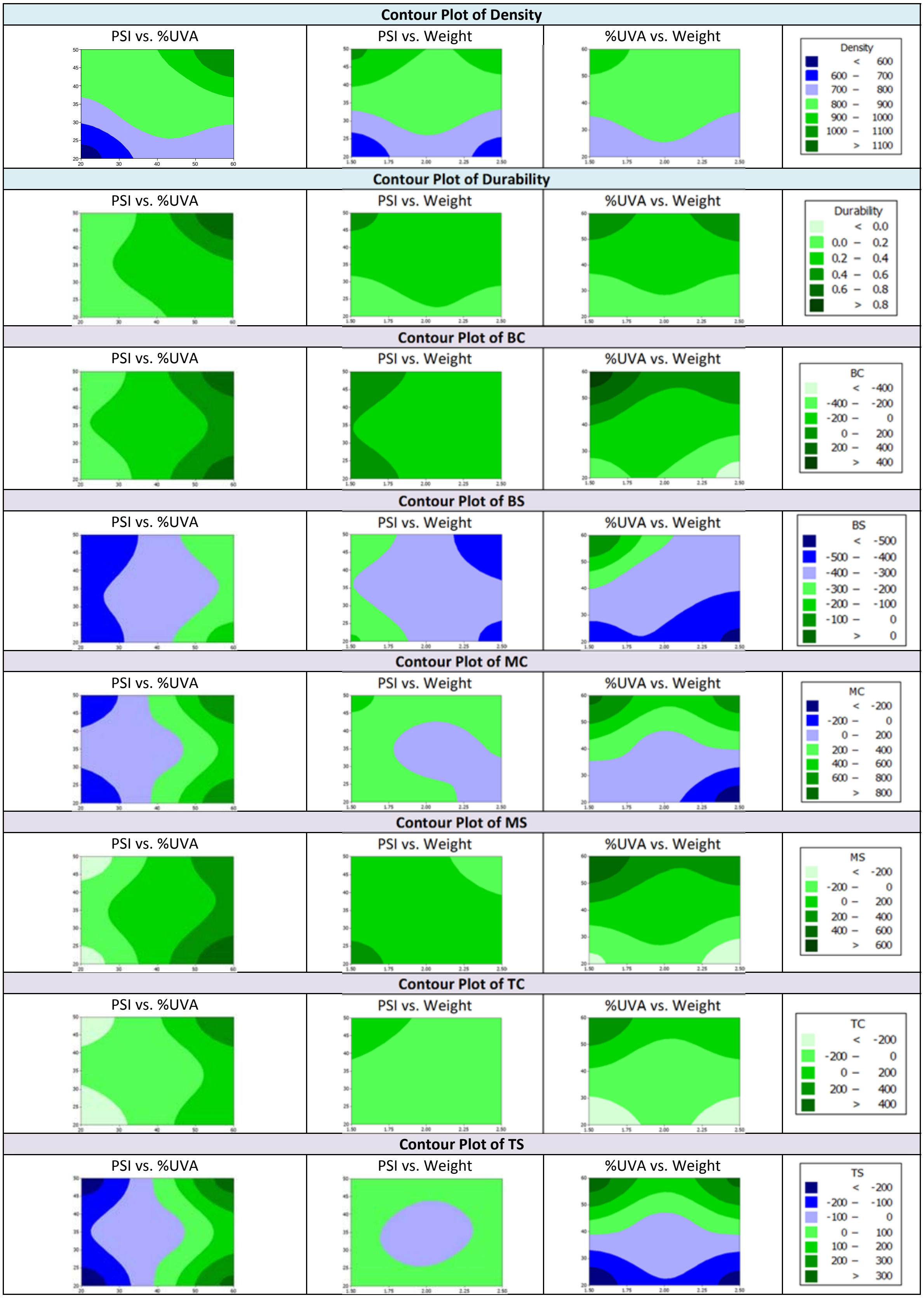

Figure 6.5 The desirability functions result for density and durability of biomass pellets.

```
Response Optimization

Parameters

            Goal     Lower  Target  Upper  Weight  Import
Density     Maximum    500    1200   1200       1       1
Durability  Maximum      0       1      1       1       1


Global Solution

PSI      =    50
%UVA     =    60
Weight   =   1.5

Predicted Responses

Density      =   1151.72  ,   desirability =   0.931030
Durability   =      0.86  ,   desirability =   0.864732

Composite Desirability = 0.897269
```

Figure 6.6 The desirability functions result for the temperature profiles

```
Response Optimization

Parameters

    Goal     Lower  Target  Upper  Weight  Import
TC  Maximum   -400     500    500       1       1
TS  Maximum   -300     400    400       1       1
MC  Maximum   -300     900    900       1       1
MS  Maximum   -400     700    700       1       1
BC  Maximum   -500     600    600       1       1
BS  Maximum   -600       5      5       1       1

Global Solution

PSI      =    50
%UVA     =    60
Weight   =   1.5

Predicted Responses

TC   =   435.330  ,   desirability =   0.928144
TS   =   378.352  ,   desirability =   0.969074
MC   =   813.033  ,   desirability =   0.927527
MS   =   471.276  ,   desirability =   0.792069
BC   =   477.608  ,   desirability =   0.888734
BS   =    -6.996  ,   desirability =   0.980172

Composite Desirability = 0.912059
```

Since the temperature profiles can replace the density and durability as surrogate response variables, the predicting model of density and durability using the six temperature profiles is developed in this study. In this case, the first PCA values of the temperature profiles become the input variables. The simple linear regression model is used to forecasting the density and durability when the six locations temperature profiles of the biomass pellet are recorded. Equation (12) and (13) shows the simple linear regression model of density and durability.

According to the results of regression analysis using the Minitab 16 shown in Figure 6.7 and Figure 6.8, both linear models are adequate to predict density and durability. Therefore, those two models can be used to predict the density and durability of the biomass pellets when the temperature profiles are recorded from the six-location of a biomass pellet are given. This implies that a non-destructive test is feasible and the critical quality characteristics can be estimated.

$$Density = \beta_{d0} + \alpha_{d1}TC + \alpha_{d2}TS + \alpha_{d3}MC + \alpha_{d4}MS + \alpha_{d5}BC + \alpha_{d6}BS \qquad \textbf{(12)}$$

$$Durability = \beta_{u0} + \alpha_{u1}TC + \alpha_{u2}TS + \alpha_{u3}MC + \alpha_{u4}MS + \alpha_{u5}BC + \alpha_{u6}BS \qquad \textbf{(13)}$$

Figure 6.7 Regression analysis of density versus six-location temperature profiles.

Regression Analysis: Density versus TC, TS, MC, MS, BC, BS

```
The regression equation is
Density = 1273 + 1.31 TC + 0.655 TS - 0.679 MC - 0.597 MS - 0.273 BC + 0.383 BS

Predictor     Coef  SE Coef      T      P
Constant    1272.8    132.8   9.58  0.000
TC          1.3114   0.4382   2.99  0.010
TS          0.6551   0.2401   2.73  0.017
MC         -0.6788   0.3352  -2.02  0.064
MS         -0.5975   0.2647  -2.26  0.042
BC         -0.2729   0.4673  -0.58  0.569
BS          0.3825   0.5009   0.76  0.459

S = 63.4781   R-Sq = 90.4%   R-Sq(adj) = 85.9%

Analysis of Variance

Source          DF      SS     MS      F      P
Regression       6  491094  81849  20.31  0.000
Residual Error  13   52383   4029
Total           19  543477
```

Figure 6.8 Regression analysis of durability versus six-location temperature profiles.

```
Regression Analysis: Durability versus TC, TS, MC, MS, BC, BS

The regression equation is
Durability = 0.834 + 0.00202 TC + 0.00170 TS - 0.00117 MC - 0.000965 MS
             - 0.000270 BC + 0.000243 BS

Predictor        Coef    SE Coef      T      P
Constant       0.8339     0.2095   3.98  0.002
TC          0.0020177  0.0006914   2.92  0.012
TS          0.0017021  0.0003789   4.49  0.001
MC         -0.0011686  0.0005289  -2.21  0.046
MS         -0.0009652  0.0004176  -2.31  0.038
BC         -0.0002702  0.0007374  -0.37  0.720
BS          0.0002434  0.0007903   0.31  0.763


S = 0.100164   R-Sq = 92.0%   R-Sq(adj) = 88.3%

Analysis of Variance

Source          DF       SS       MS      F      P
Regression       6  1.49320  0.24887  24.81  0.000
Residual Error  13  0.13043  0.01003
Total           19  1.62362
```

6.5 Conclusion and Future Study

Density and durability of the biomass pellets are major quality characteristics of interests for determining the quality of pellets during the manufacturing. However, quality engineers have to intervene the manufacturing process of pelleting for destructive testing. This study investigates whether the temperature profiles recorded from the six-location of a pellet can be the surrogate response variables for density and durability. We have shown that temperature profiles are capable of replacing density and durability. However, conventional multi-response optimization methods cannot handle profiles as response variables. This study applies a PCA approach to transform the profile response variables into a vector form.

The experimental results show that the optimal input variable solutions from the density/durability responses and temperature-profile responses are identical. That is, when the pelleting pressure is set to 50 psi, ultrasonic power is set to 60%, and the pellet weight is 1.5 gram, the density/durability responses and the temperature-profile responses are all maximized using the desirability functions. Therefore, the temperature profiles collected from the six-location of a pellet can be used as the surrogate variables to the density and durability of the biomass pellets during the pelleting process of cellulosic manufacturing. Moreover, this study also contains a predicting model of density and durability so that users can use the six-location temperature profiles to forecast the density and durability. The regression analysis results show that the linear models are adequate to predict the density and durability when the temperature profiles are given.

For future studies, other dimension reduction methods should be explored since this study applies the PCA to reduce the dimensionality of the response variables and only the first principal component is used to represent the entire dataset. This method may not be adequate if the first PC's cumulative proportion variance is not high enough, e.g. lower than 90% of entire variability. Moreover, the proposed method cannot be applied to other responses such as, surface or images. Much more research is needed in these areas.

Reference

ASAE Standards. (2003). *S269.4: Cubes, pellets, and crumbles – definitions and methods for determining density, durability and moisture content.* St. Joseph, MI: ASABE.

Derringer, G. and Suich, R. (1980), "Simultaneous Optimization of Several Response Variables," *Journal of Quality Technology*, 12(4):214-219.

Faborode M.O. (1990). "Analysis of extrusion compaction of fibrous agricultural residues for fuel applications," *Biomass*, 21(2):115-128.

Feng, Q., Cong, W.L. Zhang, M., Pei, Z.J., and Ren, C.Z. (2011). "An experimental study on charring of cellulosic biomass in ultrasonic vibration-assisted pelleting," *International Journal of Manufacturing Research*, 6(1): 77-86.

Jolliffe, I.T. (2002). *Principal Component Analysis*, Springer-Verlag New York, Inc., New York, NY.

Kaliyan N., Morey R.V., White M.D., and Doering A. (2009). "Roll-press briquetting and pelleting of corn stover and switchgrass" *Transaction of the ASABE* 52(2):543-555.

Lynd, L. R. (2003), *Cellulosic ethanol fact sheet, National commission on energy policy forum: the future of biomass and transportation fuels, available at*: http://www.agmrc.org/media/cms/IV_1CB41D0EF05F2.pdf.

Mani, S., Tabil, L.G. ,and Sokhansanj, S. (2003), "An overview of compaction of biomass grinds", *Powder Handling and Processing*, 15(3):160-168.

Reece F.N. (1966). "Temperature, pressure and time relationships in forming dense hay wafers," *Transaction of ASABE*, 9(6):749-751.

Rubin, E.M.. (2008), "Genomics of cellulosic biofuels", *Nature*, 454(14):841-845.

Shiau, J.J.H., Huang, H.L., Lin, S.H., and Tsai, M.Y. (2009). "Monitoring Nonlinear Profiles with Random Effects by Nonparametric Regression," *Communications in Statistics-Theory and Methods*, 38(10), 1664-1679.

Sokhansanj, S., Mani, S. and Zaini, P.(2005), "Binderless pelletization of biomass", *ASABE Paper No.056061*, American Society of Agricultural and Biological Engineers, St. Joseph., MI.

Van Dam J.E.G., Van Den Oever M.J.A., Teunissen W., Keijsers E.R.P., and Peralta A.G. (2004), "Process for production of high density/high performance binderless boards from whole coconut husk: Part 1: Lignin as intrinsic thermosetting binder resin," *Industrial Crops and Products*, 19(3):207-216.

Zhang, P.F., Deines, T.W., Nottingham, D., Pei, Z.J., Wang, D.H., and Wu, X.R. (2010), "Ultrasonic vibration-assisted pelleting of biomass: a designed experimental investigation on pellet quality and sugar yield," *Proceedings of the ASME 2010 International Manufacturing Science and Engineering Conference*, Erie, PA, USA, October 12-15.

Zhang, P.F. and Pei, Z.J. (2010) "Effects of Ultrasonic Treatments on Cellulose in Cellulosic Biofuel Manufacturing: a Literature Review," *Proceedings of the ASME International Conference on Manufacturing Science and Engineering (MSEC)*, Erie, PA, USA, October 12-15.

Zhang, P.F., Denies, T., Pei, Z.J., Nottingham, D., Wang, D.H., and Wu, X.R. (2010) "Ultrasonic Vibration-assisted pelleting of biomass: a Designed Experimental Investigation on Pellet Quality and Sugar Yield," *Proceedings of the ASME International Conference on Manufacturing Science and Engineering (MSEC)*, Erie, PA, USA, October 12-15.

Zhang, P.F. (2011). *Ultrasonic Vibration-Assisted Pelleting of Cellulosic Biomass for Ethanol Manufacturing* (Doctoral dissertation). Kansas State University, Manhattan, KS.

Zhang, Q. (2013). *Investigations on Power Consumption, Pelleting Temperature, Pellet Quality, and Sugar Yield in Pelleting of Cellulosic Biomass* (Doctoral dissertation). Kansas State University, Manhattan, KS.

Appendix

Figure A 6-1 Analysis of variance for density, durability, TC, TS, MC, MS, BC, and BS.

Analysis of Variance for Density (coded units)

Source	DF	Seq SS	Adj SS	Adj MS	F	P
Main Effects	3	1116149	1116149	372050	3278.50	0.000
PSI	1	799578	799578	799578	7045.88	0.000
%UVA	1	311440	311440	311440	2744.41	0.000
Weight	1	5131	5131	5131	45.21	0.000
2-Way Interactions	3	33460	33460	11153	98.28	0.000
PSI*%UVA	1	10000	10000	10000	88.12	0.000
PSI*Weight	1	21787	21787	21787	191.99	0.000
%UVA*Weight	1	1673	1673	1673	14.74	0.001
3-Way Interactions	1	10156	10156	10156	89.49	0.000
PSI*%UVA*Weight	1	10156	10156	10156	89.49	0.000
Curvature	1	5811	5811	5811	51.21	0.000
Residual Error	27	3064	3064	113		
Pure Error	27	3064	3064	113		
Total	35	1168640				

Analysis of Variance for Durability (coded units)

Source	DF	Seq SS	Adj SS	Adj MS	F	P
Main Effects	3	2.63180	2.63180	0.87727	6106.37	0.000
PSI	1	0.65399	0.65399	0.65399	4552.24	0.000
%UVA	1	1.97742	1.97742	1.97742	13764.16	0.000
Weight	1	0.00039	0.00039	0.00039	2.70	0.112
2-Way Interactions	3	0.71720	0.71720	0.23907	1664.06	0.000
PSI*%UVA	1	0.65399	0.65399	0.65399	4552.24	0.000
PSI*Weight	1	0.06281	0.06281	0.06281	437.23	0.000
%UVA*Weight	1	0.00039	0.00039	0.00039	2.70	0.112
3-Way Interactions	1	0.06281	0.06281	0.06281	437.23	0.000
PSI*%UVA*Weight	1	0.06281	0.06281	0.06281	437.23	0.000
Curvature	1	0.00022	0.00022	0.00022	1.55	0.224
Residual Error	27	0.00388	0.00388	0.00014		
Pure Error	27	0.00388	0.00388	0.00014		
Total	35	3.41591				

Analysis of Variance for TC (coded units)

Source	DF	Seq SS	Adj SS	Adj MS	F	P
Main Effects	3	2656388	2656388	885463	1254.04	0.000
PSI	1	103634	103634	103634	146.77	0.000
%UVA	1	2488071	2488071	2488071	3523.75	0.000
Weight	1	64683	64683	64683	91.61	0.000
2-Way Interactions	3	118278	118278	39426	55.84	0.000
PSI*%UVA	1	16181	16181	16181	22.92	0.000
PSI*Weight	1	487	487	487	0.69	0.414
%UVA*Weight	1	101610	101610	101610	143.91	0.000
3-Way Interactions	1	2640	2640	2640	3.74	0.064
PSI*%UVA*Weight	1	2640	2640	2640	3.74	0.064
Curvature	1	24056	24056	24056	34.07	0.000
Residual Error	27	19064	19064	706		
Pure Error	27	19064	19064	706		
Total	35	2820425				

Analysis of Variance for TS (coded units)

Source	DF	Seq SS	Adj SS	Adj MS	F	P

Main Effects	3	2497152	2497152	832384	2838.57	0.000
PSI	1	1059	1059	1059	3.61	0.068
%UVA	1	2496090	2496090	2496090	8512.10	0.000
Weight	1	3	3	3	0.01	0.922
2-Way Interactions	3	19523	19523	6508	22.19	0.000
PSI*%UVA	1	195	195	195	0.67	0.422
PSI*Weight	1	15631	15631	15631	53.30	0.000
%UVA*Weight	1	3697	3697	3697	12.61	0.001
3-Way Interactions	1	6365	6365	6365	21.71	0.000
PSI*%UVA*Weight	1	6365	6365	6365	21.71	0.000
Curvature	1	23406	23406	23406	79.82	0.000
Residual Error	27	7917	7917	293		
Pure Error	27	7917	7917	293		
Total	35	2554364				

Analysis of Variance for MC (coded units)

Source	DF	Seq SS	Adj SS	Adj MS	F	P
Main Effects	3	6657115	6657115	2219038	2083.16	0.000
PSI	1	13848	13848	13848	13.00	0.001
%UVA	1	6276526	6276526	6276526	5892.20	0.000
Weight	1	366741	366741	366741	344.28	0.000
2-Way Interactions	3	34616	34616	11539	10.83	0.000
PSI*%UVA	1	1489	1489	1489	1.40	0.247
PSI*Weight	1	1861	1861	1861	1.75	0.197
%UVA*Weight	1	31267	31267	31267	29.35	0.000
3-Way Interactions	1	29711	29711	29711	27.89	0.000
PSI*%UVA*Weight	1	29711	29711	29711	27.89	0.000
Curvature	1	98627	98627	98627	92.59	0.000
Residual Error	27	28761	28761	1065		
Pure Error	27	28761	28761	1065		
Total	35	6848831				

Analysis of Variance for MS (coded units)

Source	DF	Seq SS	Adj SS	Adj MS	F	P
Main Effects	3	4360681	4360681	1453560	747.48	0.000
PSI	1	176865	176865	176865	90.95	0.000
%UVA	1	3894756	3894756	3894756	2002.84	0.000
Weight	1	289060	289060	289060	148.65	0.000
2-Way Interactions	3	158389	158389	52796	27.15	0.000
PSI*%UVA	1	98094	98094	98094	50.44	0.000
PSI*Weight	1	3981	3981	3981	2.05	0.164
%UVA*Weight	1	56314	56314	56314	28.96	0.000
3-Way Interactions	1	23670	23670	23670	12.17	0.002
PSI*%UVA*Weight	1	23670	23670	23670	12.17	0.002
Curvature	1	3039	3039	3039	1.56	0.222
Residual Error	27	52505	52505	1945		
Pure Error	27	52505	52505	1945		
Total	35	4598285				

Analysis of Variance for BC (coded units)

Source	DF	Seq SS	Adj SS	Adj MS	F	P
Main Effects	3	3883653	3883653	1294551	2508.39	0.000
PSI	1	8240	8240	8240	15.97	0.000
%UVA	1	3234453	3234453	3234453	6267.23	0.000
Weight	1	640961	640961	640961	1241.96	0.000
2-Way Interactions	3	46599	46599	15533	30.10	0.000

PSI*%UVA	1	3380	3380	3380	6.55	0.016
PSI*Weight	1	1475	1475	1475	2.86	0.102
%UVA*Weight	1	41744	41744	41744	80.89	0.000
3-Way Interactions	1	499	499	499	0.97	0.334
PSI*%UVA*Weight	1	499	499	499	0.97	0.334
Curvature	1	53198	53198	53198	103.08	0.000
Residual Error	27	13934	13934	516		
Pure Error	27	13934	13934	516		
Total	35	3997884				

Analysis of Variance for BS (coded units)

Source	DF	Seq SS	Adj SS	Adj MS	F	P
Main Effects	3	1012837	1012837	337612	615.92	0.000
PSI	1	15272	15272	15272	27.86	0.000
%UVA	1	647771	647771	647771	1181.76	0.000
Weight	1	349794	349794	349794	638.14	0.000
2-Way Interactions	3	107441	107441	35814	65.34	0.000
PSI*%UVA	1	386	386	386	0.70	0.409
PSI*Weight	1	43	43	43	0.08	0.781
%UVA*Weight	1	107011	107011	107011	195.22	0.000
3-Way Interactions	1	33440	33440	33440	61.01	0.000
PSI*%UVA*Weight	1	33440	33440	33440	61.01	0.000
Curvature	1	19058	19058	19058	34.77	0.000
Residual Error	27	14800	14800	548		
Pure Error	27	14800	14800	548		
Total	35	1187575				

Chapter 7 A Visualization Decision Support Tool for Multivariate SPC Diagnosis using Marginal CUSUM Glyphs

Paper Title:
A Visualization Decision Support Tool for Multivariate SPC Diagnosis using Marginal CUSUM Glyphs

Published in:
Chang, S. and Chou, S.H., (2010) "A Visualization Decision Support Tool for Multivariate SPC Diagnosis using Marginal CUSUM Glyphs", *Quality Engineering*, 22:182-198.

Author's Name:
Dr. Shing I Chang and Shih-Hsiung Chou

Authors' Affiliations:
Department of Industrial and Manufacturing Systems Engineering, Kansas State University, USA.

Abstract

A marginal CUSUM glyph is proposed to visualize and decompose out-of-control signals over time. The proposed visualization tool, consisting of a two-sided CUSUM and star glyphs, is capable of indicating when and which variables contributing to the cause. Complementing traditional multivariate control charts after indicating that the process under monitoring is out of control, the proposed method provides a visualization tool with additional diagnostic information. In addition, the proposed tool is capable of handling responses with high dimensions. Extensive simulation results conducted for up to 20 dimensions provide a user guideline of how to implement the proposed methodology.

Keywords: Visualization, Multivariate SPC, CUSUM, Multivariate CUSUM

7.1 Introduction

Multivariate control charts such as Hotelling T^2 are often used for a process of multiple quality characteristics. The look of a multivariate control chart often mimics that of a univariate control chart such as $\bar{X}$ chart consisting of three horizontal lines enclosing dots connected by straight line segments. Unlike a univariate process, an out-of-control point on a multivariate control chart does not reveal which quality characteristics contribute to the problem without further analysis. A visualization tool is needed for users to make diagnostic related decisions such as when the out-of-control conditions start to take place as well as which quality characteristics are responsible. Although multiple univariate control charts, one for each quality characteristic, can be implemented as additional visual aids, this approach does not work when the number of quality characteristics is large. Not only is it difficult to control the overall type I error but scanning many univariate control charts simultaneously won't provide effective visual aid.

Many high-dimensional data visualization techniques have been developed to explore or to present datasets with multiple dimensions. Chen *et al*. (2008) summarized five tools visualizing high-dimensional datasets; they are the mosaic plots, scatter plot matrix, parallel coordinate plot, trellis displays, and star glyphs. The *Mosaic Plots*, proposed by Hartigan and Kleiner (1984), provide contingency tables used to display the relationship among two or more categorical variables. Mosaic plots consist of groups of rectangles whose sizes are corresponding to values in contingency tables. Users can interpret the mosaic plot by looking at its sizes and the positions of the rectangles. Figure 7.1 (a) shows an example of the mosaic plot for a 2009 automobile dataset (collected from Automotive.com http://www.automotive.com/index.html). The mosaic plot displays the number of cars by country and prices under the aspects of horse power (hp) and miles per gallon (mpg). Although the mosaic plot is a well-known visualization tool to multivariate datasets, it can only cope with categorical datasets, meaning that data has to be put into categories. It is difficult to apply a mosaic-plot approach to monitor a statistic process when quality characteristics are quantitative. In the car example, horse power is categorized into two classes – 0-350 and 350-850. In addition, a mosaic plot can only handle a small number of factors, e.g. four factors are considered in the car example in Figure 7.1 (a). A mosaic plot will not be able to handle problems with much larger number of factors.

A *Scatter Plot Matrix* is another visualization tool to view all the pair-wise scatter plots into a matrix. Each scatter diagram displays the relationship between any two-variable pairs. The scatter plot matrix can be potentially used for process monitoring. Figure 7.1 (b) displays an example of scatter plot for a three-dimensional dataset. The dataset was generated from the multivariate normal distribution with one-step mean shifted, i.e. μ=(5,10,20) change to μ=(7,12,22) and $\sum=\begin{bmatrix} 1 & 0 & 0.3 \\ 0 & 1 & 0 \\ 0.3 & 0 & 1 \end{bmatrix}$, where μ is a vector of mean and $\sum$ is a variance-covariance matrix. Examining Figure 7.1 (b), users can easily identify that var1 and var3 are corrected, but it is very difficult to distinguish there is a mean shift by looking at this plot. Montgomery (2008) gave an example of using principal component analysis and scatter plot with 95% confidence ellipse to show out-of-control points. Although the scatter plot matrix is a good visualization tool to display the pair-wise relationships in a snap shot, it has some limitations. First, a scatter plot presents all data points in a snapshot. Users only can see some points plot outside an ellipse but the time sequence of the plotting points is lost. Second, a scatter plot cannot handle hyper-dimensional data, such as a 50-dimensional or 100-dimensional data set. In fact, 20 dimensions will post a challenge for pair-wise displays. There will be 20 x 20 boxes needed to be displayed simultaneously.

Figure 7.1 (a) The Example of the Mosaicplot for 2009 Automobile Dataset; (b) The Example of the Scatter Plot Matrix for the Three-Dimensional Dataset.

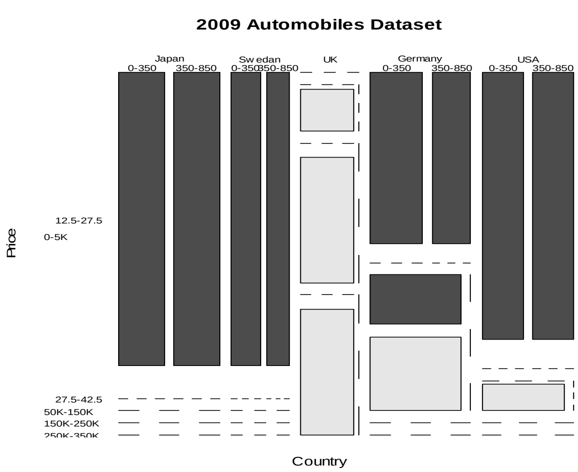

(a)

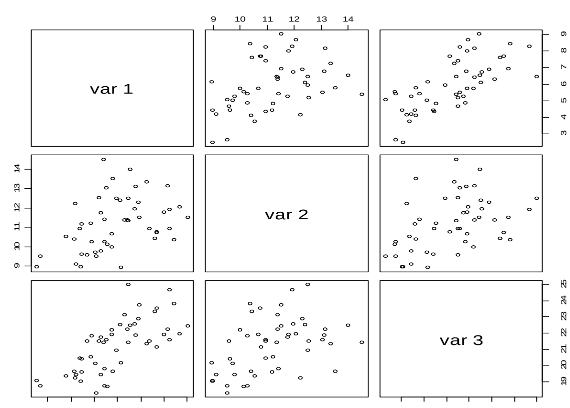

(b)

The third multivariate visualization tool is the *Parallel Coordinate Plot*. A parallel coordinate plot contains coordinate axes (vertical or horizontal) in parallel that can accommodate many variables at a time in the same plant. The number of parallel axes is corresponding to the number of variables. For each parallel axes, the bottom of line is the minimum value of the variable, while the maximum value of the variable is at the end of the line. A particular observation is represented by a line that connects the vertical line at the specific height, which is the proportion of value of the observation to length of vertical line. Figure 7.2 (a) is a simple example of the parallel coordinate plot. The dataset consists of a three-dimensional data with five observations generated from the multivariate normal distribution. Although a parallel coordinate plot can handle high-dimensional data, too many observations on the same plot tends to lose its effectiveness. As shown in Figure 7.2 (b), it is difficult to make out the changes made on an individual response among 100 observations with 20 dimensions each. Therefore, it is hard to tell if any out-of-control signal occurs.

Figure 7.2 (a) An Simple Example of 5 observations, 3-dimensional dataset; (b) Example of 100 observations, 20-dimensional dataset with one step mean shift.

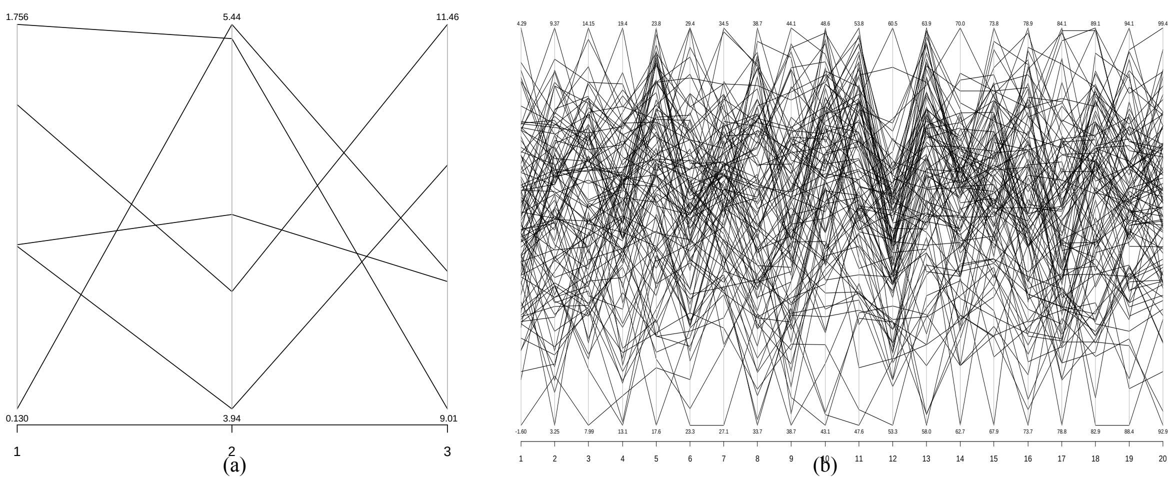

Although there were many techniques to visualize the multivariate data about its quantities or relationship, it is difficult to apply these techniques to visualize data for the purpose of statistical process control for multivariate processes. On the other hand, multivariate control charts based on Hotelling's T^2 statistic (Jackson, 1985), multivariate cumulative sum (MCUSUM; Woodall and Ncube, 1985; Crosier, 1988; Pignatiello and Runger, 1990), multivariate exponentially weighted moving average (MEWMA; Lowry, *et al.*, 1992) cannot effectively indicate which variable(s) contribute to an out-of-control signal.

Hawkins (1991) proposed a procedure called regression adjustment. Essentially, the regression adjustment is a set of univariate control charts of the residuals from the regression of each variable on all others. He further used regression adjustment to each variable to analyze out-of-control-caused variables. Since each variable contains at least one chart, it needs a large number of charts as many as the number of variables for high-dimensional datasets. Another method is based on decomposition of the Hotelling's T^2 statistic which indicates caused out-of-control variables. Mason, Tracy and Young (1995) decomposed T^2 to interpret signals called MYT decomposition. Suppose p=3, there are 3!=6 combinations of decompositions of one T^2 value. For example $T^2 = T_1^2 + T_{2\cdot 1}^2 + T_{3\cdot 1,2}^2$. It would lead to a very large number of combinations when p is large. Examples shown in Mason and Young (2002) demonstrated the use of the decomposed terms, first, to confirm the data structure based on a historical data set and, second, to identify the causes of an out-of-control signal. Furthermore, Runger, Alt, and Montgomery (1996) used a similar concept to decompose an out-of-control signal. They used $d_i = T^2 - T_{(i)}^2$ as an indicator to show the contribution of the i^{th} variable. T^2 is the current value of statistic and $\mathrm{T}_{(\mathrm{i})}^2$ is the value of the statistic for all process variables except the i^{th} one. Then, d_i is a major contributor to T^2 if d_i is large. Note that decomposition is usually applied to the latest T^2 value when the process is deemed out of control.

These methods introduced above can help diagnose **which** variables contribute to an out-of-control signal based on the latest point that causes this out-of-control signal. In order to discover the information **where** or **when** the responsible variables went out of control, additional procedures are required. As pointed out by one reviewer, the conditional terms in MYT decomposition can be viewed as squared standardized residuals from a regression. Control charts can be established on the squared root of the signaling decomposition terms so that one can track where or when the problem began. In this study, we introduce a novel technique that combines CUSUM control charts and glyphs to provide a visualization decision support tool to indicate **when and which** variable(s) are out of control. As shown in Figure 7.3 and Figure 7.4, a trellis displays and star glyphs are very effective visualization tool for multivariate datasets. Features of these visualization approaches are applied to the proposed method in this study.

The rest of this paper is organized as follows. Section 2 introduces backgrounds of the trellis displays and star glyphs as well as the standardized two-side CUSUM and the multivariate CUSUM. Section 3 is the proposed method using marginal CUSUM Glyphs followed by the experimental design of the proposed simulation study. Next, the computational results of simulations are showing in section 4. Section 5 consists of conclusions and future studies.

7.2 Background

This section summarizes the trellis displays and star glyphs. In addition, the multivariate control charts adopted in the proposed visualization tool are also introduced in this section. Although both Exponential Weighted Moving Average (EWMA) and Cumulative Sum (CUSUM) control charts are effective detection and diagnosis tools for univariate processes, Hawkins (1993) stated that the CUSUM chart is a little better. In addition, Lowry *et al*. (1992) and Lowry and Montgomery (1995) both concluded that the multivariate EWMA can be as good as a multivariate CUSUM chart to detect small mean shifts. Thus, the proposed method will adopt two CUSUM charts: standardized two-side CUSUM (SD2CUSUM) and Multivariate CUSUM (MCUSUM). To investigate if any out-of-control signal occurred, users first run MCUSUM as a preliminary step of process monitoring so that the overall type I error is under control. If the MCUSUM provide an out-of-control signal, users can show all observations that are before the out-of-control signal in marginal CUSUM glyphs on the trellis display.

7.2.1 Trellis Displays

A trellis display is a lattice-like arrangement to lay out plots into rows, columns, and pages on multiple panels. The plots on the panels can be histogram, kernel density plot, theoretical quantile plot, two-sample quantile plot, stripchart, bar plot, scatter plot, parallel coordinate plot, etc (Sarkar, 2008). Each panel contains a subset of the data graphed by plots. For example, Yates (1935) studied a split-plot experiment. The structure of the oats data set is including 72 rows and 4 columns, and its attributes are including six blocks (I, II, III, IV, V, and VI), three varieties (Victory, Golden Rain, and Marvellous), four concentrations of nitrogen, and yield. Figure 7.3 shows the trellis display of the Oats data with block I and II. The yield of oats is plotted against concentration of nitrogen for three varieties of oats and two blocks. In this paper, the idea of lattice-like arrangement of the trellis display is applying to the proposed multivariate visualization tool. The block assignment will be replaced by the time sequence while the star glyphs will be adopted to represent each multivariate observation on panels. The star glyphs are introduced in next section.

Figure 7.3 A Trellis displays of the Oats data.

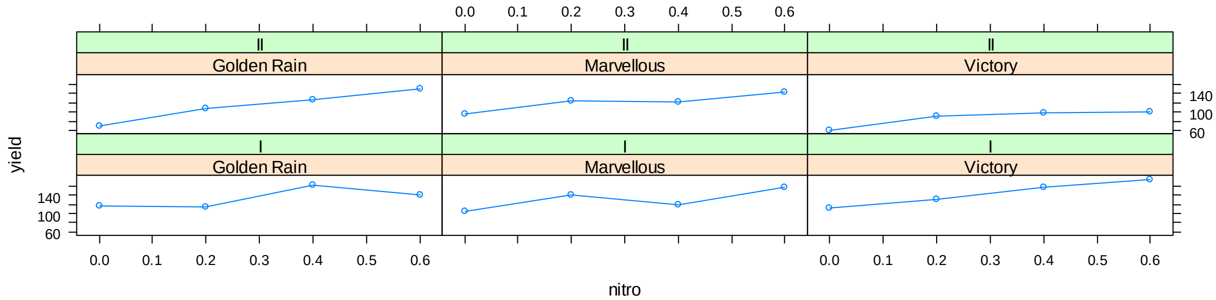

7.2.2 Star Glyphs

Star glyphs (also called star plot) display a multivariate data set in a geometrical shape such as hexagon for six dimensional data. In a star glyph, each individual graphic represents an observation. A star contains n spikes that radiate from the center with even space. The angle between each spike is equal to $360/n$ degree. Each spike has a value on it with the same proportion of the variable for that observation, which means observations must be standardized before stars are constructed. At the end of the point of each spike is usually connected to each other by line segments. To demonstrate the star glyph, five cars with seven attributes are used as an example. The seven attributes are: miles per gallon (mpg), weight of lbs (weight), horsepower (hp), engine displacement in cubic inches (disp.), number of cylinders (cyl.), torque of Newton-Meter (Torque), and price in US dollar (Price).

Figure 7.4 shows five examples of star glyphs. The graphic (a) to (e) are five different sedan vehicles with seven attributes for star glyphs demonstration, while graphic (f) shows the basis of variable assignment in which each spike represents one attribute. The longer the spike the large the values for that attribute. The car "Saab 9-3 2.0T" shown in Figure 7.4 (b) has high mpg, less weight, low horse power, small engine displacement, four cylinders, small torque, and lowest price compared to the other cars. A side-by-side comparison with Bentley demonstrates why the mpg of Bentley seems to disappear. The Saab has 29 mpg while the Bentley only has 14 mpg. However, the sticker prices are the opposite: Saab \$30,360 vs. Bentley \$224,990. The function of star glyphs called "stars" in the R language (http://www.r-project.org/) in its graphics package was used to generate these star glyphs in Figure 7.4.

Figure 7.4. Examples of Star glyphs where (f) Represents the Legend

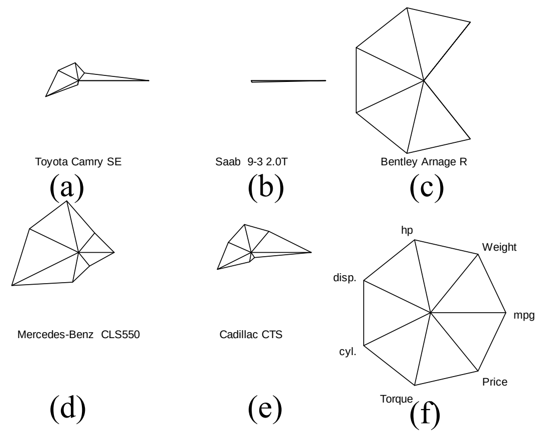

7.2.3 Standardized Two-Side Univariate CUSUM (SD2CUSUM)

The standardized two-side univariate CUSUM (SD2CUSUM) essentially is a tabular CUSUM with the standardized observations. This control chart is mainly designed for a process with only one quality characteristic. To run this procedure, it is necessary to obtain a phase I data set, so that mean μ_0 and standard deviation σ can be estimated. The data collected during a phase I process is often deemed a nominal representation of the underlying process for future observations to follow. Basically, the tabular CUSUM accumulates the differences between observations and the target. Two types of tabular CUSUM statistics are one for positive mean shifts and the other for negative mean shifts. Specifically, the positive part deals with the observations that are above the target, while the negative part copes with those below the target. Let x_i be the one dimensional i^{th} observation on the process. Note that the statistic of the negative part is a positive number as well. However, when these two statistics are plotted on the same chart, the CUSUM statistic for the negative shifts are plotted below the center line as showed in Figure 7.5. The statistics of the tabular CUSUM is showing below (Hawkins, 1993).

$$C_i^+ = \max[0, x_i - (\mu_0 + K) + C_{i-1}^+] \tag{1}$$

$$C_i^- = \max[0, (\mu_0 - K) - x_i + C_{i-1}^-] \tag{2}$$

where the C^+ and C^- represent the positive and negative parts of tabular CUSUM. The starting values are $C_0^+ = C_0^- = 0$. K is called the reference value (or called the allowance or slack value). Usually, K is about half of the absolute difference between the target value μ_0 and the out-of-control value of mean μ_1 to be detected, i.e.,

$$K = \frac{|\mu_1 - \mu_0|}{2} \tag{3}$$

K can also be expressed in standard deviation form in terms of $\delta = |\mu_1 - \mu_0|/\sigma$, which provides the magnitude of the shift to be detected. And K then becomes $\frac{\delta}{2}\sigma$ or $K = k\sigma$, $k = \frac{\delta}{2}$.

Figure 7.5. An Example of the CUSUM Chart. The first 25 dataset was generated from $N(10,1^2)$, while the rest 5 dataset was from $N(12,1^2)$.

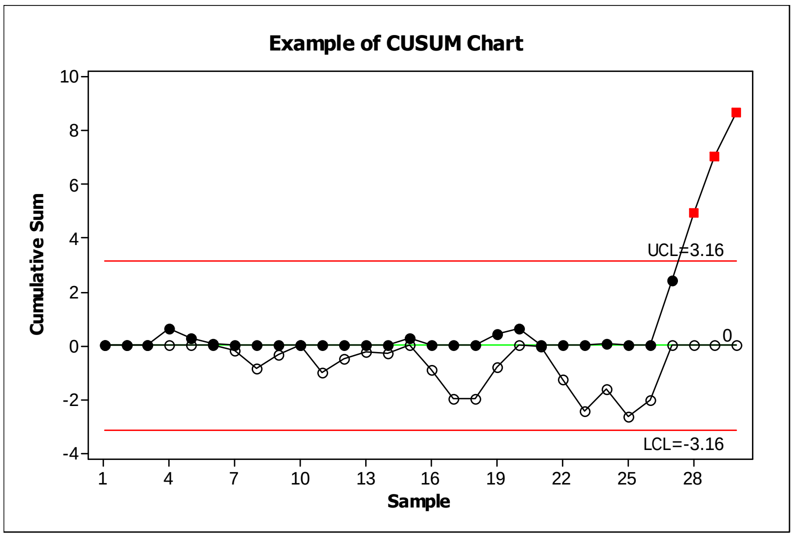

The following steps in equations (4) to (6) are taken to standardize the original data set. Specifically, the i^{th} observation is standardized as

$$y_i = \frac{x_i - \mu_0}{\sigma} \tag{4}$$

where σ is from the phase I estimate or known, and the equation (5) and (6) become

$$C_{p,i} = \max[0, y_i - k + C_{p,i-1}] \tag{5}$$

$$C_{n,i} = \max[0, -k - y_i + C_{n,i-1}] \tag{6}$$

where $C_{p,i}$ is the i^{th} observation statistic of standardized two-side CUSUM for positive mean shifts, while $C_{n,i}$ is the i^{th} observation statistic for negative mean shifts.

To decide whether the observation is out-of-control or not, H is the critical value for an out-of-control signal. If either C_i^+ or C_i^- is larger than H, it is considered that the process is out of control. Montgomery (2008) suggested that H be 5 times the process standard deviation σ, i.e,

$H=h\sigma$, where h=5. Since the process has been standardized, the detection criterion can be revised to whether $C_{p,i}$ or $C_{n,i}$ is larger than h or not.

Furthermore, since the CUSUM procedure is based on the accumulated difference between observations and the target, a delay phenomenon will affect when an out-of-control signal is detected. For example, if a process has a mean shift at xi, the system will not give an alarm until xj, i<j because of this phenomenon. Montgomery (2008) provided an example of finding the last-in-control observation, and in this paper, a pseudocode of tabular CUSUM is implemented in Figure 7.6, where N+ is the counter that records the number of consecutive periods that the upper-side CUSUM $C_{p,i}$ values are larger than zero, while N- is the counter for the lower-side CUSUM $C_{n,i}$. And the last-in-control position l is equal to o-N+ or o-N-, where o is the stopping counter number when the first out-of-control signal takes place during the phase II monitoring.

Figure 7.6 Pseudocode of Procedure of Tabular CUSUM

Procedure of Tabular CUSUM

set i=1, $C_{p,0}$ and $C_{n,0}$
while $C_{p,i}$ and $C_{n,i}$ smaller than h do
  calculate $C_{p,i}$ and $C_{n,i}$ by using (5) and (6).
  if $C_{p,i} > 0$ then $N^{+}= N^{+}+1$
  else $N^{+}==0$
  if $C_{n,i} > 0$ then $N^{-}= N^{-}+1$
  else $N^{-}==0$
  i++
end while
out-of-control $o=i$
last-in-control $l = o- N^{+}$ or $o- N^{-}$
print $C_{p,i}$, $C_{n,i}$, o, and l for all i.

7.2.4 The Multivariate CUSUM Chart

For processes with multiple quality characteristics, a multivariate CUSUM should be implemented. Multivariate control charts are often recommended over running multiple univariate control charts simultaneously because the overall type I error can be controlled to a desired level. Crosier (1988) proposed one of the better multivariate CUSUM schemes in term of the average run length (ARL) performance called vector-valued CUSUM. The main idea of this multivariate CUSUM (MCUSUM) is similar to that of the univariate CUSUM, except that MCUSUM multiples the statistic by a weight.

Let X_i be i^{th} observation on the process. X_i is from a multivariate normal distribution with mean T and variance-covariance $\sum$ which are known or can be estimated from a phase I data set. The statistics of MCUSUM is as below.

$$C_i = [(S_{i-1} + X_i - T)'\Sigma^{-1}(S_{i-1} + X_i - T)]^{1/2} \tag{7}$$

then

$$\begin{cases} S_i = 0 & \text{if } C_i \le k \\ S_i = (S_{i-1} + X_i - T)(1 - \frac{k}{C_i}) & \text{if } C_i > k \end{cases} \tag{8}$$

where S_0=0 and k>0

An out-of-control signal is generated when

$$y_i = [S_i'\Sigma^{-1}S_i]^{1/2} > h \tag{9}$$

where k is a reference value and h is a decision interval for the process.

The chosen value of k and h values for in-control ARL of 200 and 500 can be found in Crosier's study (1988). In this study, we reorganize their result in Table 7-1.

Table 7-1 Chosen value of *k* and *h* with different kinds of dimension *p* under two in-control ARLs.

	In-Control ARL's of 200		In-Control ARL's of 500	
p	*h*	*k*	*h*	*k*
2	5.50	0.5	6.65	0.5
5	9.46	0.5	10.9	0.5
10	14.9	0.5	17.2	0.5
20	24.7	0.5	28.0	0.5

7.3 The Proposed Marginal CUSUM Glyphs

The proposed framework first relies on the MCUSUM described in the previous section to detect any process shift so that the overall type I error is desirable. If the type I error is excessive, too many false alarms will be triggered. Operators may become placid and ignore a true process shift that may prove to be costly in the future. Therefore, in this study, the proposed method uses the multivariate control chart as the primary detection method, while the marginal univariate control chart described in section 7.2.3 is used as the diagnostic tool once the multivariate control chart signals an out-of-control observation.

The proposed diagnostic tool, the marginal CUSUM glyphs, is presented in this section. The proposed method, integrating marginal CUSUM into one glyph, is a visualization tool for a decision support system dealing with multivariate quality characteristics. Specifically, glyphs plotted over time are organized in panels of trellis. Every row contains two time series glyphs, i.e., C_{pi} and C_{ni}. C_{pi} is a glyph of i^{th} observation for the upper (positive)-side CUSUM statistic, while C_{ni} is a glyph of the same observation for the lower (negative)-side CUSUM statistic. Each vertex in the glyph represents a response that shares equal space around 360 degrees. When a CUSUM statistic becomes large, the corresponding vertex would grow in length. On the other hand, an in-control process would have all vertices close to the center "dot." Finally, a circle with the radius h encircles the center dot, and this circle represents a control limit for each glyph. If a few responses are responsible for an out-of-control MCUSUM signal, their marginal CUSUM would show abnormality in the glyph over time leading to the out-of-control moment, and those spikes would excess the circle. The following steps describe the main procedure of the proposed marginal CUSUM glyphs.

Step 1: Run MCUSUM until it provides an out-of-control signal at location or time τ assuming one sample is taken for each sample period.

Step 2: Run SD2CUSUM procedure to generate $C_{p,i}$, $C_{n,i}$ and record any out-of-control o, and last-in-control location l for each dimension. The out-of-control position for the i^{th} dimension o_i is the location that excesses the control limit h, while the last-in-control location l_i is equal to $o_i - N^+$ or $o_i - N^-$ for dimension i where N^+ and N^- are defined in section 2.3.

Step 3: Construct star glyphs staring from sample periods 1 to τ for both positive and negative glyphs. Each glyph consists of a circle with radius of h and spikes with length of $C_{p,i}$ or $C_{n,i}$ radiating from the center of a circle. We choose to start the spikes from 3 o'clock position and move the spikes in counterclockwise direction with identical angle between any adjacent spikes.

Step 4: Print out out-of-control o and last-in-control l for each dimension, and display the marginal CUSUM glyphs. Out-of-control signals indicate *which* variables contribute statistics of MCUSUM, while last-in-control locations show *when* these variables become out-of-control.

With a stable and in-control process, a glyph on the trellis panel should present a “dot” with some tiny spike inside of a circle. However, users might not see some small change by looking at a “dot”, for a tiny spike might be difficult to distinguish. Instead of a “dot”, users can add a constant c on both $C_{p,i}$ and $C_{n,i}$ to expend a “dot” into a polygon shape. The new statistics showing in equation (10) and (11) denoted $CC_{p,i}$ and $CC_{n,i}$ would replace the original $C_{p,i}$ and $C_{n,i}$. Also the same c is required to be added to the radius h to maintain the same scale of threshold as shown in equation (12). This new limit is denoted as H.

$$CC_{p,i} = c + \max[0, y_i - k + C_{p,i-1}] \tag{10}$$

$$CC_{n,i} = c + \max[0, -k - y_i + C_{n,i-1}] \tag{11}$$

$$H=c+h \tag{12}$$

7.3.1 An Example to Demonstrate the Use of the Proposed Method

An example of 5-dimensional, 20 observations with one sigma mean shift example is presented in this section. The dataset is shown in column of x_1 to x_5 in Table 2. It was generated from the multivariate normal distribution. The first 10 observations was simulated as in-control data from a multinormal distribution with mean vector μ_0=(5,10,15,20,25) and variance-covariance matrix shown in equation (13), while the last 10 observations represented out-of-control data from μ_1=(**6**,10,**16**,20,**26**), i.e. a small mean shift at the first, third and fifth variables, and its variance-covariance structure same as that of the first 10 observations.

$$\Sigma = \begin{bmatrix} 1 & 0.3 & 0.3 & 0.3 & 0.3 \\ 0.3 & 1 & 0.3 & 0.3 & 0.3 \\ 0.3 & 0.3 & 1 & 0.3 & 0.3 \\ 0.3 & 0.3 & 0.3 & 1 & 0.3 \\ 0.3 & 0.3 & 0.3 & 0.3 & 1 \end{bmatrix} \tag{13}$$

A Scatter plot of this example is shown in Figure 7.7, in which the dots represent the first 10 observations, while the squares are for the last ten. The ellipses are 95% confidence contours based on the normal assumption. The solid-line ellipses are for the first 10 observations, while the dash-line ellipses are for the last 10. Note that, in reality, one would not know in advance when such a shift takes place or if it takes place at all. Even with dots and squares it is difficult to identify the process status.

At the beginning of the proposed method, the MCUSUM is applied. After using the equations (7), (8), and (9) with h=9.46 and k=0.5, the statistic of MCUSUM is showing in the column of C in Table 2 and its control chart is showing in Figure 7.8. The out-of-control signal occurred starting at 15th observation.

At this point, the diagnostic process begins. The first step is to standardize every dimension by using equation (4) where σ=1 and μ_0=(5,10,15,20,25). Next, the procedure of two-side CUSUM is applied via equations (5) and (6) with h=5 and k=0.5. The marginal CUSUM statistics are shown in Table 7-3.

To Determine Which Variables Contribute to the Out-of-control Signal

The data of $C_{p,i}$ and $C_{n,i}$ where i=1 to 15 in Table 7-3 are used to construct the proposed glyphs. After applying the traditional star glyphs described in section 7.2.2 for each $C_{p,i}$ and $C_{n,i}$, the soild-line circle with radius=h is also added on each of glyph. In Figure 7.9, the proposed glyphs are shown. The graph of "basic" is an elementary glyph of a scale. Note that the star glyphs are not visible when the process is in control, where the values of $C_{p,i}$ and $C_{n,i}$ are close to zero. Therefore, a constant c is added to $C_{p,i}$,$C_{n,i}$ and h according to equations (10) to (12). In this case, the glyphs with c=3 are shown in Figure 7.10. There are three spikes exceeding the circle, between CC_{p14} and CC_{p20} indicating that the means of variables x_1, x_3, and x_5 have shifted. In addition, there is no spike exceeding the circle in any of C_n or CC_n. One can conclude that no negative mean shift occurred.

<u>To Determine When Shifts Took Place</u>

In Table 7-3, the 14th observation of C_p statistic in the first dimension is 5.83, which is larger than h=5. Thus, it is deemed that the first dimension has shift at 14th observation on positive-side CUSUM. Moreover, since the correspond $N_{p,1}$ of 14th observation is 6, the last-in-control observation is 14-6=8th observation according to the definition of last-in-control in section 7.2.3. Using the same philosophy, the third and the fifth dimensions are found to shift at 16th and 17th, respectively. And their last-in-control locations are at 10th observation for the third dimension, and 11th observation for the fifth dimension. And there is no shift indicated in negative-side CUSUM. The proposed method indicates that variables x_1, x_3, and x_5 make contribution to the out-of-control signal at location 8th, 10th, and 11th, respectively.

Table 7-2. 5-dimensional, 20 observations dataset.

	x_1	x_2	x_3	x_4	x_5	C
1	4.79858	10.0034	15.0335	19.2843	25.0273	0.463891
2	4.85333	9.1170	14.8924	18.3470	21.8418	2.607937
3	4.32499	8.9170	16.2335	19.6594	25.6710	1.775256
4	5.23184	10.2377	14.3568	18.8797	25.0120	2.239928
5	6.76232	8.4736	14.8295	18.7632	25.3518	3.221392
6	3.93670	10.0544	14.8085	18.3438	26.4359	2.147643
7	4.98181	8.9128	12.3676	20.7162	24.5627	2.440458
8	4.57178	12.2499	15.3191	20.6362	26.2305	2.130893
9	5.85859	9.7962	14.5142	20.2430	24.0448	0.772875
10	6.95341	9.3181	15.1976	20.6888	24.6941	1.788469
11	7.15771	8.9142	15.6287	19.4212	25.4814	3.296222
12	6.23149	9.7179	16.4945	19.4940	26.2335	5.596017
13	6.16967	9.5291	17.2668	19.7801	26.9197	7.212117
14	6.45825	10.9076	15.4995	19.0572	25.7781	8.722549
15	7.39763	10.4058	15.5910	21.2973	25.9004	11.45267
16	5.26227	10.2907	17.4474	21.4488	25.6842	13.99988
17	5.42656	12.8401	18.6317	19.5853	25.1729	15.96414
18	7.06759	10.2345	16.2082	19.4704	26.4889	15.93851
19	7.20849	10.2192	13.8677	19.0505	26.8322	16.17303
20	6.00803	10.2438	15.9425	20.9734	26.3481	18.32671

Figure 7.7. The scatter plot of the given example.

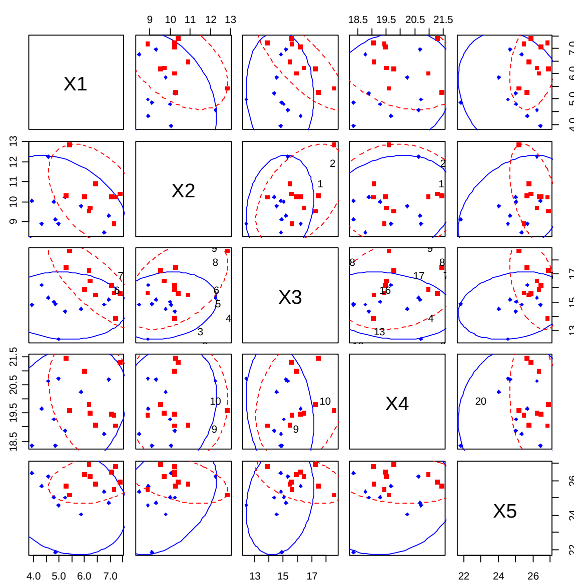

Figure 7.8. MCUSUM control chart of the given example.

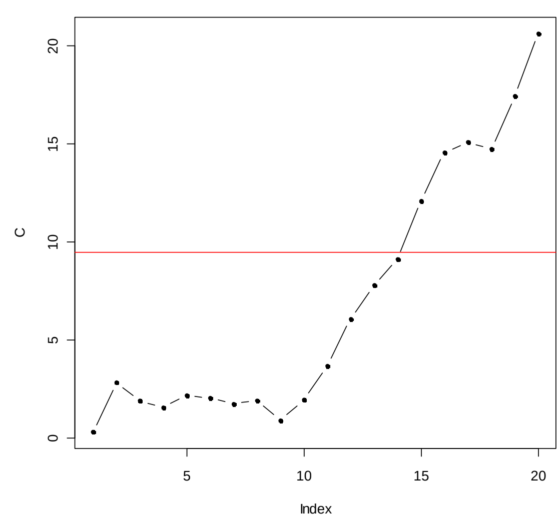

Table 7-3. The result of two-side standardized CUSUM for the given example.

(a) SD2CUSUM for Positive Mean Shifts

i	$C_{p,i,1}$	$N_{p,i,1}$	$C_{p,i,2}$	$N_{p,i,2}$	$C_{p,i,3}$	$N_{p,i,3}$	$C_{p,i,4}$	$N_{p,i,4}$	$C_{p,i,5}$	$N_{p,i,5}$
1	0.00	0	0.00	0	0.00	0	0.00	0	0.00	0
2	0.00	0	0.00	0	0.00	0	0.00	0	0.00	0
3	0.00	0	0.00	0	0.73	1	0.00	0	0.17	1
4	0.00	0	0.00	0	0.00	0	0.00	0	0.00	0
5	1.26	1	0.00	0	0.00	0	0.00	0	0.00	0
6	0.00	0	0.00	0	0.00	0	0.00	0	0.94	1
7	0.00	0	0.00	0	0.00	0	0.22	1	0.00	0
8	0.00	0	1.75	1	0.00	0	0.35	2	0.73	1
9	0.36	1	1.05	2	0.00	0	0.10	3	0.00	0
10	1.81	2	0.00	0	0.00	0	0.28	4	0.00	0
11	3.47	3	0.00	0	0.13	1	0.00	0	0.00	0
12	4.20	4	0.00	0	1.12	2	0.00	0	0.73	1
13	4.87	5	0.00	0	2.89	3	0.00	0	2.15	2
14	5.83	6	0.41	1	2.89	4	0.00	0	2.43	3
15	7.73	7	0.31	2	2.98	5	0.80	1	2.83	4
16	8.90	8	0.00	0	4.81	6	0.78	2	5.53	5
17	9.06	9	0.00	0	6.64	7	0.19	3	6.75	6
18	9.35	10	0.00	0	7.00	8	0.00	0	6.44	7
19	8.93	11	0.00	0	6.12	9	0.00	0	7.75	8
20	11.18	12	0.87	1	7.04	10	0.16	1	9.56	9

(b) SD2CUSUM for Negative Mean Shifts

i	$C_{n,i,1}$	$N_{n,i,1}$	$C_{n,i,2}$	$N_{n,i,2}$	$C_{n,i,3}$	$N_{n,i,3}$	$C_{n,i,4}$	$N_{n,i,4}$	$C_{n,i,5}$	$N_{n,i,5}$
1	0.00	0	0.00	0	0.00	0	0.22	1	0.00	0
2	0.00	0	0.38	1	0.00	0	1.37	2	2.66	1
3	0.18	1	0.97	2	0.00	0	1.21	3	1.49	2
4	0.00	0	0.23	3	0.14	1	1.83	4	0.98	3
5	0.00	0	1.25	4	0.00	0	2.57	5	0.12	4
6	0.56	1	0.70	5	0.00	0	3.72	6	0.00	0
7	0.08	2	1.29	6	2.13	1	2.51	7	0.00	0
8	0.01	3	0.00	0	1.31	2	1.37	8	0.00	0
9	0.00	0	0.00	0	1.30	3	0.63	9	0.46	1
10	0.00	0	0.18	1	0.60	4	0.00	0	0.26	2
11	0.00	0	0.77	2	0.00	0	0.08	1	0.00	0
12	0.00	0	0.55	3	0.00	0	0.08	2	0.00	0
13	0.00	0	0.52	4	0.00	0	0.00	0	0.00	0
14	0.00	0	0.00	0	0.00	0	0.44	1	0.00	0
15	0.00	0	0.00	0	0.00	0	0.00	0	0.00	0
16	0.00	0	0.00	0	0.00	0	0.00	0	0.00	0
17	0.00	0	0.00	0	0.00	0	0.00	0	0.00	0
18	0.00	0	0.00	0	0.00	0	0.01	1	0.00	0
19	0.00	0	0.00	0	0.00	0	0.00	0	0.00	0
20	0.00	0	0.00	0	0.00	0	0.00	0	0.00	0

Figure 7.9. The CMCUSUM glyphs of the given example with *c*=0.

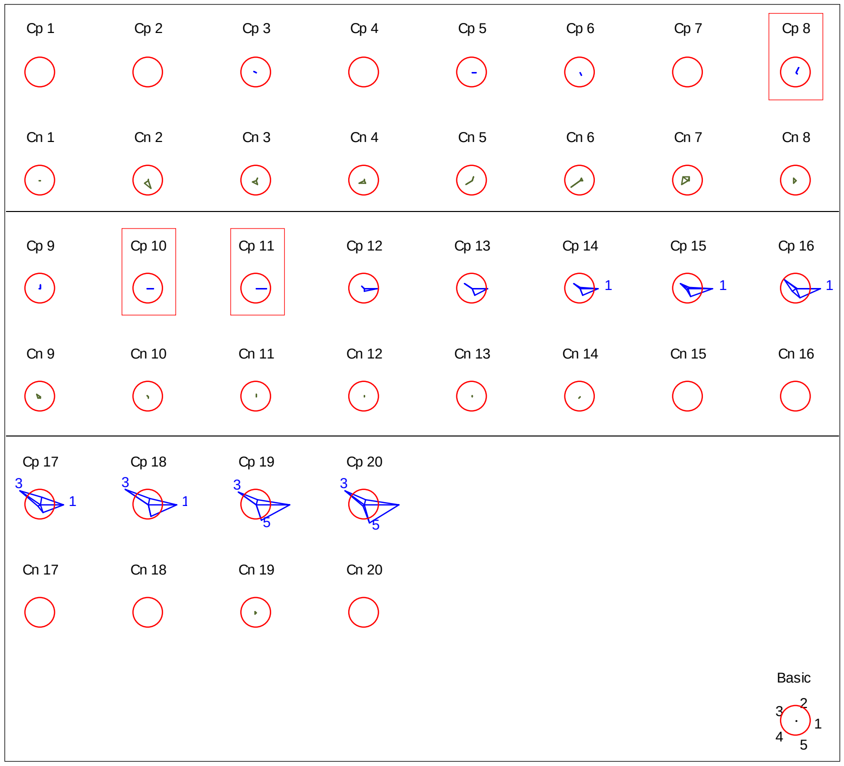

Figure 7.10. The CMCUSUM glyphs of the given example with *c*=3.

7.4 A Simulation Study

To examine the capability of the proposed method, a simulation study is planned to explore magnitude of *h*, number of dimensions, number of dimensions shifted, and type of correlation-coefficient structures. Figure 7.11 shows the detailed experimental plan of the proposed study. The design is to test the capability of the proposed method at different types of value of *h* in terms of absolute value of deviation between true shift location and calculated shift location. Each factor combination is repeated 1000 times. Each run contains 100 observations with 1σ mean shifts taking place at 31st observation for all planned dimensions. For example, considering a five-dimensional, 100 observations dataset with three of five dimensions having a step mean shift, the simulation data set would have the first 30 observations generated from the multivariate normal distribution with μ_0, while the last 70 observations are from μ_1. The means of the non-shifted dimensions stay at the same magnitudes. The variance shift is not considered in this study.

Figure 7.11. Experimental design of the proposed method at different types of *h*.

Magnitude of h:
h=3, 4, 5, 6, 7, 8

Number of Dimension:
dim=3, 5, 10, 20

Number of Dimensions Shifted:
1. Small: 1/3 of number of dimensions shifted—3(1); 5(2); 10(3); 20(5)
2. Medium: half of number of dimensions shifted—3(2); 5(3); 10(5); 20(10)
3. Large: All of number of dimensions shifted—3(3); 5(5); 10(10); 20(20)

Note: 3(2) means two out of three dimensions are shifted.

Types of Correlation-Coefficient Structure:
ρ=0, 0.5, 0.9

Input Data Series Type:
Multivariate Normal Distribution

Magnitude of h

Since *h* is the major criterion of setting the control limit of CUSUM, it is necessary to test the proposed method under different magnitudes of *h*. The smaller the value of *h* the more quickly the SD2CUSUM detects a shift. However, the type I error would increase. On the other hand, if *h* has been increased, the type II error would increase. In this paper, six types of value of *h* are applied to, *i.e., h*=3, 4, 5, 6, 7, and 8.

Number of Dimensions

The number of dimensions is one of the factors considered in implementing multivariate control charts, especially in visualization of multivariate dataset. In this study, four dimensions are considered. They are 3, 5, 10, and 20. This factor allows us to study how effective the proposed method is when the dimension increases.

Number of Dimensions Shifted

There are three different levels of number of dimensions shifted in this study: small, medium, and large. For small level, 1/3 of number of dimensions shifted. For example, if one dimension has 1σ mean shift in a three-dimensional dataset, this case is in the small level category. That is, the first 30 observations follow multivariate normal distribution with μ_0=(5, 10, 15), while the last 70 observations are generated from multivariate normal distribution with μ_1=(**6**, 10, 15). The notation of this case is 3(1). In addition, the other small number of dimension shifted cases has 2, 3, and 5 dimensions shifted for 5, 10, and 20 dimensions, respectively. For the medium level, half of number of dimensions shifted, while all of number of dimensions has shifted for large number of dimensions shifted cases. Note that the goal of this factor is to study the effect of how wide-spread mean shifts are to the responses rather than the magnitude of the shifts.

Types of Correlation-Coefficient Structure

Different types of variance-covariance structures are also considered in this simulation. Without the loss of generality, three types of correlation-coefficient matrices are used to study no, medium and high correlations among the responses. The correlation-coefficient structure for the simulated data that generated from multivariate normal distribution is the following.

$$\Sigma = \begin{bmatrix} 1 & \cdots & \rho \\ \vdots & \ddots & \vdots \\ \rho & \cdots & 1 \end{bmatrix}, \text{ where } \rho=0,\ 0.5, \text{ and } 0.9 \tag{14}$$

7.4.1 Simulation Results and Discussions

This section shows the computational results of the proposed simulation study using 1,000 runs for each combination – 216,000 runs in total. The performance of the proposed method is measured by four statistics: the **correct identification percentage**, the **average**

absolute value of deviation, **type I error rate (false alarm rate), and type II error rate**. These four statistics will be applied to the last-in-control signals. The first one is the bigger the better, while the rest of which are the smaller the better. The correct identification percentage indicates how accurate the system is to identify which responses are responsible for the out-of-control signal. The average absolute value of deviation measures the distance between true location of a mean shift and its calculated location among all dimensions that exhibit mean shifts. Specifically, it is calculated the follows:

$$\textbf{Average absolute value of deviation} = \frac{\sum_{i=1}^{m} |l_i - t_i|}{m} \tag{15}$$

where l_i is the calculated location of i^{th} dimension of dataset, t_i is the true location of i^{th} dimension, and m is the number of dimensions that are identified correct out of control. Under the measure of those out-of-control dimensions, the type I error rate, or the false alarm rate, is the probability when the proposed method indicates a dimension is out of control while, in truth, it is not. The type II error rate, on the other hand, is the probability when it fails to identify a shifted dimension. The desired result for the correct identification percentage is 100%, while that of the other three statistics is the closer to zero the better.

The suggestion of h for the proposed method provides a guideline for implementing the proposed method and will be discussed. The simulation results are shown in Figure 7.12 to Figure 7.14, and their corresponding tables are available from the authors upon request. For example, Figure 7.12(a) indicates the simulation results of small number of dimensions shifted with ρ=0. Each sub-chart consists of four performance measures – correct identification percentages (correctness), average absolute value of deviation(dev), type I error rate (in %) (type I), and type II error rate (in %)(type II). Specifically Figure 7.12 (a) summarizes the simulation result of small number of dimensions shifted under different h with ρ=0, while Figure 7.12 (b) and 12(c) are for ρ=0.5 and ρ=0.9 respectively. Next level down, Figure 7.12 (a-1) to (a-4) depict four performance criteria respectively. For example in Figure 7.12 (a-1), correct identification percentage plots against the dimension. Although h=3 and 4 have the highest correct identification percentages, they also have high deviation and type I error rate. Therefore, ***h*=5** is a more balanced control limit for this case because it has larger correct identification percentages and lower type II error rate than those of h=6, 7, and 8. Although values of deviation and type I error rate at h=6, 7, and 8 are lower than those of h=5, they are close to each other.

In the case of small number of dimensions shifted with ρ=0.5 as shown in Figure 7.12(b), h=4, 5, and 6 have the top three highest percentages of correct identification. The control limit h=4, however, have higher values of deviation and type I error rate than those of h=5 and h=6. The differences between h=5 and 6 for all criteria and dimensions are small. Thus, ***h*= 5 or 6** is the recommended control limit for this case if the correct identification percentage and accuracy of where a process shift takes place are important. Note that h=7 and 8 are chosen due to their poor correct identification percentages 88.3% and 78.1% as oppose to those(98.3% and 95.9%) of h= 5 and 6.

Finally the case of ρ=0.9 with small number of dimensions shifted is considered, h=5, 6, 7, and 8 have larger correct identification percentages than that of h=3 and 4. Moreover, h=7 and 8 have very small value of deviation and type I error rate shown in Figure 7.12 (c-3). However, Figure 7.12 (c-4) indicates high type II error rate in 3 and 5 dimensional datasets of h=7 or 8 may not be acceptable. Therefore, it is suggested that ***h*=5 or 6** is used as the control limit in this case. In summary, ***h*=5** is a good choice for all dimensions and covariance structure when the number of dimensions exhibiting shifts is small.

In the case of the medium number of dimensions shifted, half of response variables contain mean shifted. The simulation results are shown in Figure 7.13. In Figure 7.13 (a-1), ***h*=5** performs a better result than any others for all ρ because it has high correctness rate, small deviation, type I error rate, and type II error rate for last-in-control signal.

The final situation is when all dimensions shift. Since all mean levels of dimensions have shifted, there is no type I error occurred in this case. The computational results are shown in Figure 7.14 (a-1) to (c-4). All of them show that h=5 has the best choice among h because of its balanced performance in terms of acceptable correct identification percentages, small deviation and type II error rate. Thus, ***h*=5** is a recommended control limit for the proposed method when large number of dimensions shifted happened. From the above analysis, ***h*=5** seems to provide the best balanced performance for all dimensions, covariance structure, and number of dimensions exhibiting shifts.

Figure 7.12.Performance statistics for small level of number of dimensions shifted with (a) ρ=0, (b) ρ=0.5, and (c) ρ=0.9 under different h.

The y axes of plots (1) to (4) are correct classification percentage, average absolute value of deviation, type I error rate in percentage, and type II error rate in percentage, respectively. The x axis represents the numbers dimension for last-in-control location.

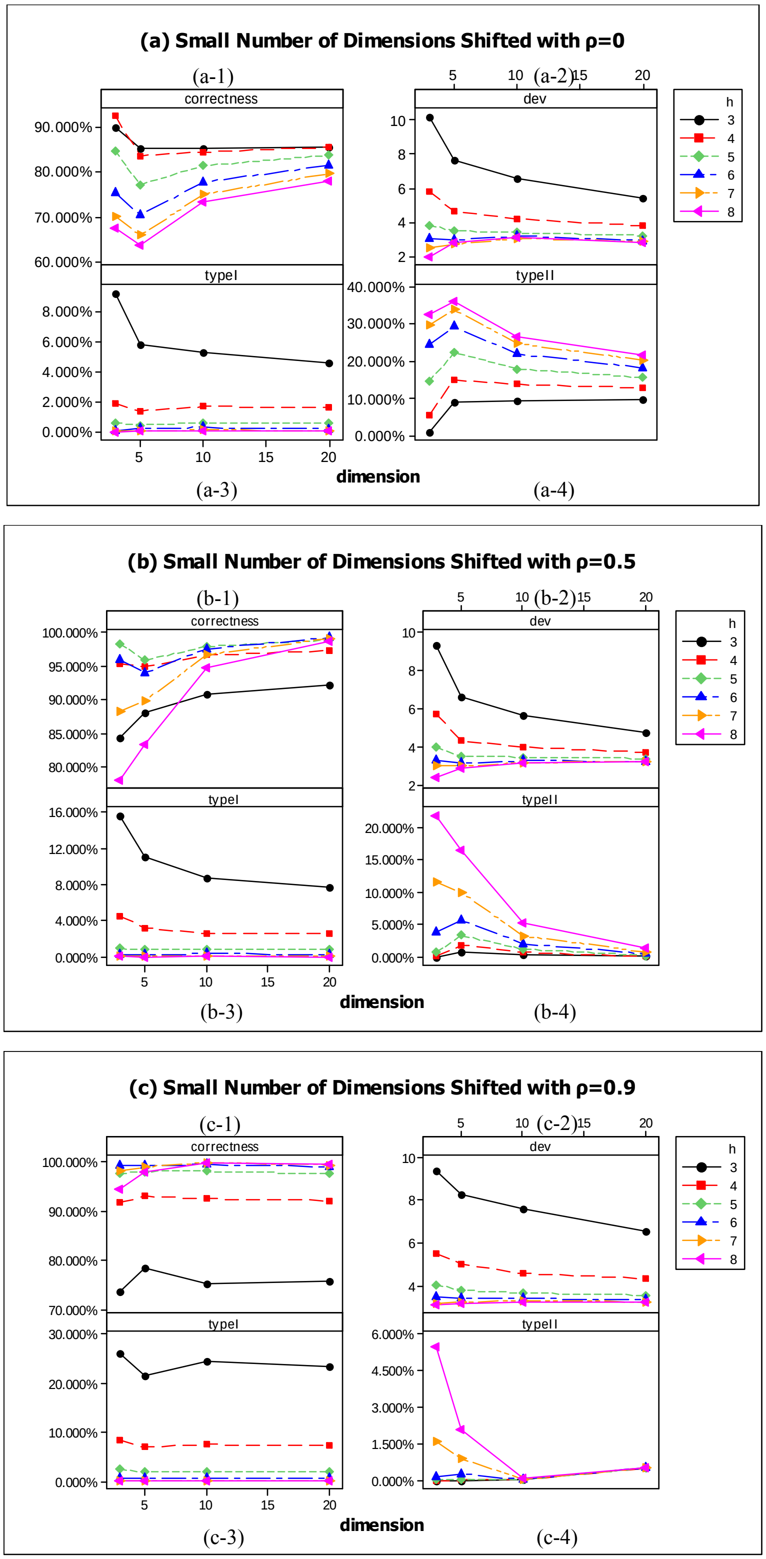

Figure 7.13. Performance statistics for medium level of number of dimensions shifted with (a) ρ=0, (b) ρ=0.5, and (c) ρ=0.9 under different h.

The y axes of plots (1) to (4) are correct classification percentage, average absolute value of deviation, type I error rate in percentage, and type II error rate in percentage, respectively. The x axis represents the numbers dimension for last-in-control location.

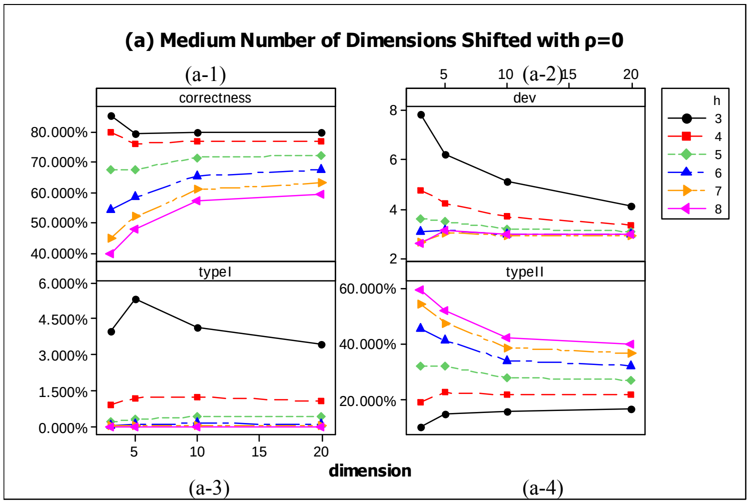

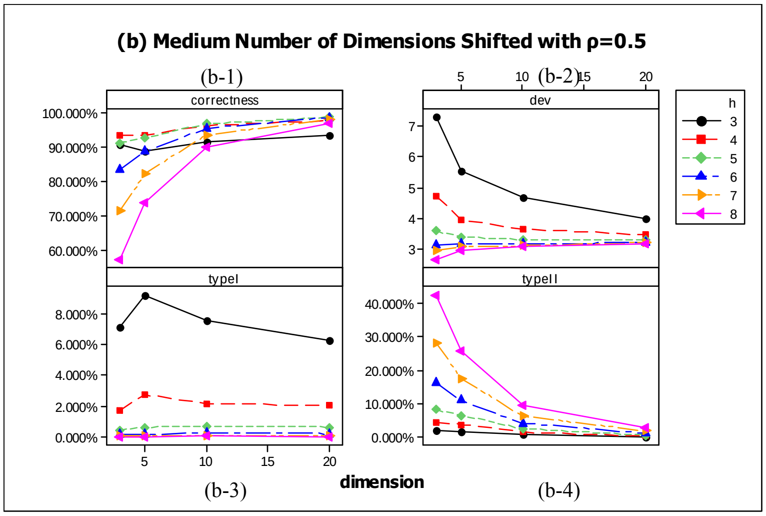

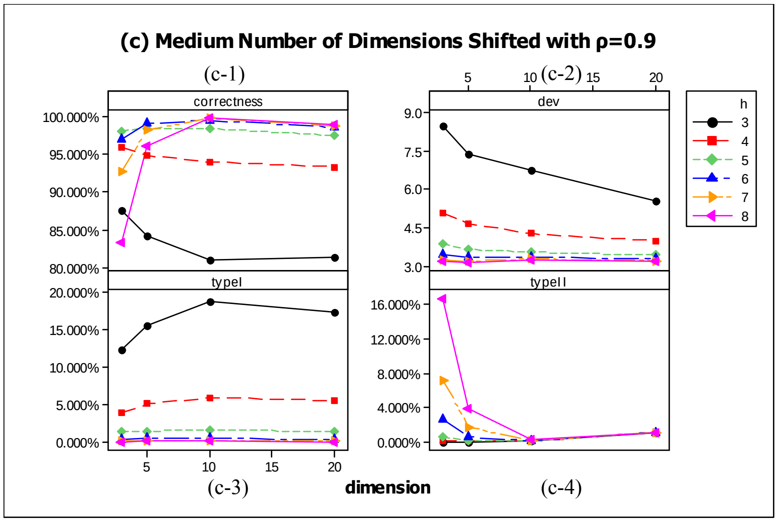

Figure 7.14. Performance statistics for large level of number of dimensions shifted with (a) ρ=0, (b) ρ=0.5, and (c) ρ=0.9 under different h.

The y axes of plots (1) to (3) are correct classification percentage, average absolute value of deviation, and type II error rate in percentage, respectively. The x axis represents the numbers dimension for last-in-control location.

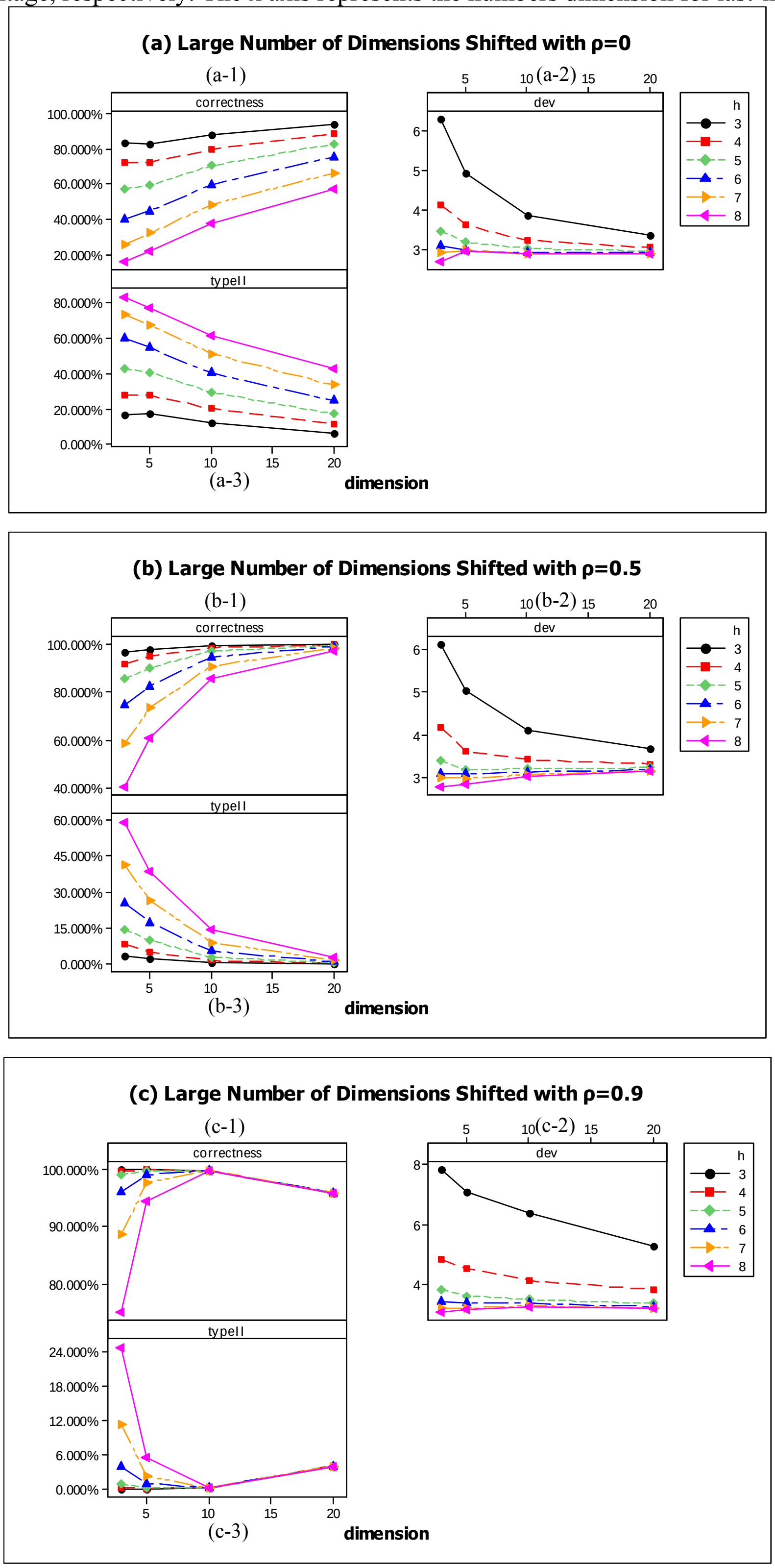

Figure 7.15. Simulation results of small number of dimensions shifted.

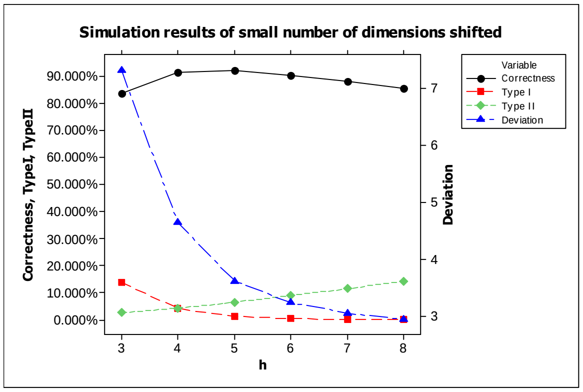

Table 7-4. Simulation results of small number of dimensions shifted.

h	Correct ident. %	Type I Err. Rate (%)	Type II Err. Rate (%)	Avg. abs. value of Deviation
3	83.733%	13.698%	2.569%	7.328
4	91.650%	4.127%	4.223%	4.645
5	92.446%	1.145%	6.409%	3.620
6	90.725%	0.349%	8.926%	3.238
7	88.421%	0.099%	11.480%	3.056
8	85.760%	0.030%	14.210%	2.943

Figure 7.16. Simulation results of medium number of dimensions shifted.

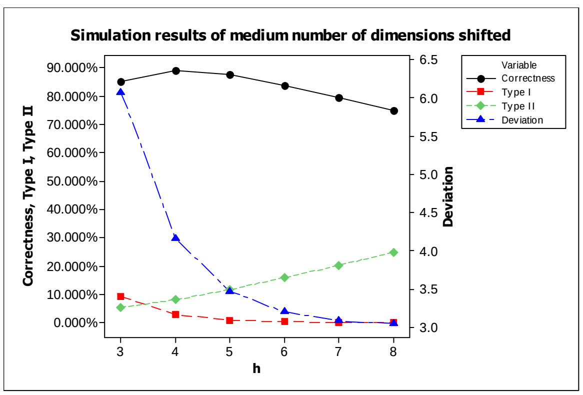

Table 7-5. Simulation results of medium number of dimensions shifted.

h	Correct ident. %	Type I Err. Rate (%)	Type II Err. Rate (%)	Avg. abs. value of Deviation
3	85.394%	9.323%	5.282%	6.082
4	89.114%	2.811%	8.075%	4.164
5	87.591%	0.788%	11.620%	3.469
6	83.887%	0.223%	15.890%	3.202
7	79.725%	0.064%	20.211%	3.084
8	75.119%	0.020%	24.861%	3.046

Figure 7.17. Simulation results of large number of dimensions shifted.

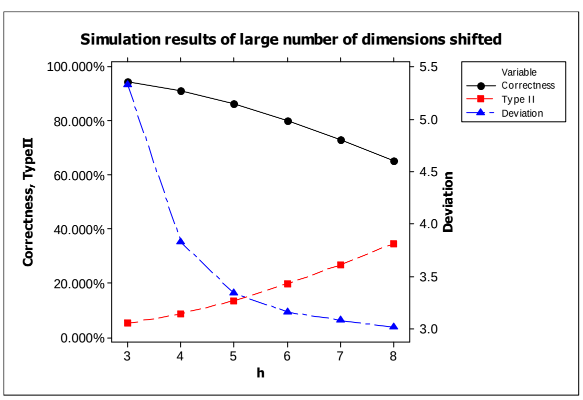

Table 7-6. Simulation results of large number of dimensions shifted.

h	Correct ident. %	Type II Err. Rate (%)	Avg. abs. value of Deviation
3	94.884%	5.116%	5.332
4	91.264%	8.736%	3.832
5	86.474%	13.526%	3.336
6	80.167%	19.833%	3.159
7	73.063%	26.937%	3.080
8	65.346%	34.654%	3.010

Table 7-4 to 7.6 present the simulation results in another perspective by averaging performance statistics over all covariance structures and dimensions. For example, the correct identification percentages of *h*=3 is an average value of different types of ρ and different numbers of dimensions when h=3. Figure 7.15 to 7.17 correspond to Table 7-4 to 7.6. An *h* should be chosen so that the correct identification percentage is as large as possible while the rest of the performance statistics are as small as possible. Note that y axis on the left in Figure 7.15 to 7.17 are percentages for criteria correct identification percentage, type I error rate in percentage, and type II error rate in percentage while that on the right-hand side is for the deviation from the true change point.

Figure 7.15 to 7.17 provide an overall guideline for choosing *h* that is determined by three criteria – correct identification percentage, type II error rate, and average absolution deviation. An ideal choice of h provides a high correct identification percentage, a low type II error rate, and a small deviation from the true out-of-control location. However, users may not know what kind of underlying covariance structure among responses or number of responses that may have shifted in practice. These three figures suggest that *h*=5 and 6 provide the best overall balanced performance because the line segments of these three *h* values are very close together. Note that *h*=5 was recommended earlier from the analyses based on Figure 7.12 to 14. The overall comparisons here provide further confirmation. For example, if a user chooses *h*=5 to a situation where medium number of dimensions may be likely to shift, it will provide 87.6% correct identification percentage, 0.79% type I error rate, 11.6% type II error rate, and 3.5 of its average deviation from the true spot. This user should contemplate whether *h*=6 is a better choice because the criterion values of this new choice are 83.9% correct identification percentage, 0.22% type I error, 15.9% type II error, and 3.2 as its average deviation. Do the gains in type I error (-0.57%) and average deviation (-0.3) outweigh the loss in correct identification (-3.7%) and type II error rate (+4.3%)?

Because there are multiple criteria present in this problem, a solution is generally reached by considering the trade off of all criteria. Eventually a compromised solution is generated. This type of problems often referred to as the multi-criteria decision making is beyond the scope of this work. Please refer to Triantaphyllou (2000) for more details.

7.5 Conclusions and Future Study

This study provides a visualization tool for making quality-related decision when the number of dimensions is large such as 20. The proposed method, the marginal CUSUM glyphs, can help users not only decompose the traditional multivariate control chart, such as, Hotelling's T^2, multivariate EWMA, or multivariate CUSUM, but also visualize the original dataset. The proposed method provides the information which variable are responsible as well as where or when a variable is out of control. From the simulation results, the proposed method is capable of detecting mean shifts. In this study, according to the simulation results, h=5 and 6 are recommended to be applied to all situations regardless of the covariance structure among responses or how many of them exhibiting shifts. The tables and figures based on the simulation results also provide a user guideline for choosing other values of h via the correct classification percentage, magnitude of deviation, and false alarm rate and type II error rate.

For future research, the following issues can be studied. First, the effect of outliers should be considered. Outliers can make the statistics of SD2CUSUM increase dramatically to cause unnecessary out-of-control signals. To deal with this issue, filtering the dataset may be necessary. Techniques of outlier identification for high dimensional dataset include MVE/MCD (Rousseeuw, 1985; Rousseeuw and van Driessen, 1999), OGK estimator (Maronna and zamar, 2002), and PCOut (Filzmoser *et al.,* 2008).

In this study, the highest number of dimension is 20. It is not a trivia task to expand the proposed method to response dimension over 100 or more. The angles between spikes for 50 and 100 dimensions are 7.2 and 3.6 respectively. The more spikes are within a circle in a star glyph the more clutter they cause. When a process is in control, cluttering is not an issue because all spikes are within the circles of control limits. Users do not need distinguish individual dimension. However, when there are many spikes that exceed control limit circles, it depends on how close these spikes are located. If they are equally spaced or far apart, the results of display are usually satisfactory. On the other hand, if all out-of-control spikes are adjacent to each other, users need to consult with the corresponding diagnostic report to make out which spikes exceed the circles. Another way to address high dimension problem is to reduce the number of dimensions, such as using principle component analysis (PCA). However, once PCA is applied to the original dataset, the original domain is transferred to a much reduced domain. It is hard to identify which original dimensions contribute to an out-of-control signal.

The proposed glyphs are competent in demonstrating out-of-control responses due to mean shifts. However, this version does not consider the changes due to data structure changes among responses. One possible solution is to consider the use of colors and angles in addition to the expansion of the current visualization from two dimensional to three dimensional space. It would be a major undertaking. Finally, the situation in which the number of dimensions is larger than the number of observation is challenging. Neither can the proposed method nor traditional multivariate control charts cope with this situation because the estimate of the variance-covariance structure becomes a nontrivial task. Boyles (1996) and Chang and Ho (2001) have provided some ground work in this area.

References

Boyles, R. A. (1996). “Multivariate Process Analysis with Lattice Data.” *Technometrics*, 38(1): 37-49.

Chang, S. I and E. S. Ho (2001). “Multivariate Statistical Process Control for Inspection Data from Coordinate Measuring Machines.” *International Journal of Industrial Engineering – Theory, Applications and Practices*, 8(4): 347-358.

Chen, C., Härdle, W., & Unwin, A. (2008). *Handbook of data visualization (springer handbooks of computational statistics)*. New York, NY: Springer.

Crosier, R. B. (1988). “Multivariate generalizations of cumulative sum quality-control schemes.” *Technometrics*, 30(3): 291-303.

Filzmoser, P., Maronna, R., & Werner, M. (2008). “Outlier identification in high dimensions.” *Computational Statistics and Data Analysis*, 52(3): 1694-711.

Hartigan, J. A., & Kleiner, B. (1984). “A mosaic of television ratings.” *The American Statistician*, 38(1): 32-35.

Hawkins, D. M. (1991). “Multivariate quality control based on regression-adjusted variables.” *Technometrics*, 33(1): 61-75.

Hawkins, D. M. (1993). “Cumulative sum control charting: An underutilized SPC tool.” *Quality Engineering*, 5(3): 463-477.

Jackson, J. E. (1985). “Multivariate quality control.” *Communications in Statistics - Theory and Methods*, 14(11): 2657-2688.

Lowry, C. A., Woodall, W. H., Champ, C. W., & Rigdon, S. E. (1992). “A multivariate exponentially weighted moving average control chart.” *Technometrics*, 34(1): 46-53.

Lowry, C. A. & Montgomery, D. C. (1995). “A Review of Multivariate Control Charts.” *IIE Transactions*, 27(6): 800-810.

Maronna, R. A. & Zamar, R. H. (2002). “Robust estimates of location and dispersion for high-dimensional datasets*.” Technometrics*, 44(4): 307-317.

Mason, R. L., and Young, J. C. (2002). “Multivariate Statistical Process Control with Industrial Applications.” *siam/ASA*, Alexandria, Virginia.

Mason, R. L., Tracy, N. D., and Young, J. C. (1995). “Decomposition of T2 for multivariate control chart interpretation.” *Journal of Quality Technology*, 27(2): 99-108.

Montgomery, D. C. (2008). *Introduction to statistical quality control*. New York, NY: John Wiley & Sons.

Pignatiello, J. J.,Jr., & Runger, G. C. (1990). "Comparisons of multivariate CUSUM charts." *Journal of Quality Technology*, 22(3): 173-86.

The R project for statistical computing. Star (Spider/Radar) Plots and Segment Diagrams. http://wiki.r-project.org/rwiki/doku.php?id=rdoc:graphics:stars

Runger, G. C., Alt, F. B. and Montgomery, D. C. (1996). "Contributors to a Multivariate Statistical Process Control Signal." *Communications in Statistics—Theory and Methods*. 25(10): 2203-2213.

Rousseeuw, P. J. (1985). "Multivariate estimation with high breakdown point." *Mathematical Statistics and Applications*, 8, 283-297.

Rousseeuw, P. J., van Driessen, K. (1999). "A fast algorithm for the minimum covariance determinant estimator." *Technometrics*, 41(3): 212-223.

Sarkar, D. (2008). *Lattice: Multivariate data visualization with R (use R)*, 1st ed., New York, NY: Springer.

Triantaphyllou, E. (2000), *Multi-Criteria Decision Making Methods: A Comparative Study*. Boston, MA: Kluwer Acedemic Publishers.

Yates, F. (1935). "Complex Experiments." *Journal of the Royal Statistical Society* (Supplement), 2: 181-247.

Woodall, W. H., & Ncube, M. M. (1985). "Multivariate Cusum Quality-Control Procedures." *Technometrics*, 27(3), 285-292.

Chapter 8 Conclusions

In this chapter, the summaries and conclusions of each chapter will be presented, as well as the contribution and future study.

8.1 Summaries and Conclusions of this Research

The summaries and conclusions of this research are presented as following:

1. In Chapter 2, this research examined the effectiveness of removing noise using the B-Splines fitting with and without the help of wavelet transformation in nonlinear profiles. Chang and Yadama (2010) proposed a method that combines wavelet transformation and B-splines to improve profile monitoring. However, B-spline fitting is effective without the help of wavelet transformation when the monitoring of profile shape change is the only consideration, according to the experimental results in this research. Therefore, this research suggests that B-Splines fitting can be used without applying wavelet transformation first, if variance change is not considered. Otherwise, the wavelet decomposition will be useful to extract the variation change information.
2. In Chapter 3, the proposed framework monitors profile shape and variance changes simultaneously. The simulation results show that the proposed two-channel monitoring framework are capable of detecting scenarios of shape change only and both shape and variation changes. However, the proposed method would give false alarm of indication that both shape and variance changes in a profile but in fact only variance change exist. This research suggests that the causes due to variation changes should be examined first by using Paynaba and Jin's (2011) method.
3. In Chapter 4, the proposed framework that consists of FFT and the clustering/classification method as well as the dimension reduction approach is capable of monitoring waveform profiles without gold standard profile. The numerical results show that the proposed framework is capable of identifying abnormal wave profiles with minimal false alarm. The results of using the proposed method to the real world case study from the condensation water temperature profiles that collected from the curing process of the high-pressure hose products are also presented. According to the numerical results, the proposed framework in phase I (FFT+PAM+ED) constructs a solid phase I

process control chart with competitive performance in terms of false alarm rates after removing abnormal data points. In addition, the proposed framework in phase II (FFT+PAM+SVM_{RBF}+ED) dominates other famous profile analysis techniques with respect to the accuracy rate.

4. In Chapter 5, this research provides two approaches to detect process shifts in multiple nonlinear profiles, along with a simulation study for evaluating the performance of the proposed approaches in terms of average run length. According to the simulation study, the method I has better performance when the shape of profiles is changed entirely in the process, while the method II is more sensitive when the process contains partial profiles changes. Moreover, when profiles are highly correlated, the detecting power of the proposed method is much better than those cases with lower correlations. The hybrid method that combines method I and method II are also investigated so that quality engineers can diagnose each section before the process is finish without losing detecting power.
5. In Chapter 6, this research applies the PCA to the factorial experimental design when the response factor is the format of multiple nonlinear profiles. The numerical result shows the proposed method succeeded to convert the multiple nonlinear temperature profiles collected from six-location of a biomass pellet to a vector. Therefore, the conventional factorial experimental design method can be obtained directly. Also, the numerical results show the multiple temperature profiles can be used as the surrogate factors to replace the density and durability using desirability function. Finally, this research provides the predicting model for user to forecast the density and durability once the multiple temperature profiles dataset is given.
6. In Chapter 7, the proposed marginal CUSUM glyphs provide users a visualization aid to decompose the out-of-control signal of a multivariate control chart, and to diagnose the cause of out-of-control signal. Also, the proposed method gives the information of which variables are responsible as well as where or when a variable is out of control. Moreover, this research provides a guideline for choosing the parameters of the proposed method according to simulation results.

8.2 Future Study

This research explored the profile analysis in various aspects, single profile analysis, multiple profiles analysis, and profile diagnosis along with a visualization aid. However, there are still some studies that are not in the scope of this research. The following challenges can be considered in future studies.

1. Although this research provides a novel approach to monitor a process when the quality characteristics of interest are multiple nonlinear profiles, the research was conducted when shape change was the only consideration. There are remaining research subjects that when the process of interest is profile variance change only or both profiles shapes and variance are changed in the multiple profile scenrio.
2. The quality characteristics of interest in this research are profiles. In reality, it is possible the quality characteristics of interest may be a spatial dataset, an image, or a video. To develop a process monitoring tool to deal with such data formats is a potential future study.
3. The proposed visualization and diagnosis tool, marginal CUSUM glyphs, only works for the number of dimensions up to 20. It will be a challenge when the number of dimensions is over 1000 or more. A potential future study can be to investigate how large the number of dimensions the proposed method can handle, or explore other new methods to deal with the high-dimensional problem.
4. The methods proposed in this research monitored the profiles at the end of process or stage. A possible future study is to monitor the profiles on a real-time base. The possible application of real-time monitoring will help the quality engineers improve the process stability during the process rather than wait until the entire process is finished.

References

Chang, S.I. and Yadama, S., (2010). Statistical Process control for Monitoring Non-linear Profiles using Wavelet Filtering and B-Spline Approximation, *International Journal of Production Research*, 48(4), 1049-1068.

Paynabar, K. and Jin, J., (2011). Characterization of Non-linear Profiles Variations using Mixed-effect Models and Wavelets, *IIE Transactions*, 43(4), 275-290.